BSPE

해빈류의 시·공간적 변동성 연구 (I)

Temporal and Spatial Variability of Longshore Currents (I)

1993. 3.

한 국 해 양 연 구 소

제 출 문

한국해양연구소장 귀하

본 보고서를 "해빈류의 시·공간적 변동성 연구 (I)" 사업의 최종보고서로 제출합니다.

1993. 3. 31.

연구책임자 김 창 식

요 약 문

1. 제 목

해빈류의 시·공간적 변동성 연구 (I)

2. 연구의 필요성

연안에서 바닷물의 운동과 이에 따른 제반 환경요인들의 관련은 매우 복잡하다. 특히 조석에 의한 간만의 차이가 심한 천해에서는, 조석에 따른 역학요소들의 변화가 있다. 파랑의 쇄파에 의해 발생하는 해빈류(longshore currents)는 연안물리 현상의 이해 및 연안공학적 활용면에서 매우 중요한 역할을 한다. 연안에서의 퇴적물 이동, 해안선 변화, bar 또는 bump의 지형변화 등은 대부분 이러한 해빈류에 의한 반응으로 해석되며, 해빈류의 정확한 추정은 이에 따른 해적물 이동량 추정에 절대적으로 필요한 요소이다.

1970년에 Lognuet-Higgins(1970, Bowen(1969) 그리고 Thornton(1970) 등에 의해 제의된 평균 해빈류 추정 방법이 지난 20여년간 표준식으로 널리 사용되어 왔으며, 최근에는 bar가 형성된 연안에서 random wave에 의한 해빈류 추정방법이 Thorton and Guza(1968)에 의해 제의된 바 있다. 이들 기존 방법에 의한 해빈류의 추정은 조석과 다른 외력의 시간적 변화를 무시할 경우 만족할 만한 결과를 얻을 수 있었으며, 이로 인하여 추정되는 퇴적물 이동량은 관측시기, 관측시 기상 및 조석 조건 등에 의해 오차의 범위가 매우 크다.

하지만 지금까지의 연안류 관측과 예측은 조석 주기의 단편적(주로 고조시) 시간동안 수행해온 탓으로 연안류에 의한 퇴적물 이동 및 해안선 변화는 정상상태의 평균값에 의해 추정되어 왔다. 1990년 미국 동부해안(Duck, N.C)에서 수행된 DELILAH 실험은 3주간 연속으로 약 40여개의 P,U,V, sensor-pack으로부터 매초 8개씩의 자료를 관측함으로써 Hrms 및 해빈류, 연안류의 시간·공간적 변동성을 관측할 수 있는 최초의 실험이 되었다.

이렇게 연속 21일간 관측한 해빈류의 자료를 분석하여 조석과 기상변화에 의한 연안류의 시간 및 공간적 변동성을 연구하는 것은, 지금까지 사용되어오던 평균해빈류의 실제 적용성을 검토할 수 있으며, 필요시 새로운 개념의 해빈류에 의한 연안퇴적물이동에 대한 예측연구가 필요하다.

3. 연구목표

- 관측된 해빈류의 자료를 분석하여, 시·공간적 변동특성을 제시
- 시공간적 변동특성을 설명할 수 있는 개념적 모델개발
- 시공간적 변동특성에 대한 기존예측모델결과와의 비교검토
- 해빈류의 조석변화에 대한 반응 추정
- 연구결과를 국제연안공학 학술회의 (ICCE'92)와 유명 Journal (JGR Ocean)에 발표함으로써, 새로운 현상발견의 공인성을 인정받는다.

4. 연구결과

- 해빈류 및 Hrms의 조석주기에 따른 변동성은 쇄파대 내에 현저하게 나타나며,
- 변동성 크기는 20cm/s - 50cm/s 로써, 평균해빈류의 크기 20cm/s - 100cm/s에 대응하는 값이다.
- 기존 해빈류 예측모델에 조석에 따른 수심변화를 도입한 개념적 모델로, 해빈류 및 Hrms의 변동은 쇄파수심의 변화에 대한 일차적 반응임을 설명.
- 관측된 해빈류의 변동은 조석외에 기상변화에 의한 장주기 변동을 보임으로써 각종 외력에대한 계속적 연구의 필요성 강조.

5. 기대성과 및 활용방안

- 해빈류의 기존 개념을 탈피하여 변동성 이론으로 전환함으로써, 지금까지 오차의 범위가 ±200%인 해빈류 추정에 정확성 기여
- 해안선 변화 및 해저지형 변형 추정의 기본 요소인 퇴적물 이동 추정의 필수요소인 해빈류를 정확히 예측함으로써, 퇴적 침식 현상 규명에 정밀도 향상
- 저층 경계층의 과정이해 및 연안공학적 활용도 증진에 기여

Summary

Data were acquired continuously during the DELILAH experiment with the specific objective of examining variability of the longshore current at tidal frequencies. The hypothesis being that waves inside the barred profile are dependent on the depth of water over the bar where the waves break. Evidence for this was found by Howd et al (1991) in the analysis of the SUPERDUCK data, where they found high correlation of waves inside the bar with the tidal elevation. A strong tidal signature can be seen in the cross-shore array of pressure and current measurements of the DELILAH data. Waves inside the bar have a strong tidal signature, suggesting a nonlinear modulation of wave amplitudes in the surf zone due to the tides. Consequently, the temporal variation of radiation stresses drive the longshore current variability at tidal frequencies. The order of magnitudes of steady longshore current is approximately O(1 m/sec), while that of fluctuating longshore current at tidal frequencies is O(0.3 m/sec). The contribution of tidal currents to the longshore current variability at tidal frequencies seems to be negligible by nearly zero mean value outside the surf zone.

To understand a possible nonlinear process responsible for this variability of longshore current at tidal frequencies, the conservation of momentum equation including time variability is used to solve for the longshore current. Parameterization of energy dissipation due to breaking, response of longshore current to change in the onshore gradient of the a longshore momentum flux is introduced to obtain the solutions at higher order. The variability of longshore current on real topography predicted by using numerical models is compared with the data obtained during the DELILAH experiment.

목 차

제 1 장

ICCE'92 Book of Abstracts 에 게재된 논문

ICCE'92

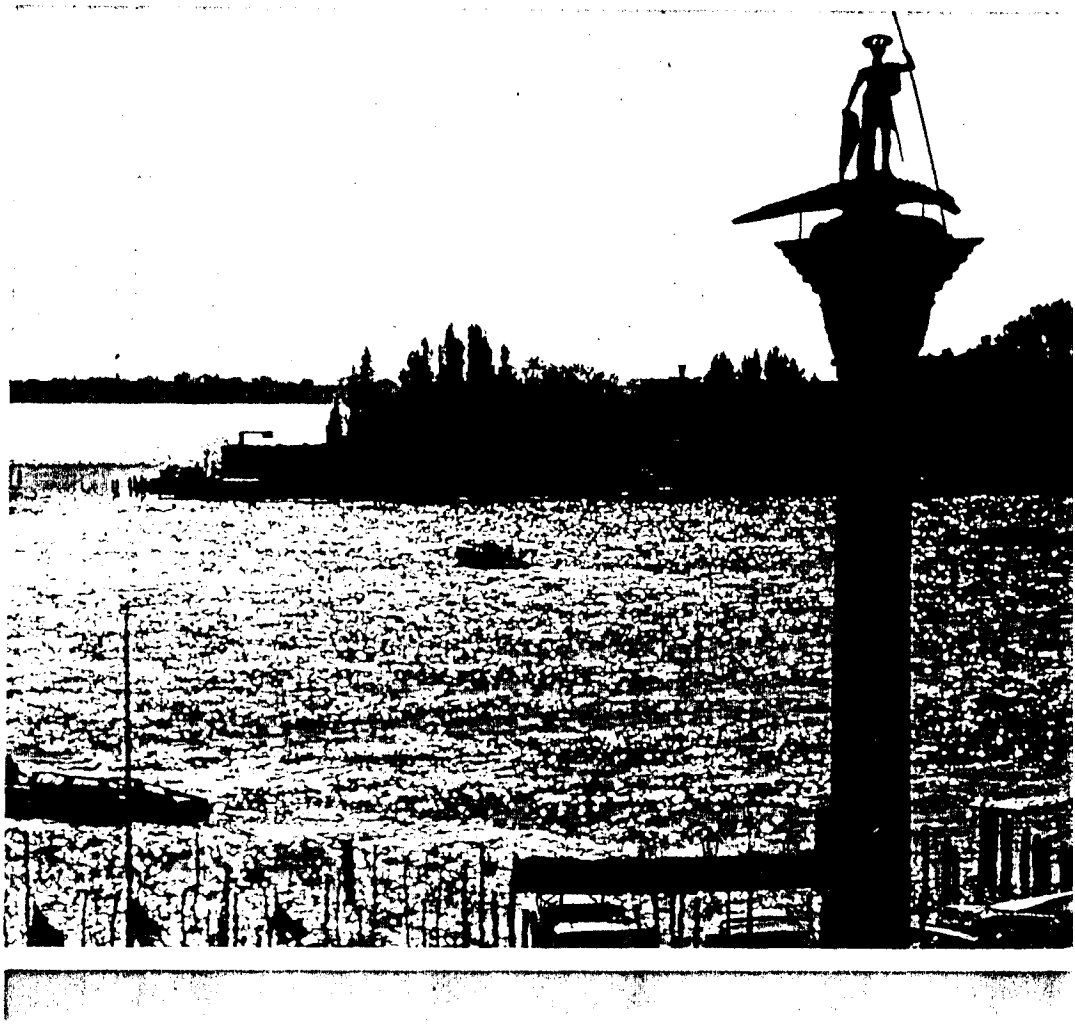

23rd International Conference on Coastal Engineering

4-9 October 1992
Venice, Italy

Book of Abstracts

Time variability of longshore currents

C.S. KIM[1] and E.B. THORNTON[2]
[1] Korea Ocean R&D Institute, Ansan POB 29, Seoul 425-600 Korea
[2] Oceanography Dept. Naval Postgraduate School, Monterey CA, USA 93943

Abstract

The mean momentum balance approach for the longshore current prediction has been widely used for nearshore application. However data acquired during a recent field experiment, DELILAH, show significant variability of wave height and longshore current in the surf zone at tidal frequencies and longer time scales. Extending the works on tidal modulation of longshore currents by Thornton and Kim, 1992 (TK92), and Kim and Thornton, 1992 (KT92), this paper presents a moving boundary approach to model numerically the temporal changes in wave height and longshore current which are perturbed by tides, winds and barometric pressure on different time scales.

Introduction

Data were acquired continuously during the DELILAH experiment with the specific objective of examining variability of the longshore current at tidal frequencies. The hypothesis being that waves inside the barred profile are dependent on the depth of water over the bar where the waves break. Evidence for this was found by Howd *et al.* (1991), and TK92, where they found high correlation of waves insides the bar with the tidal elevation. A strong tidal signature can be seen in the cross-shore array of current measurements (Figure 1). Presumably due to this variability at different time scales, it has not been possible to locate the strongest longshore current in a barred system; sometimes over the bar crest, sometimes in the bar trough (Figure 2).

The subject of the temporal variation of longshore current has been overlooked due to the lack of experimental data, but the subject is of special interest to its potential of correctly estimating sediment transport in the nearshore where tides are present.

Statement of Problem

Up until now, the mean momentum balance equation has been widely used to estimate the mean profile of longshore current. However, there is a significant temporal and spatial variation of wave height and longshore current due to the change in water depth in connection with slowly-varying forcing parameters. Based on the works of TK92, and KT92, the time scales of variation can be grouped into steady state and two slowly-varying time scales. A conceptual model for tidal modulation on near planar beach (TK92) and perturbation solution for two time scales (KT92) could not incorporate the multiple forcings by tides, unsteady winds and barometric pressure, etc.

To understand a possible nonlinear process responsible for this variability of longshore current at multi-frequencies, the conservation of momentum equation including time variability is used to solve for longshore current, and the energy equation for wave height.

Solution Technique

The equation governing the growth of wave energy E is

$$1) \qquad \frac{\partial E}{\partial t} + \frac{\partial}{\partial x}(EC_g) + S_{xy}\frac{\partial V}{\partial x} = \langle \epsilon \rangle$$

where Sxy is the radiation stress of onshore flux of y-momentum (alongshore), V is the longshore current, and $\langle \varepsilon \rangle$ is the energy dissipation due to the random wave breaking as suggested by Thornton and Guza (1986).

The time-dependent longshore current V is expressed as

$$2) \qquad \frac{\partial}{\partial t}(\rho V(h+\overline{\zeta})) + \frac{\partial}{\partial x}S_{xy} = -\tau_y{}^B + \tau_y{}^S$$

where $\overline{\zeta}$ is mean set-up, h is the slowly varying mean water depth, $\tau_y{}^B$ is the bottom friction and $\tau_y{}^S$ is the alongshore component of wind stress. Slowly-varying forcing terms are parameterized based on the field observation data.

A finite difference scheme used to solve the time-dependent momentum and energy equations is adapted to include the moving boundary at the shoreline to account for the slowly varying sea surface. The shoreline is allowed to move with unsteady water

depth, and the moving boundary is treated on a moving grid system.

Trial results are presented, which indicate substantial promise for the prediction of longshore current and associated sediment transport rate in the nearshore.

References

Howd, P.A., J. Oltman-Shay, and R.A. Holman. 1991. Wave variance partitioning in the trough of a barred beach. *J. Geophys. Res.* 96,12781-12795.

Kim, C.S. and E.B. Thornton. 1992. Tidal modulation of longshore current. II, Model. (In preparation).

Thornton, E.B. and R.T. Guza. 1986. Surf zone longshore currents and random waves: Field data and models. *J. Geophys. Res.* 16, 1165-1178.

Thornton, E.B. and C.S. Kim. 1992. Tidal modulation of longshore current. I. Field Observation. (Submitted to J. Geophys. Res.).

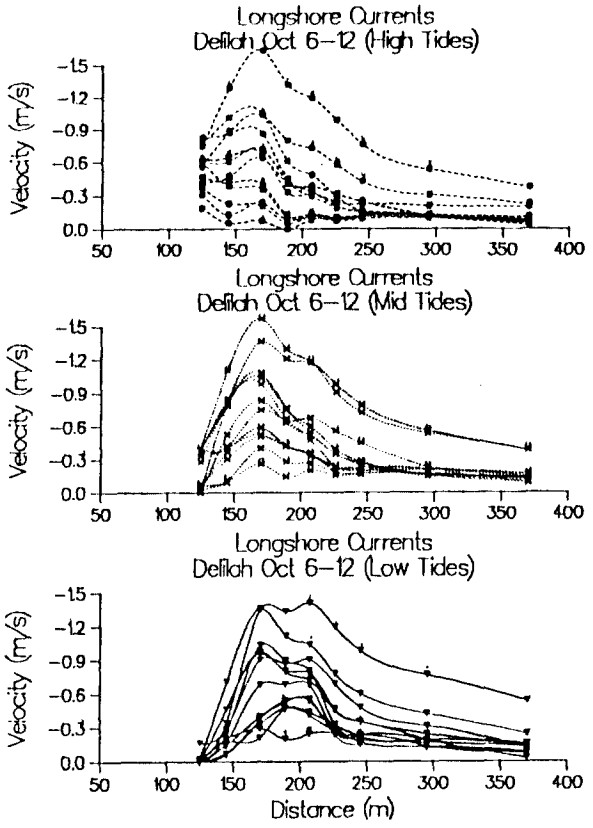

Fig. 2. Longshore currents grouped at different tidal cycles. Locations of the strongest current varied during the experiment.

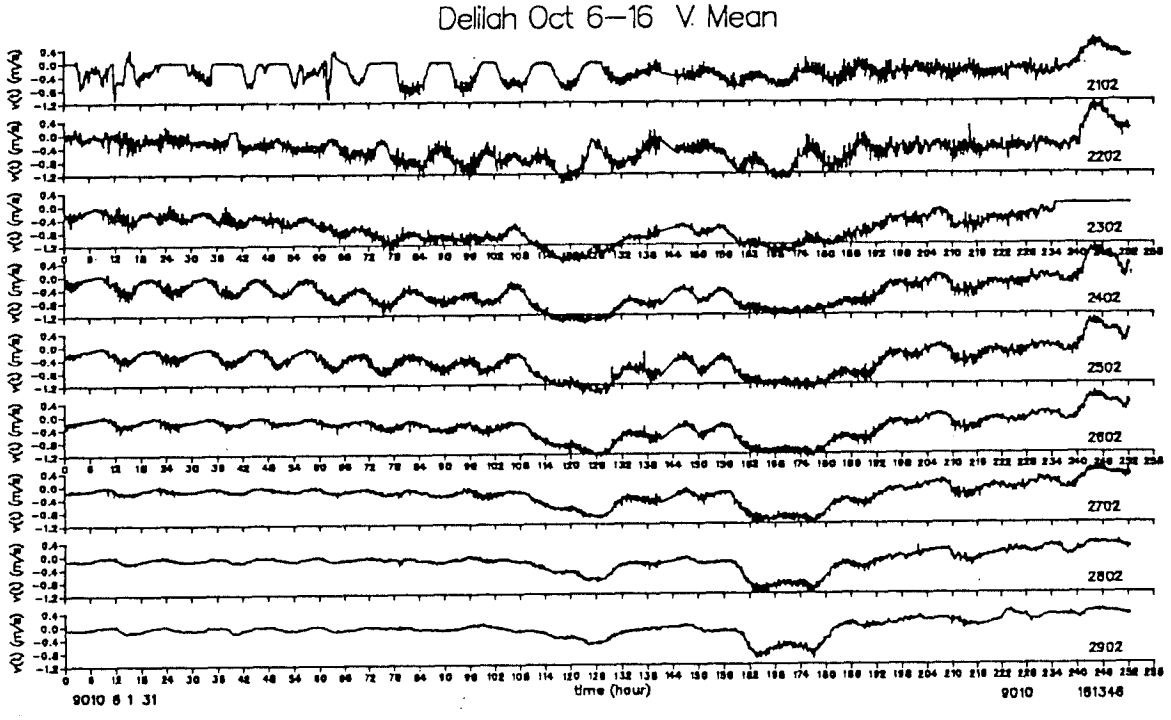

Fig. 1 Longshore velocity observations (5 min means) starting at offshore (bottom panel 2902), across the bar (panels 2702-2402), the trough (2302-2202), to the foreshore (top panel), during the DELILAH experiment from 2 to 16 October 1990, showing significant tidal signature in the surf zone.

제 2 장

ICCE '92에 발표된 내용

Time Variability of Longshore Currents Due to Tides

Chang S. Kim* and Edward B. Thornton

Oceanography Department
Naval Postgraduate School
Monterey CA USA

* Present Address
Korea Ocean R & D Institute
Seoul Korea

1. Introduction

- Motivation
- Goals
- Importance

2. Experiment (DELILAH)

- Experiment overview
- Sample observations
- Data Preparations

3. Simulation of longshore current variability due to tide

- Conceptual model
- Comparison with observation

4. Conclusion

5. On-going works

- Perturbation method (two time expansion)
- Numerical modelling (Moving boundary)

MOTIVATION

o During DELILAH Experiment, spatial and temporal variations of longshore currents at tidal frequency in the surf zone were observed.

GOALS

o To understand the underlying processes of Longshore current modulation.

o To predict the variability associated with tides, winds, atmospheric pressure and other forcings.

IMPORTANCE

Variability itself has an O(1) influence on the sediment transport.

DELILAH Experiment

o SPECIFIC OBJECTIVE

- Examining variability of longshore currents at tidal frequencies

o FRF at DUCK, North Carolina

o waves and currents continuously for 3 weeks from Oct. 2–Oct. 21, 1990.

o Beach profiles, winds, tide, atmospheric pressure

o fair to storm weathers

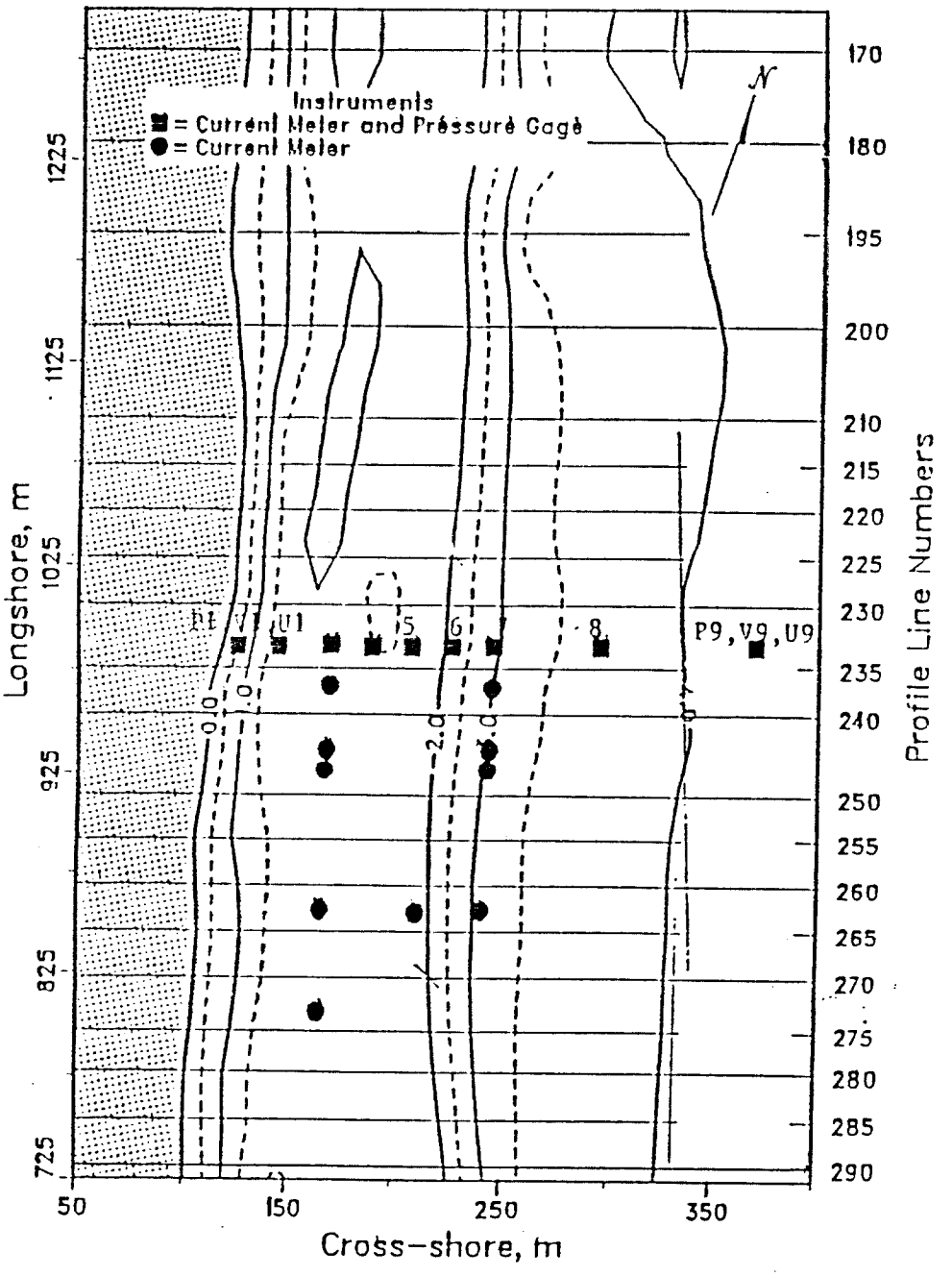

DELILAH Mini-Grid 11 OCT 90

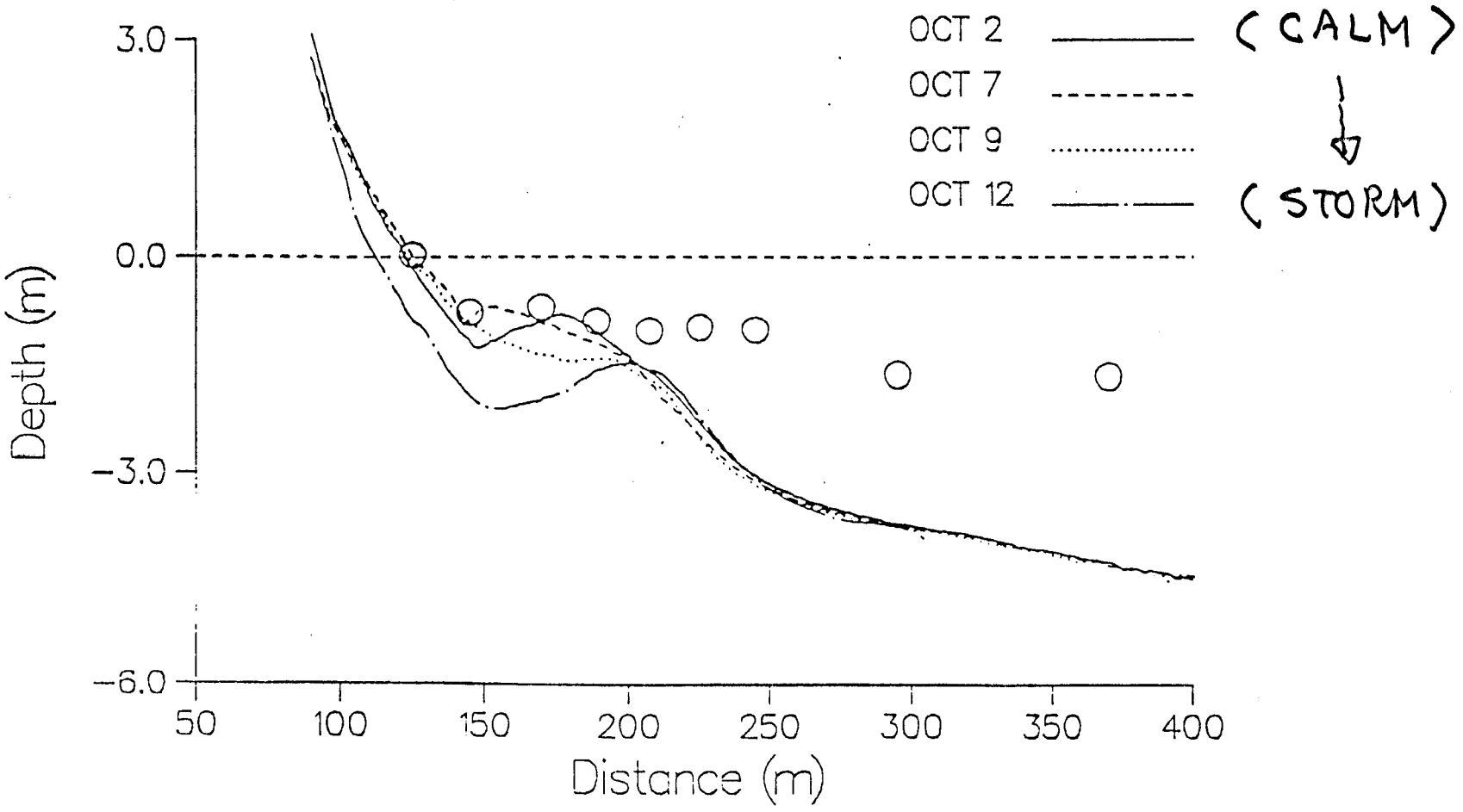
OCT 2
OCT 7
OCT 9
OCT 12
(CALM)
(STORM)
3.0
0.0
-3.0
-6.0
Depth (m)
50
100
150
200
250
300
350
400
Distance (m)

1 OCT 90

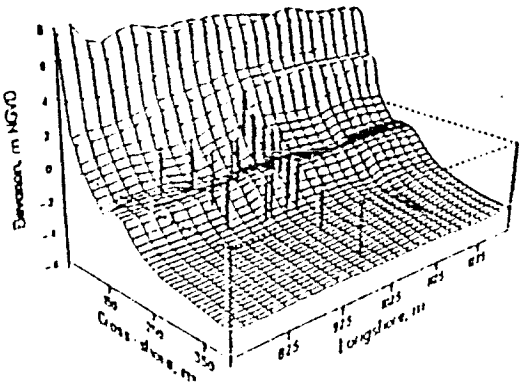

9 OCT 90

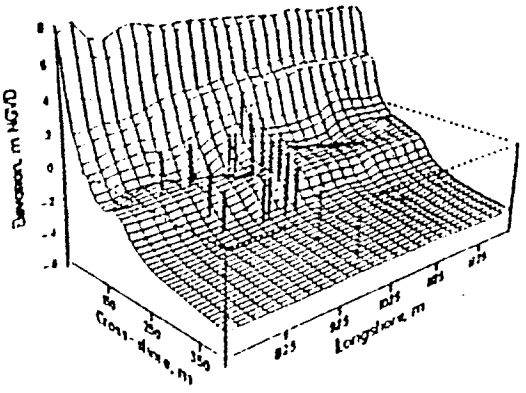

11 OCT 90

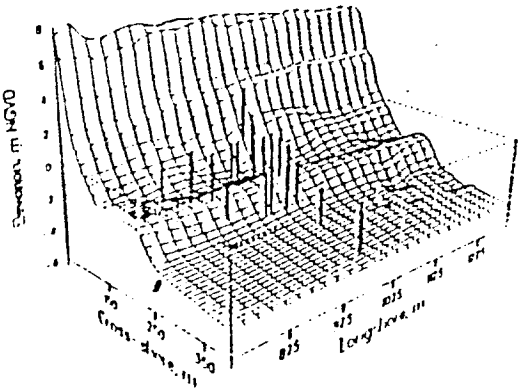

19 OCT 90

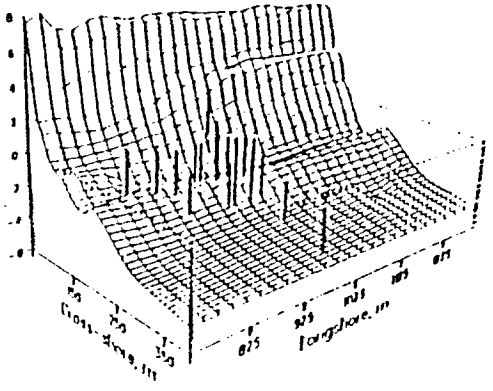

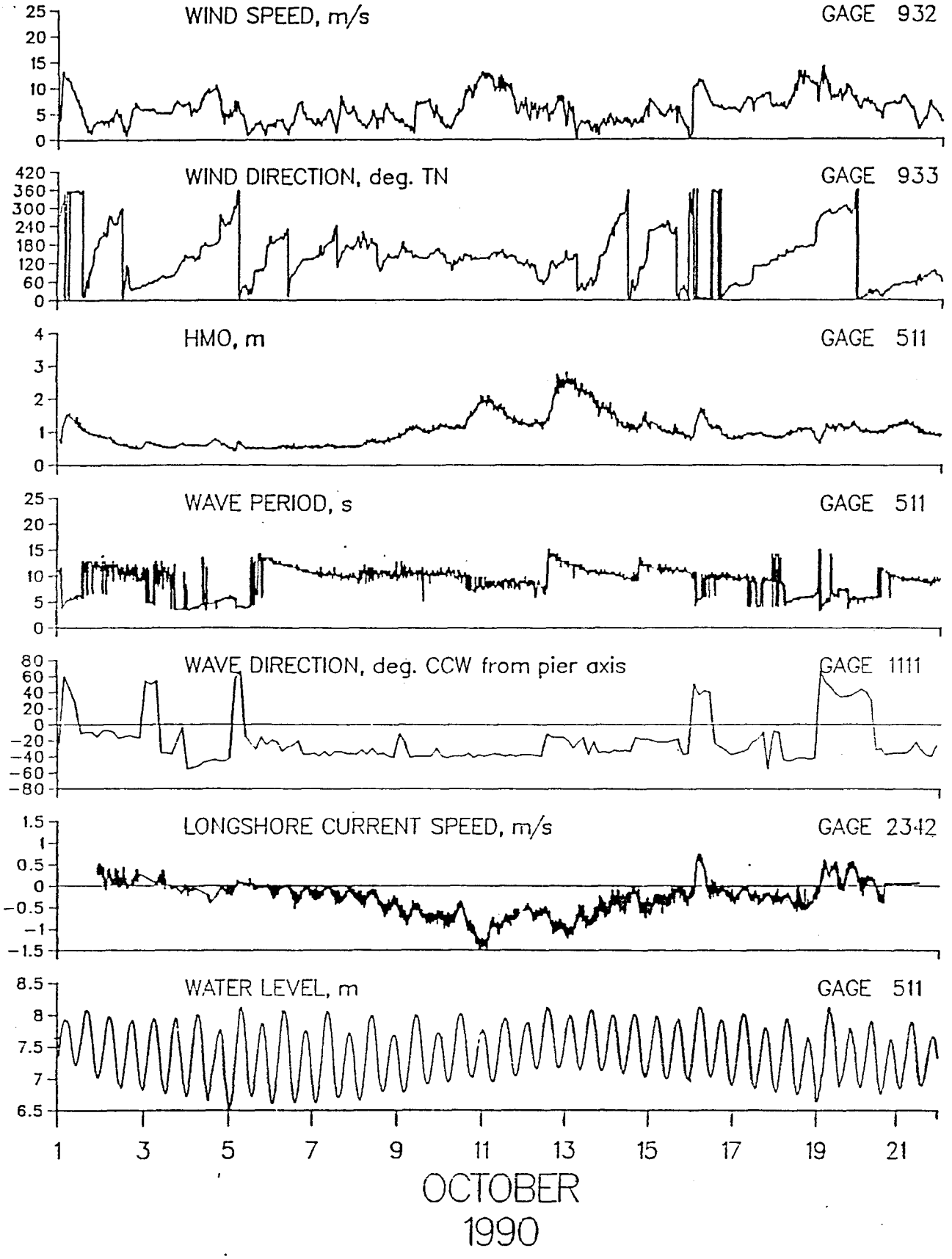
WIND SPEED, m/s
GAGE 932
25
20
15
10
5
0
WIND DIRECTION, deg. TN
GAGE 933
420
360
300
240
180
120
60
0
HMO, m
GAGE 511
4
3
2
1
0
WAVE PERIOD, s
GAGE 511
25
20
15
10
5
0
WAVE DIRECTION, deg. CCW from pier axis
GAGE 1111
80
60
40
20
0
-20
-40
-60
-80
LONGSHORE CURRENT SPEED, m/s
GAGE 2342
1.5
1
0.5
0
-0.5
-1
-1.5
WATER LEVEL, m
GAGE 511
8.5
8
7.5
7
6.5
1
3
5
7
9
11
13
15
17
19
21
OCTOBER
1990

Data Preparation

- o Most sensors at 8Hz
- o Cross-shore array of P, U, V
  (9 sensors)
- o 5-min mean for Oct. 6-16, 1990
- o Hrms and V
- o Tide

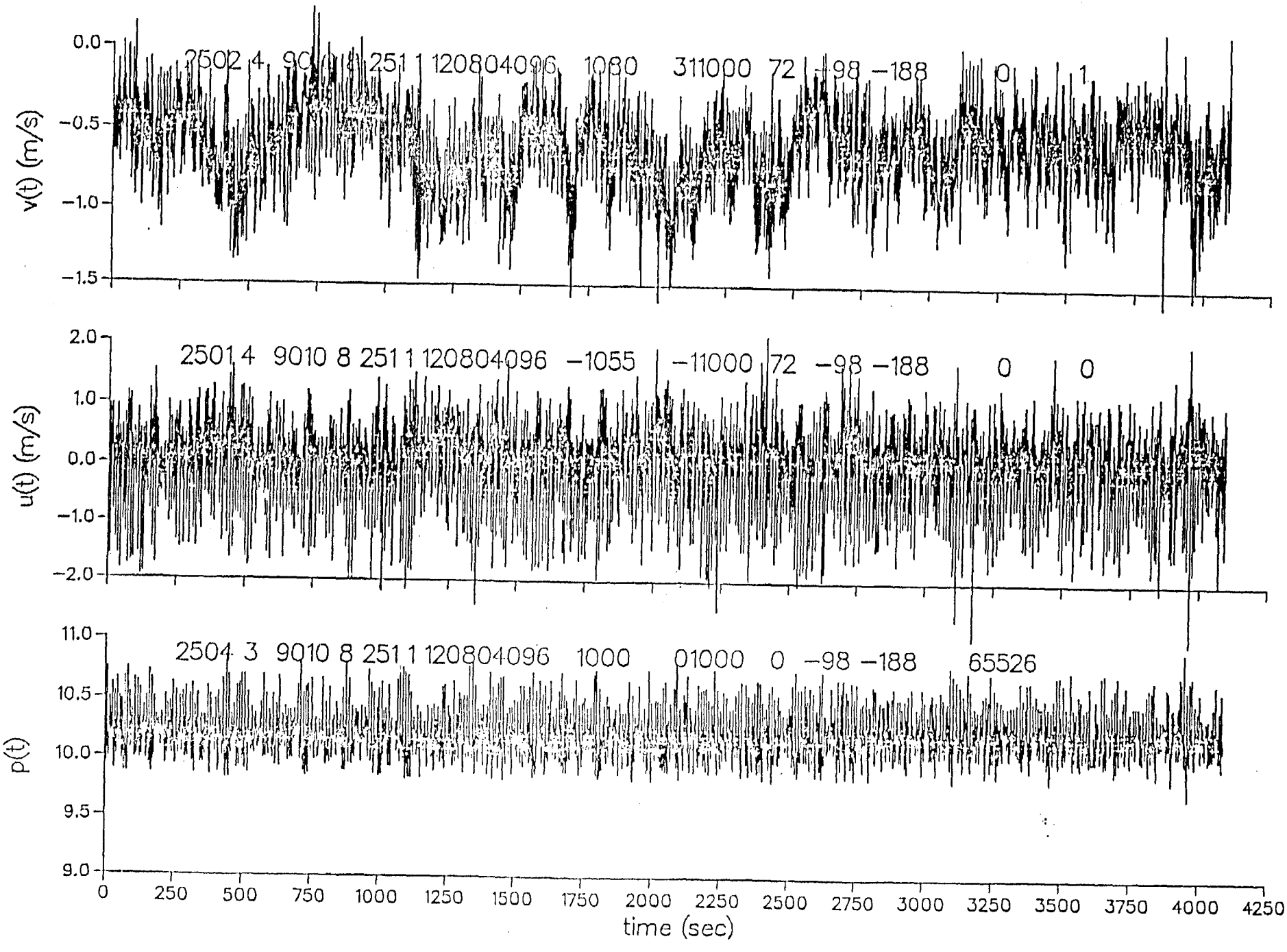
v(t) (m/s)
0.0
−0.5
−1.0
−1.5
2502 4 90 8 251 1 120804096 1080 311000 72 −98 −188 0 1
u(t) (m/s)
2.0
1.0
0.0
−1.0
−2.0
2501 4 9010 8 251 1 120804096 −1055 −11000 72 −98 −188 0 0
p(t)
11.0
10.5
10.0
9.5
9.0
2504 3 9010 8 251 1 120804096 1000 01000 0 −98 −188 65526
0 250 500 750 1000 1250 1500 1750 2000 2250 2500 2750 3000 3250 3500 3750 4000 4250
time (sec)

Delilah Oct 6–16 V Mean

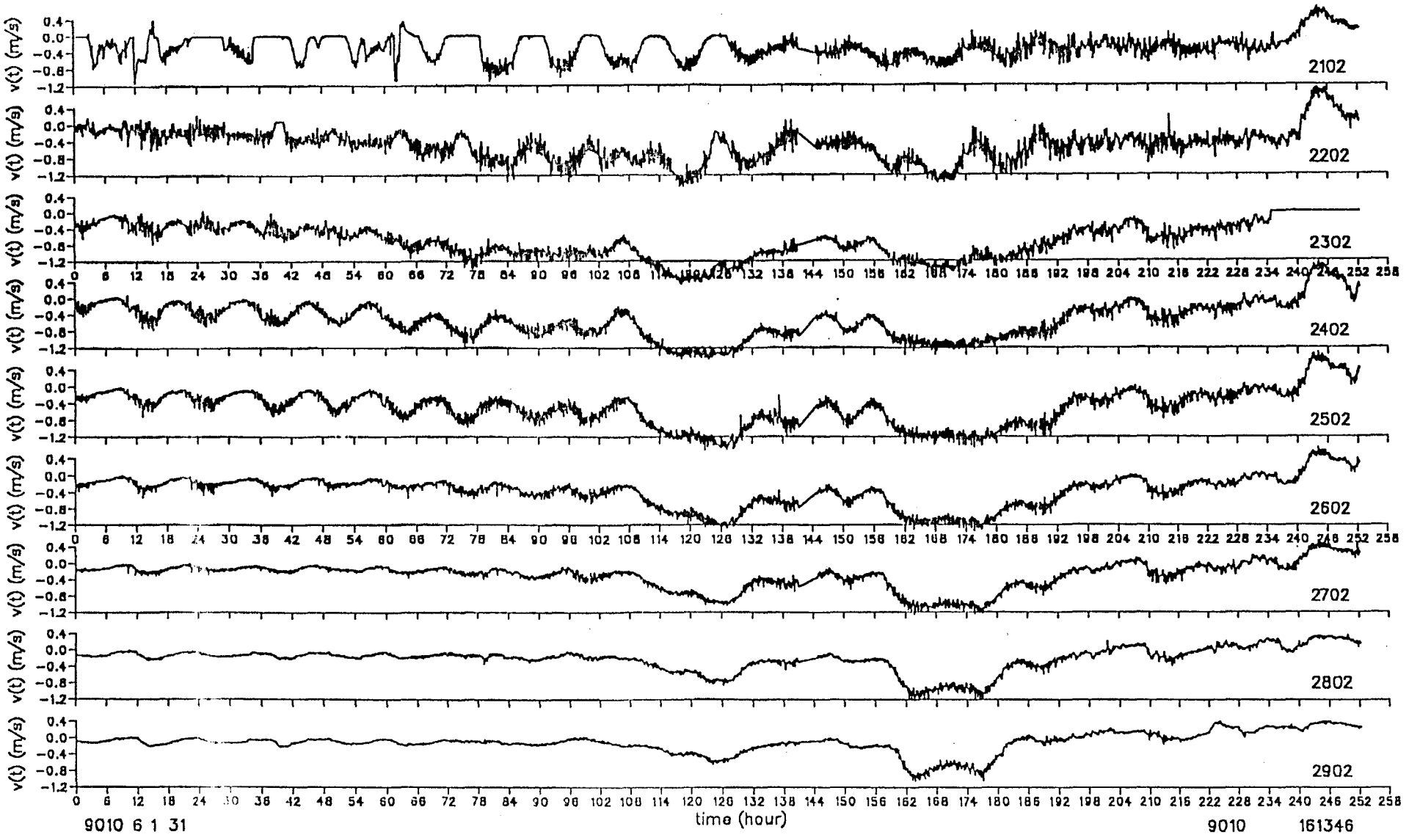

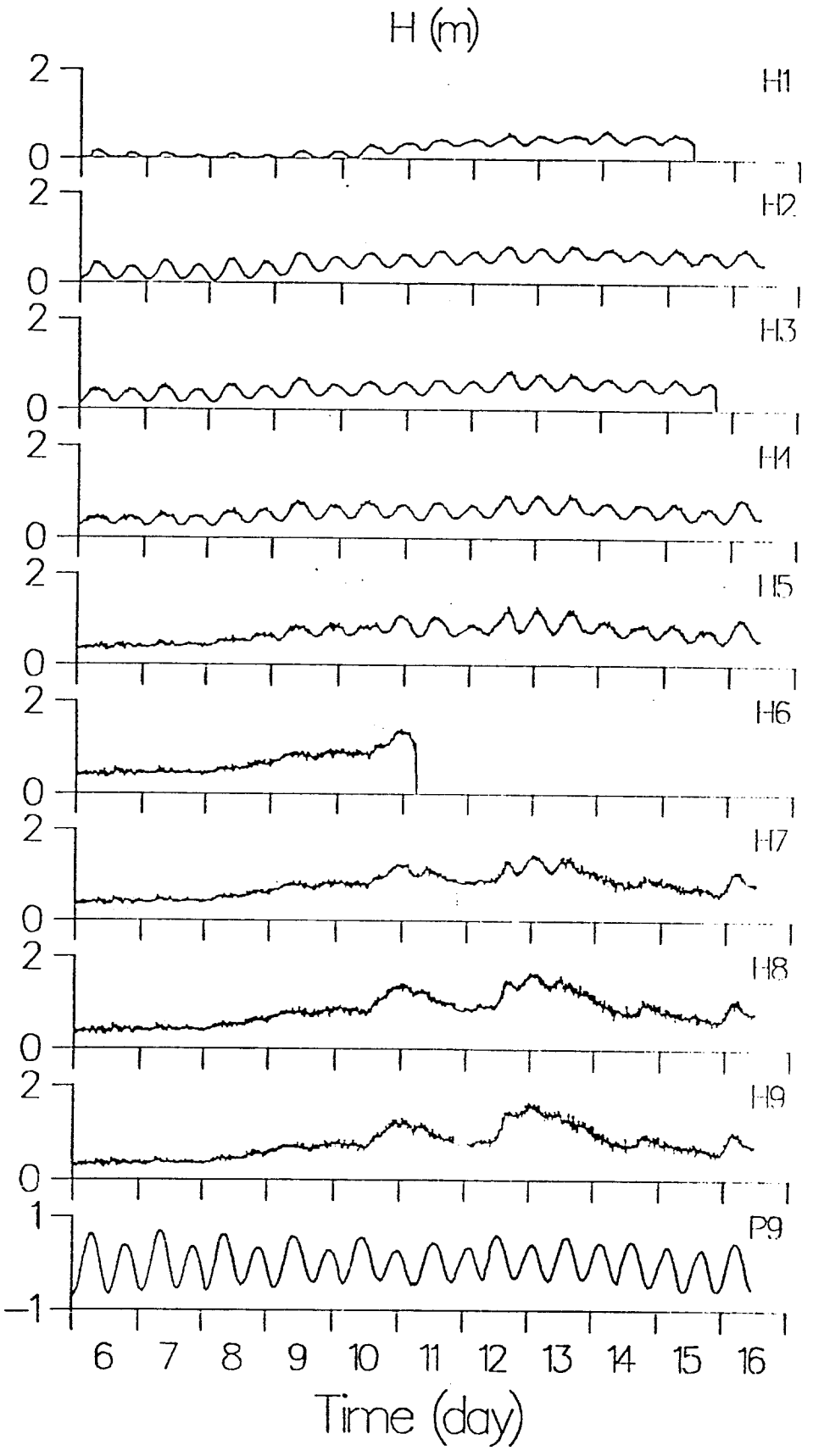
H (m)
H1
H2
H3
H4
H5
H6
H7
H8
H9
P9
2
0
1
-1
6
7
8
9
10
11
12
13
14
15
16
Time (day)

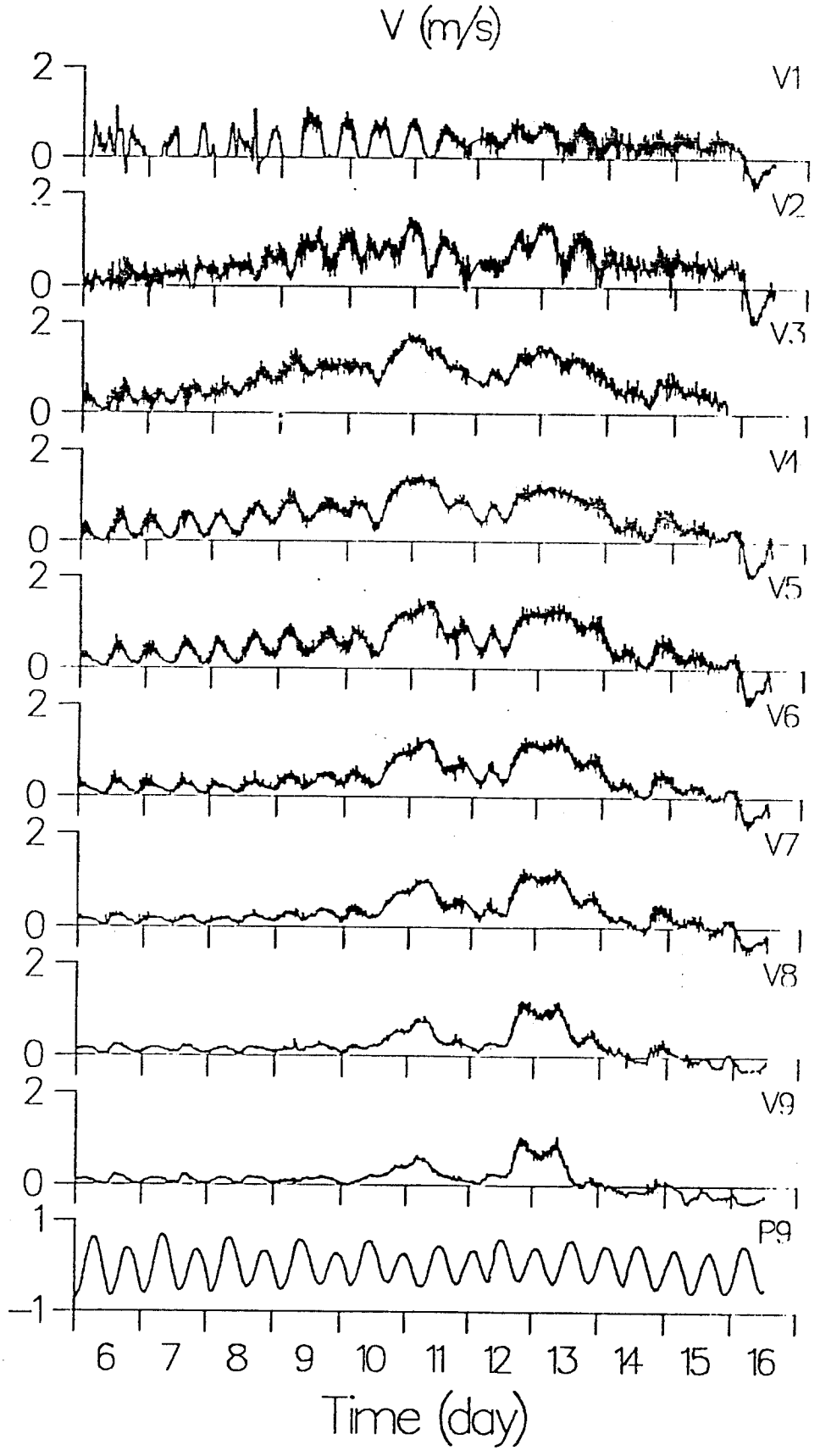
V (m/s)
2
0
V1
2
0
V2
2
0
V3
2
0
V4
2
0
V5
2
0
V6
2
0
V7
2
0
V8
2
0
V9
1
-1
P9
6
7
8
9
10
11
12
13
14
15
16
Time (day)

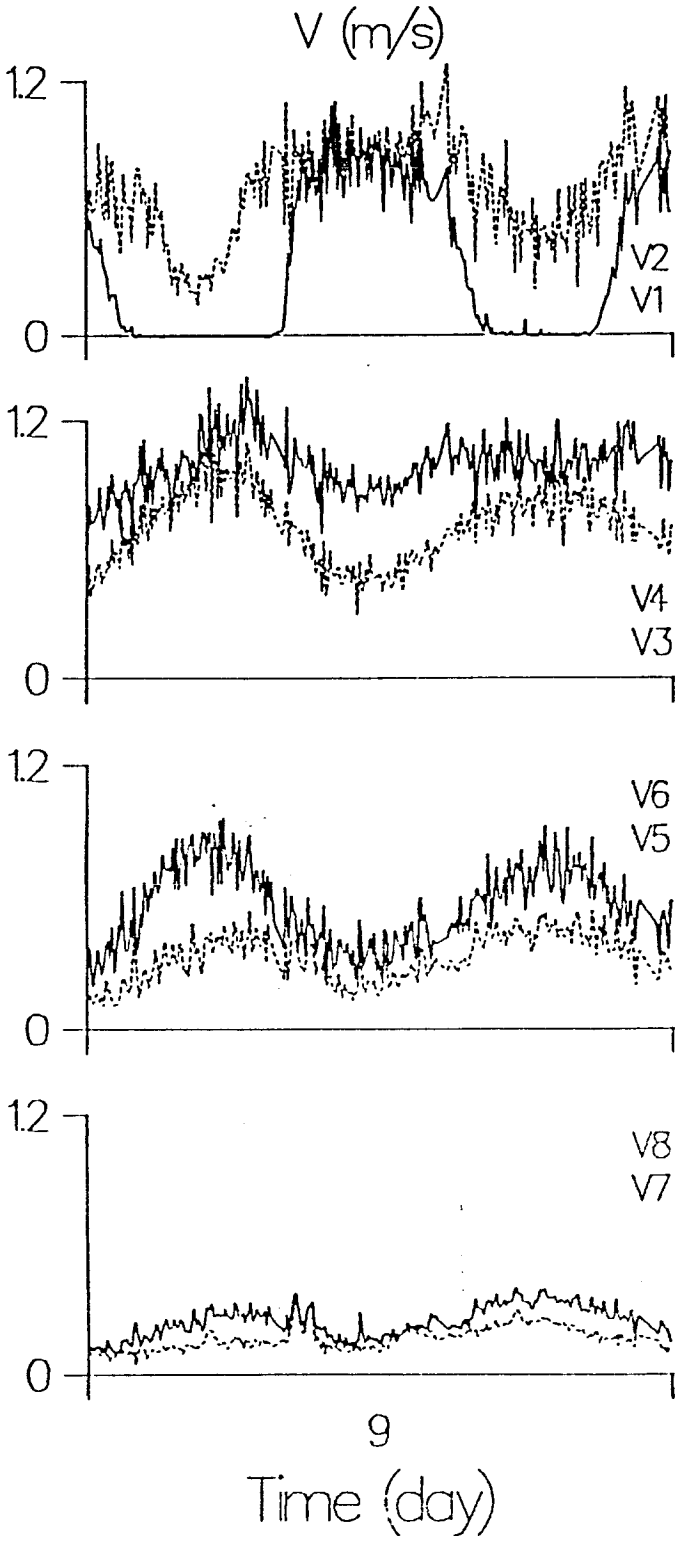
V (m/s)
1.2
0
V2
V1
1.2
0
V4
V3
1.2
0
V6
V5
1.2
0
V8
V7
9
Time (day)

Simulation of longshore current variability

o Adapts the model of Thornton and Guza (1986)

– wave height transformation

$$\frac{dEC_g \cos\alpha}{dx} = <\varepsilon_b>$$

$$E = \frac{1}{8}\rho g H_{rms}^2$$

$$<\varepsilon_b> = \frac{3}{16}\sqrt{\pi}\rho g \frac{B^3}{\gamma^4 h^5} f_p H_{rms}^2$$

– Longshore Currents

$$\frac{\partial S_{yx}}{\partial x} = -\tau_y^b$$

$$\frac{\sin\alpha_o}{C_o} <\varepsilon_b> = -\frac{d}{dx} S_{yx}' - \rho C_f \overline{|\tilde{u}| V}$$

Governing Equations

$$\frac{\partial}{\partial t}(h+\overline{\zeta})+\frac{\partial}{\partial x_i}\{U_i(h+\overline{\zeta})\}=0$$

$$\frac{\partial}{\partial t}(\rho U(h+\overline{\zeta}))+\frac{\partial}{\partial x}\{(\rho UU(h+\overline{\zeta}))+S_{xx}\}$$

$$=-\rho g(h+\overline{\zeta})\frac{\partial \overline{\zeta}}{\partial x}-\tau_x^b+\tau_x^s$$

$$\frac{\partial}{\partial t}(\rho V(h+\overline{\zeta}))+\frac{\partial}{\partial x}\{\rho UV(h+\overline{\zeta})+S_{xy}\}$$

$$=-\rho g(h+\overline{\zeta})\frac{\partial \overline{\zeta}}{\partial y}-\tau_y^b+\tau_y^s$$

$$\frac{\partial E}{\partial t}+\nabla\cdot\{E(C_g+U)\}+S_{xy}\frac{\partial V}{\partial x}+\nabla\cdot\left(\frac{1}{2}\rho hU'^3\right)$$

$$=0 \qquad , \quad x \gg x_b$$

$$=<\varepsilon> \qquad , \quad x < x_b$$

where $U' = U+\dfrac{E}{\rho Ch}$

stream velocity modified
by mass transport

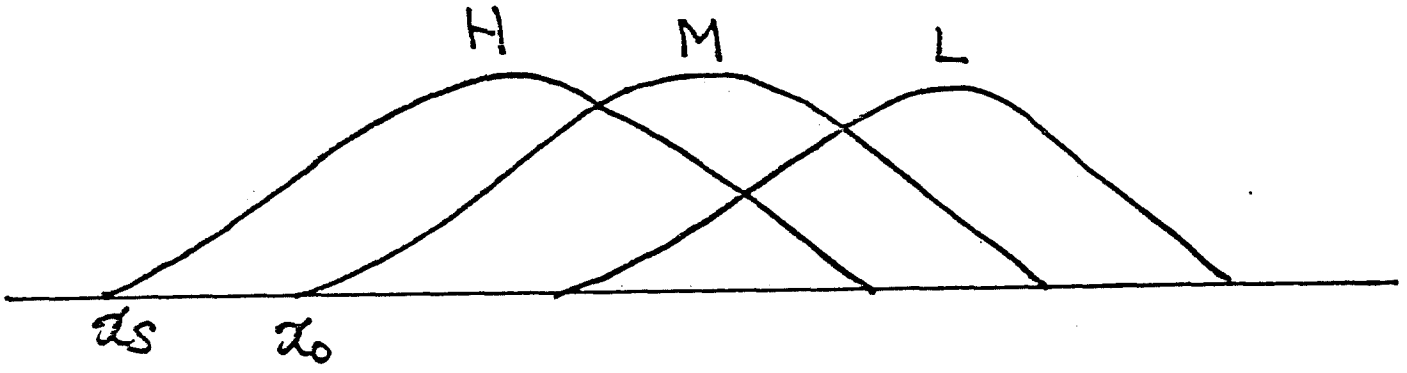

o tide : $\zeta = \zeta_T \sin \sigma t$

o shoreline : $x_s = -\dfrac{\zeta_T}{\tan \beta} \sin \sigma t$

o at t, $x = x_o - x_s$

$V(x, t) = V_o(x_o - x_s)$

$$= \int \frac{dV(x, t)}{dx} \frac{dx}{dt} dt$$

$$= \frac{dV(x_o)}{dx} \frac{\zeta_T}{\tan \beta} \sin \sigma t$$

$\therefore$ V is in-phase where $\dfrac{dV}{dx} > 0$

V is out-of-phase where $\dfrac{dV}{dx} < 0$

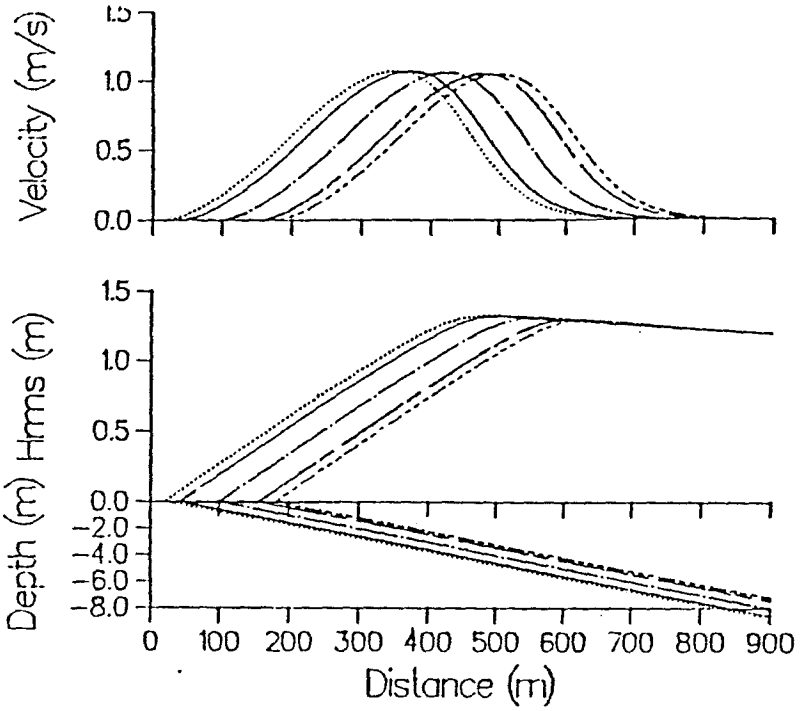
Velocity (m/s)
1.5
1.0
0.5
0.0
Depth (m) Hrms (m)
1.5
1.0
0.5
0.0
-2.0
-4.0
-6.0
-8.0
0
100
200
300
400
500
600
700
800
900
Distance (m)

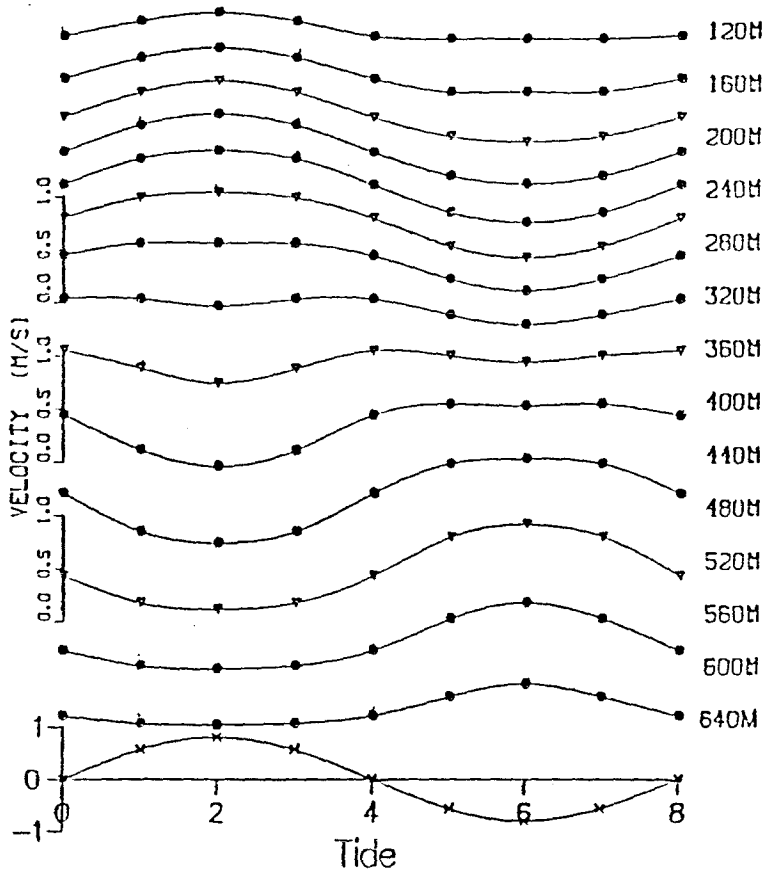
120M
160M
200M
240M
280M
320M
360M
400M
440M
480M
520M
560M
600M
640M
VELOCITY (M/S)
0.0 0.5 1.0
0.0 0.5 1.0
0.0 0.5 1.0
1
0
-1
0
2
4
6
8
Tide

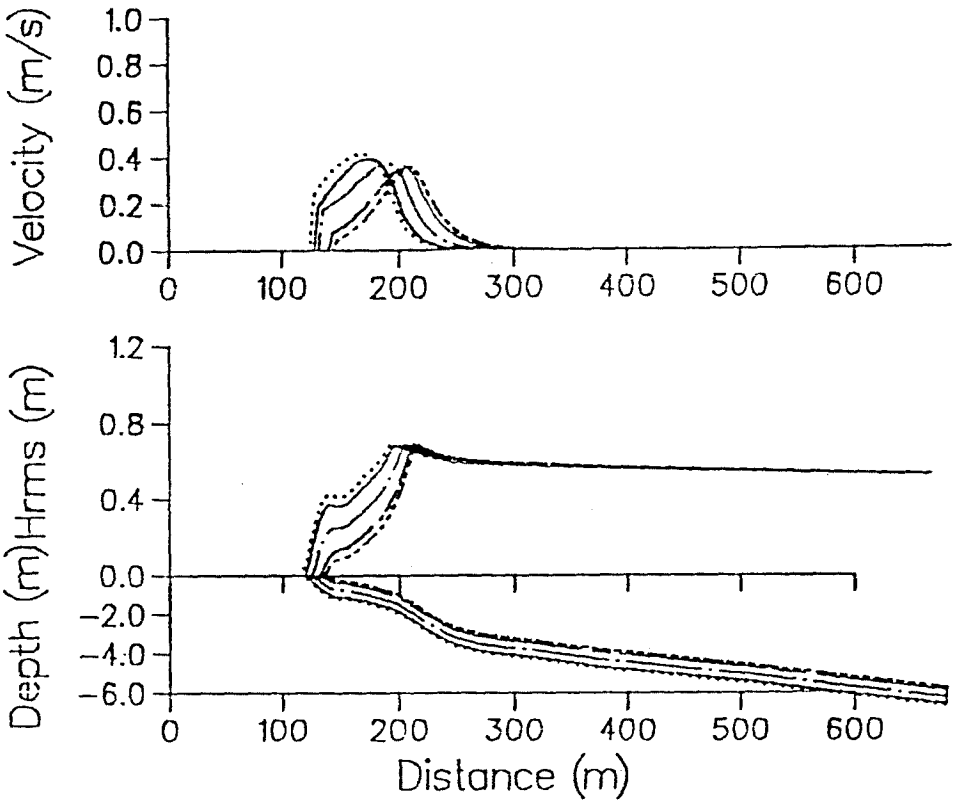
Velocity (m/s)
1.0
0.8
0.6
0.4
0.2
0.0
0
100
200
300
400
500
600
Depth (m)Hrms (m)
1.2
0.8
0.4
0.0
−2.0
−4.0
−6.0
0
100
200
300
400
500
600
Distance (m)

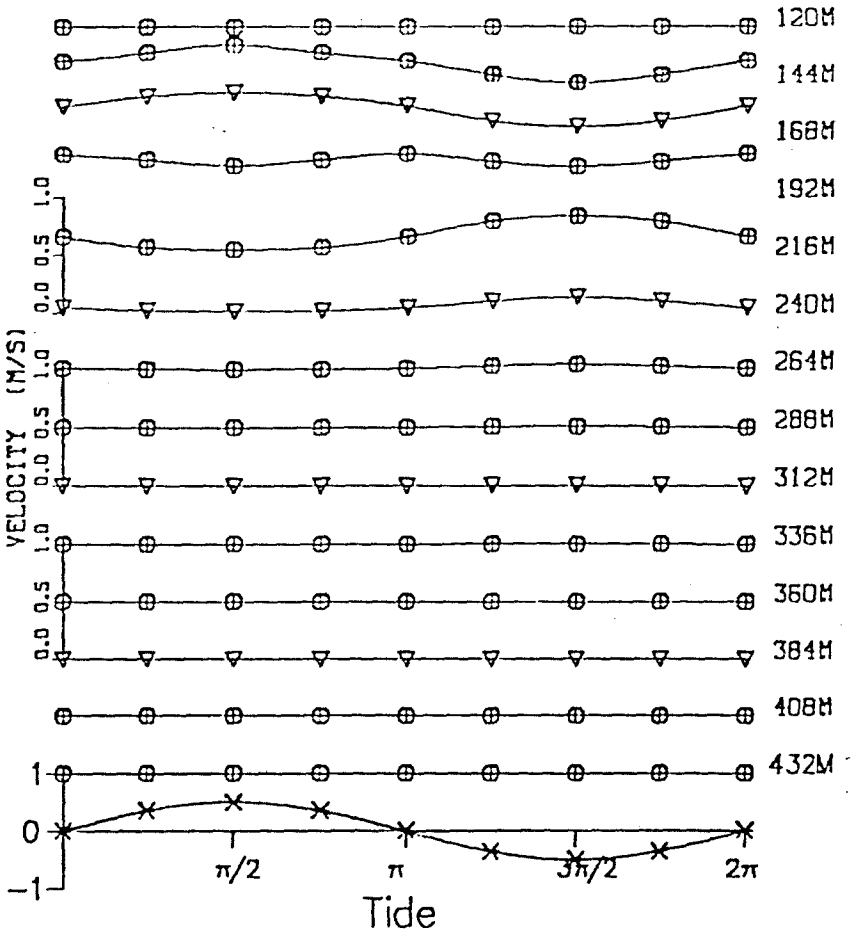
120M
144M
168M
192M
216M
240M
264M
288M
312M
336M
360M
384M
408M
432M
VELOCITY (M/S)
1.0
0.5
0.0
1
0
−1
π/2
π
3π/2
2π
Tide

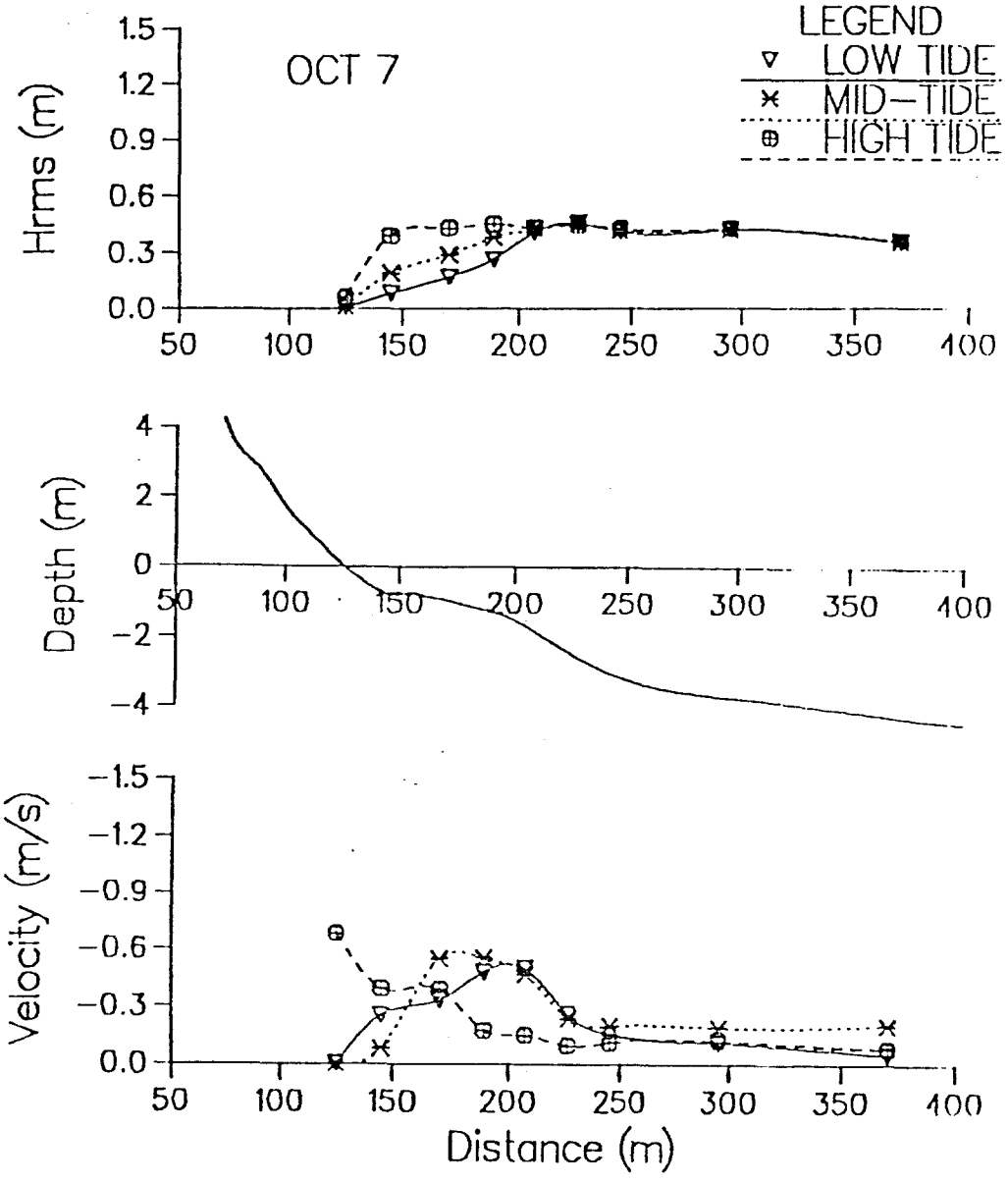
OCT 7
LEGEND
LOW TIDE
MID-TIDE
HIGH TIDE
Hrms (m)
1.5
1.2
0.9
0.6
0.3
0.0
50
100
150
200
250
300
350
400
Depth (m)
4
2
0
-2
-4
Velocity (m/s)
-1.5
-1.2
-0.9
-0.6
-0.3
0.0
Distance (m)

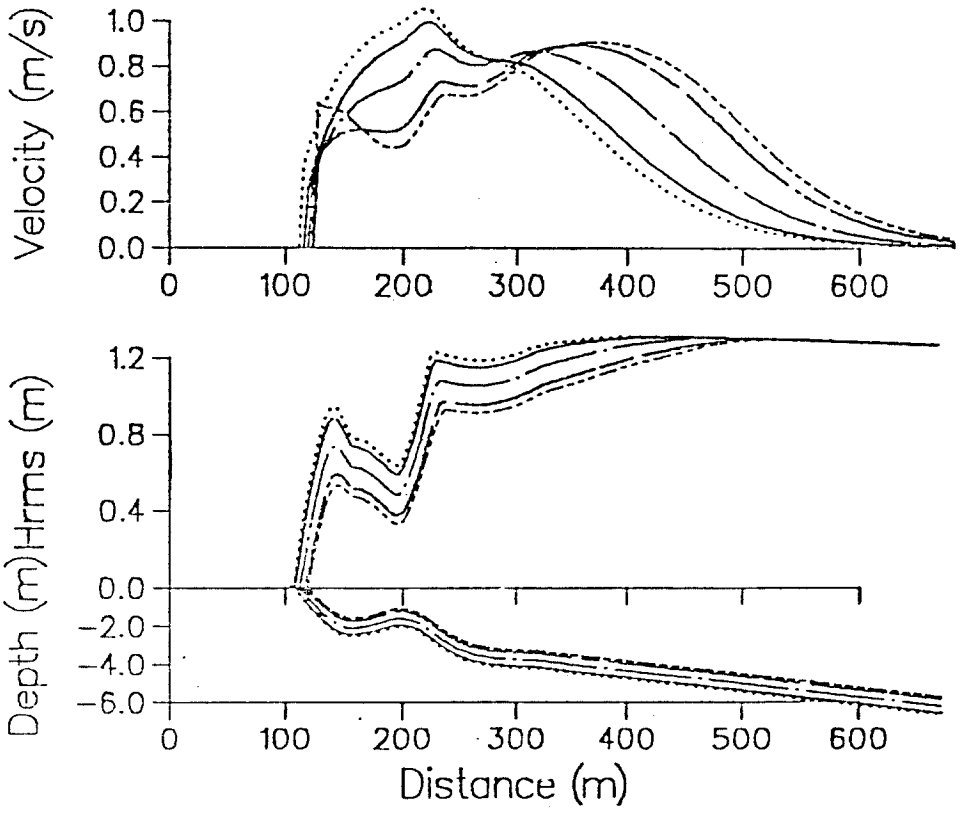
Velocity (m/s)
1.0
0.8
0.6
0.4
0.2
0.0
0
100
200
300
400
500
600
Depth (m)Hrms (m)
1.2
0.8
0.4
0.0
-2.0
-4.0
-6.0
Distance (m)

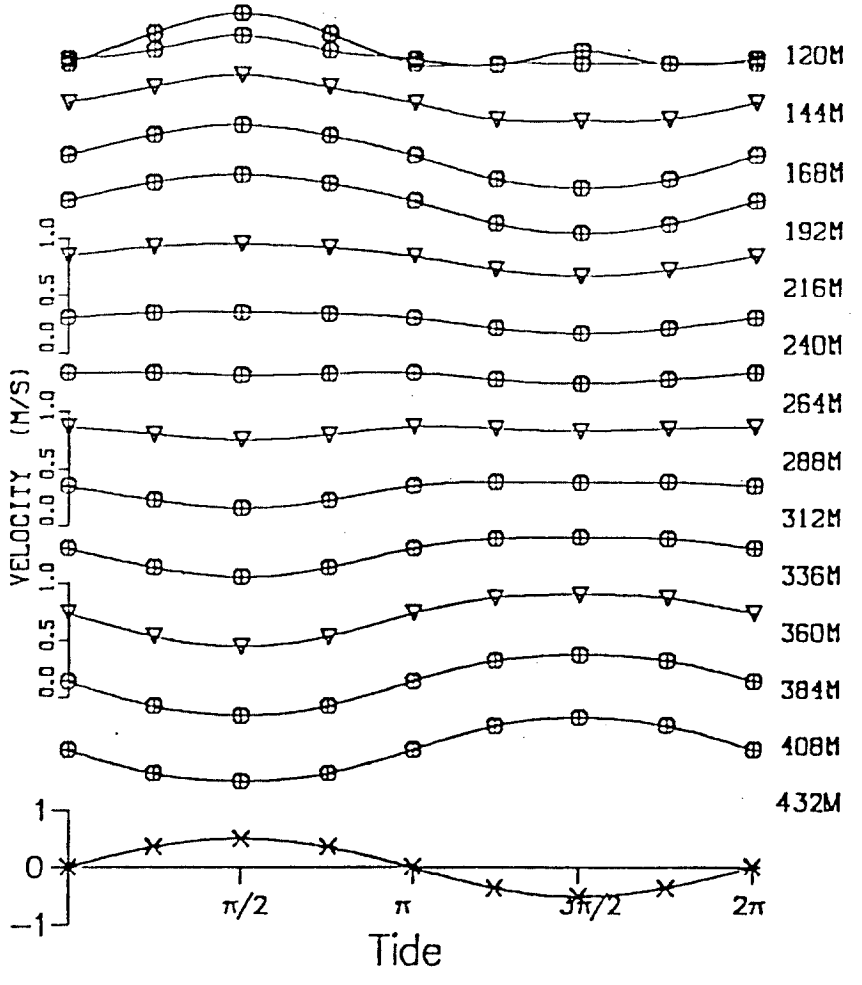
120M
144M
168M
192M
216M
240M
264M
288M
312M
336M
360M
384M
408M
432M
VELOCITY (M/S)
1.0
0.5
0.0
1
0
-1
π/2
π
3π/2
2π
Tide

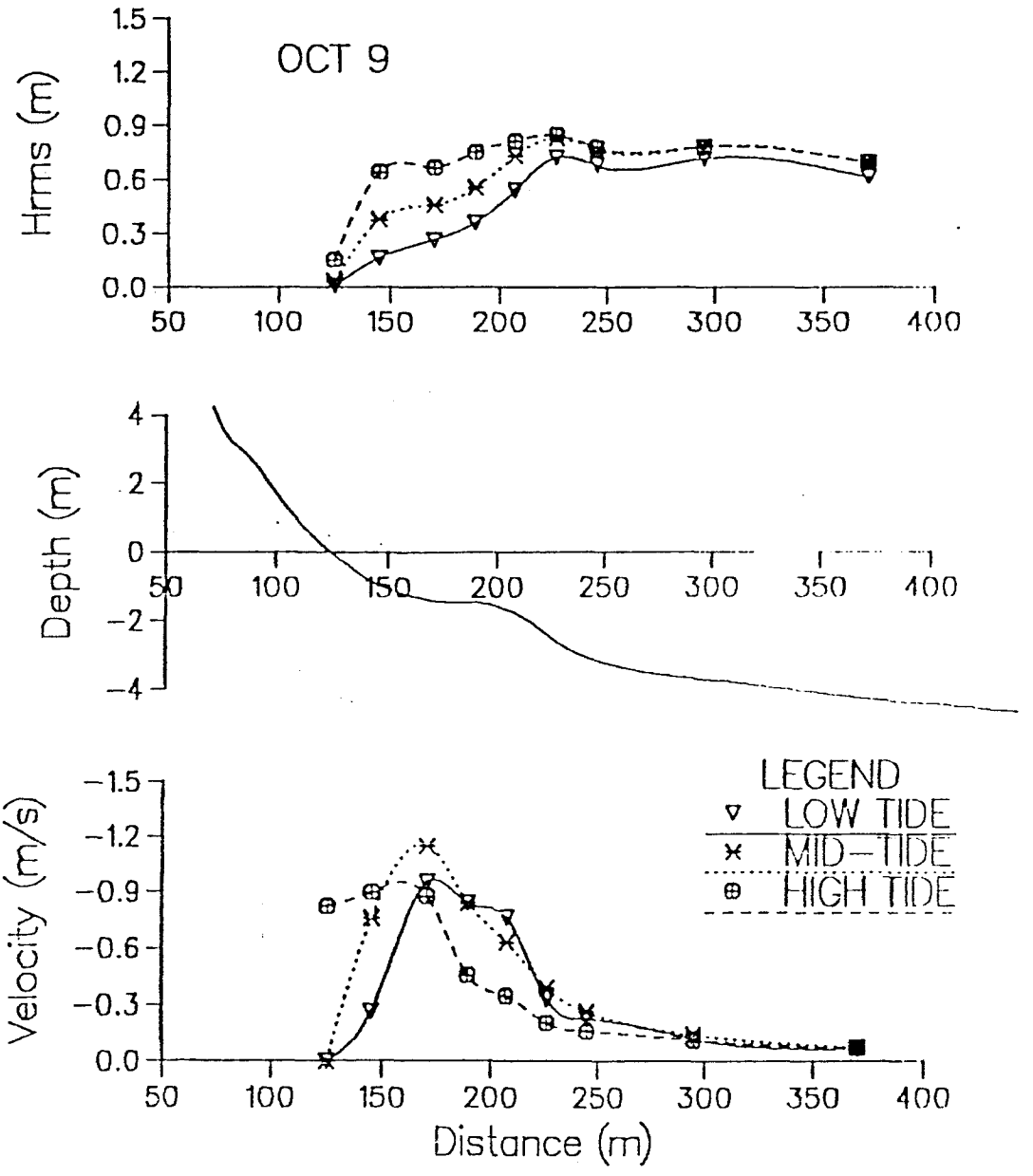
OCT 9
Hrms (m)
1.5
1.2
0.9
0.6
0.3
0.0
50
100
150
200
250
300
350
400
Depth (m)
4
2
0
−2
−4
Velocity (m/s)
−1.5
−1.2
−0.9
−0.6
−0.3
0.0
LEGEND
LOW TIDE
MID−TIDE
HIGH TIDE
Distance (m)

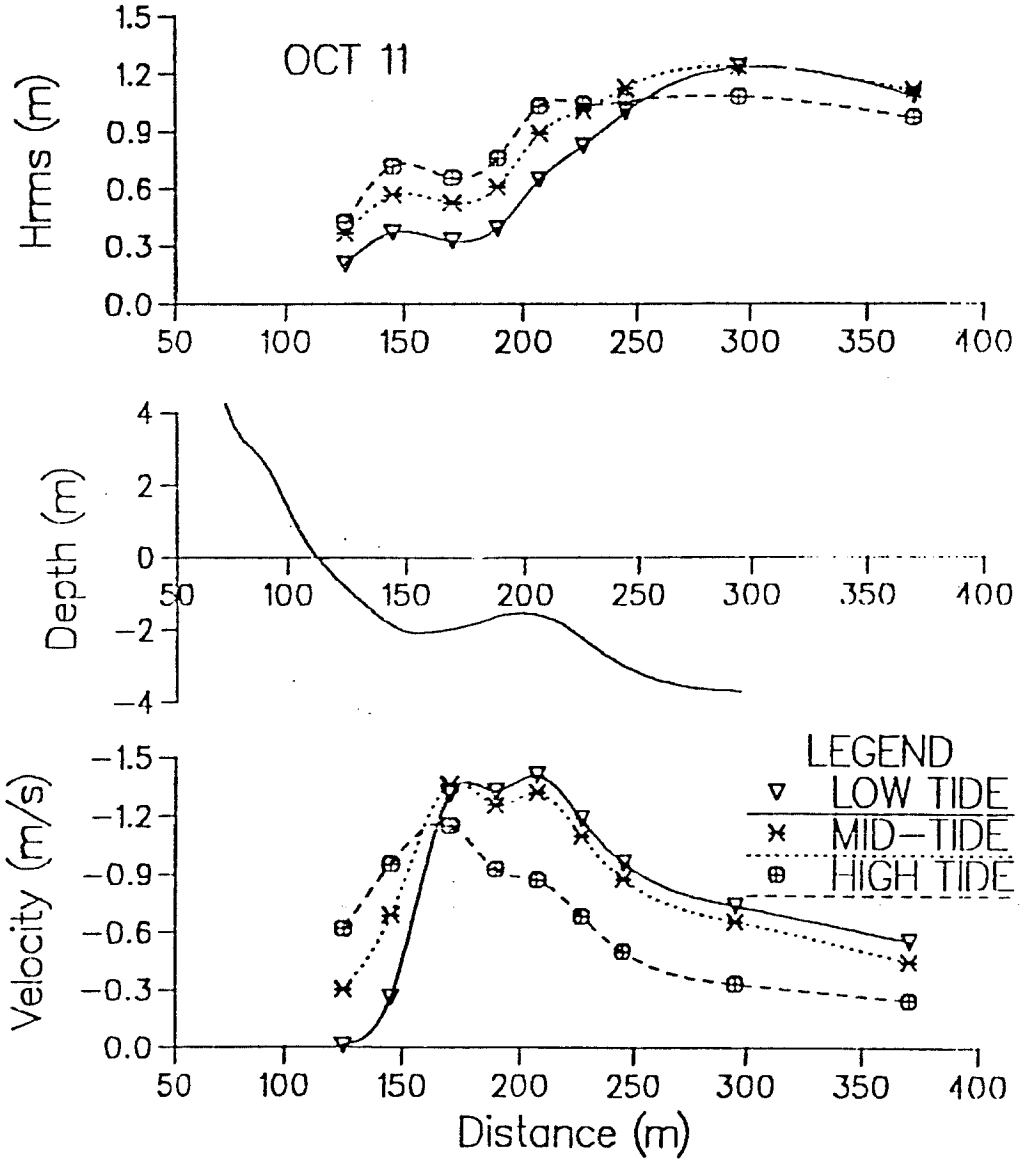
OCT 11
Hrms (m)
1.5
1.2
0.9
0.6
0.3
0.0
50
100
150
200
250
300
350
400
Depth (m)
4
2
0
−2
−4
Velocity (m/s)
−1.5
−1.2
−0.9
−0.6
−0.3
0.0
LEGEND
LOW TIDE
MID−TIDE
HIGH TIDE
Distance (m)

CROSS–SPECTRUM (P9 – V9)

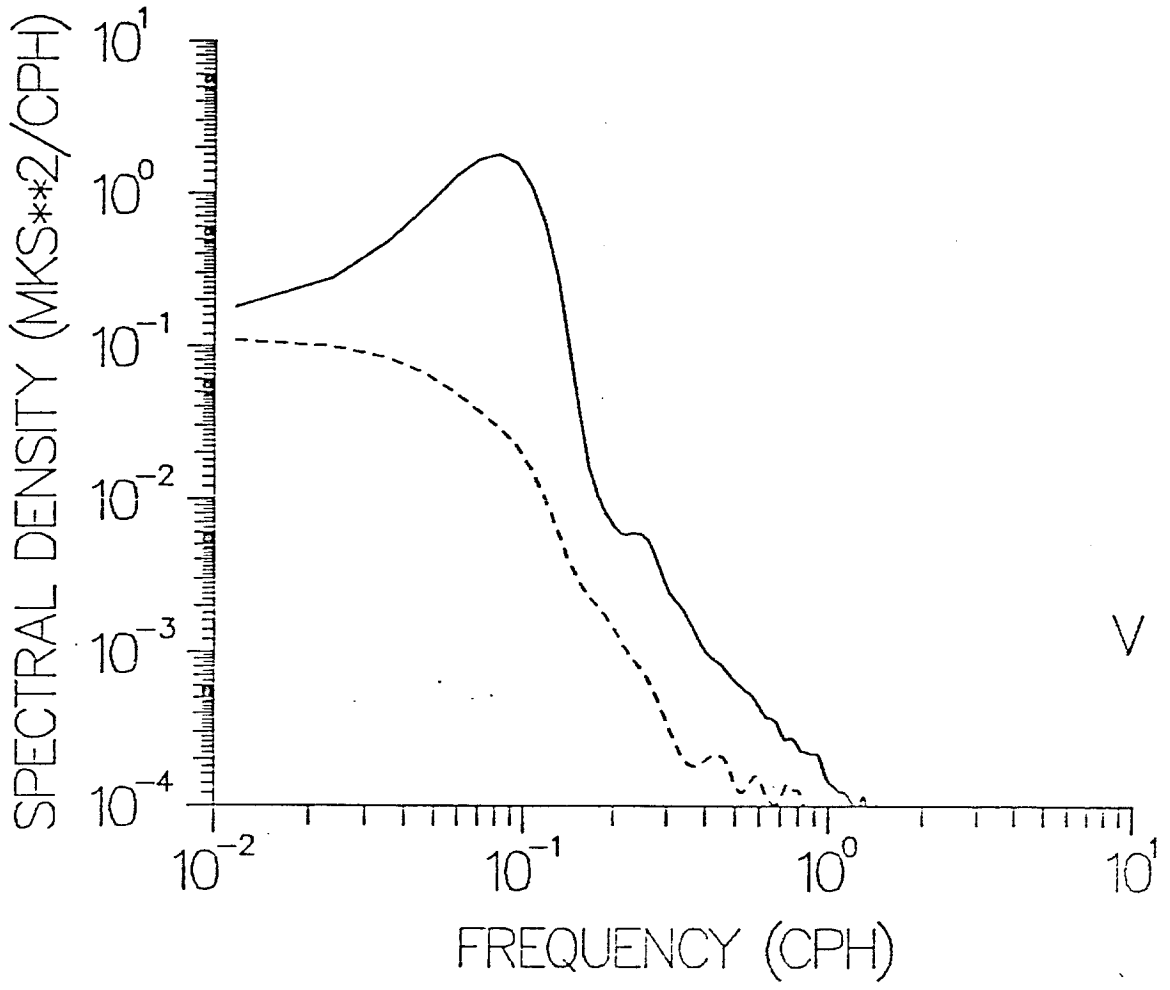

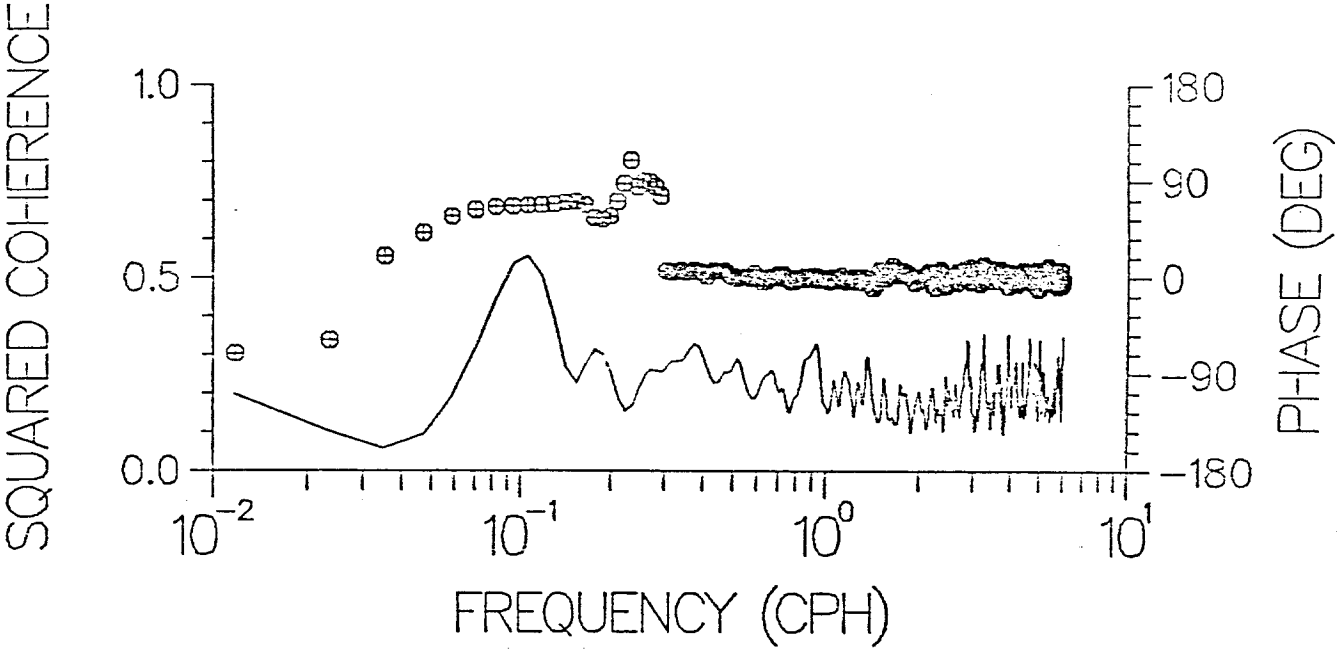

CROSS–SPECTRUM (P9 – V5)

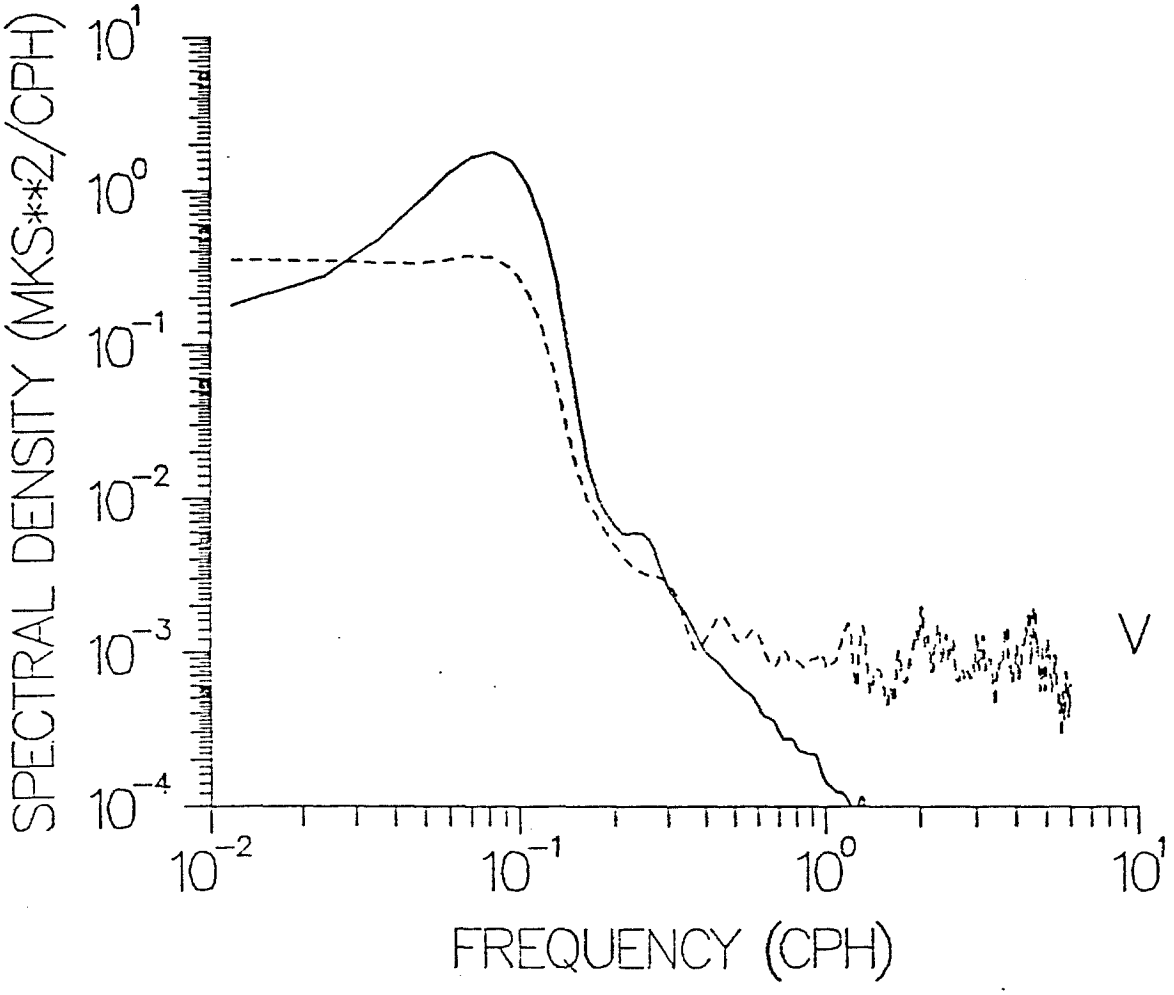

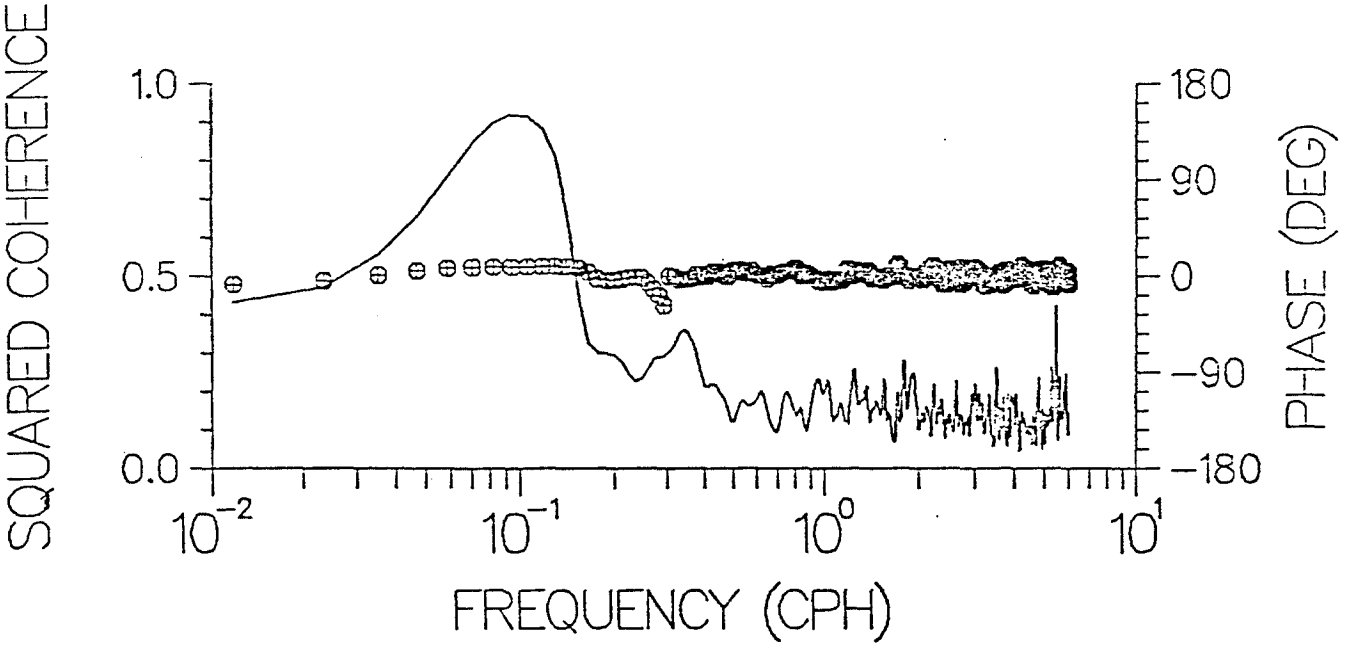

CROSS–SPECTRUM (P9 – V2)

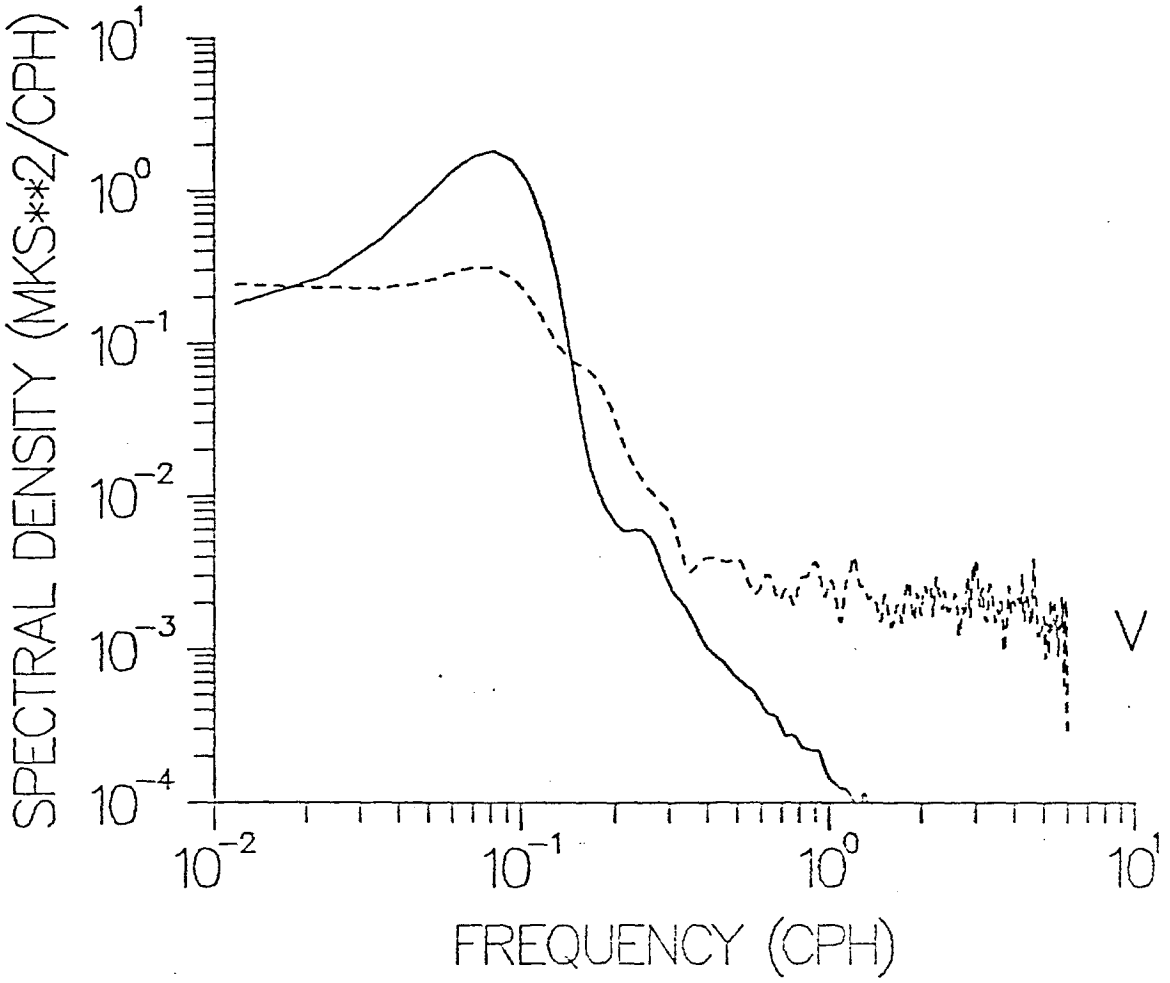

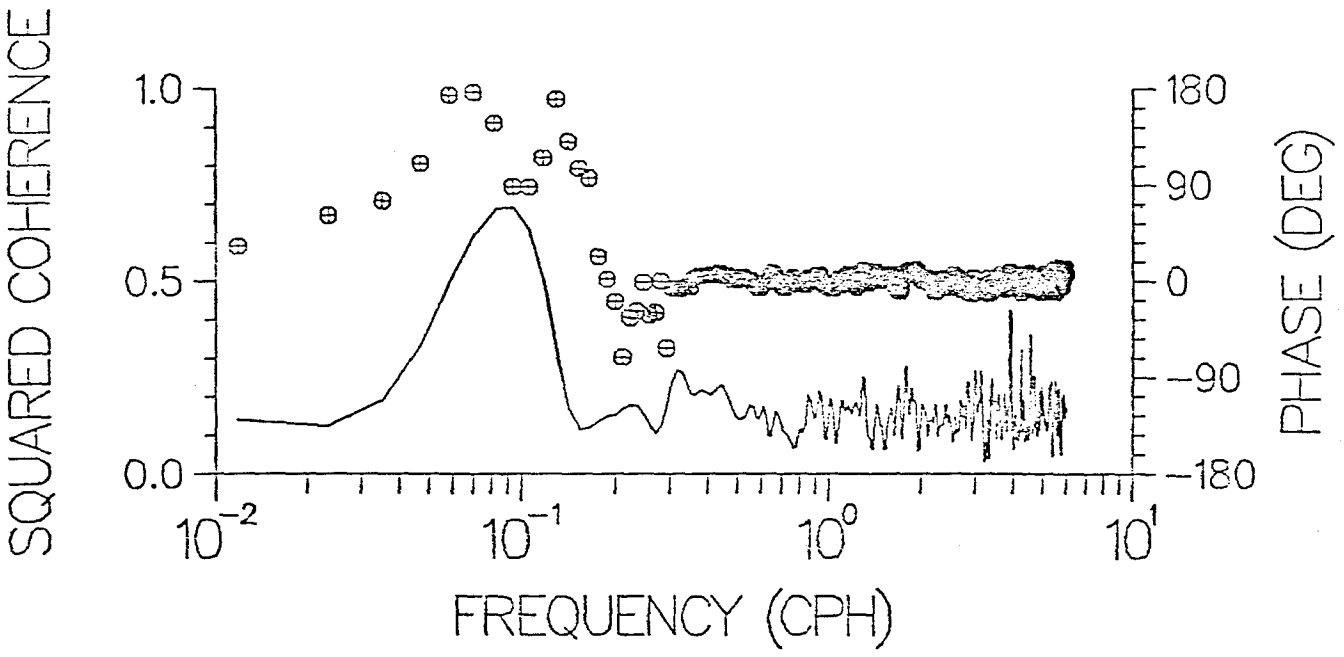

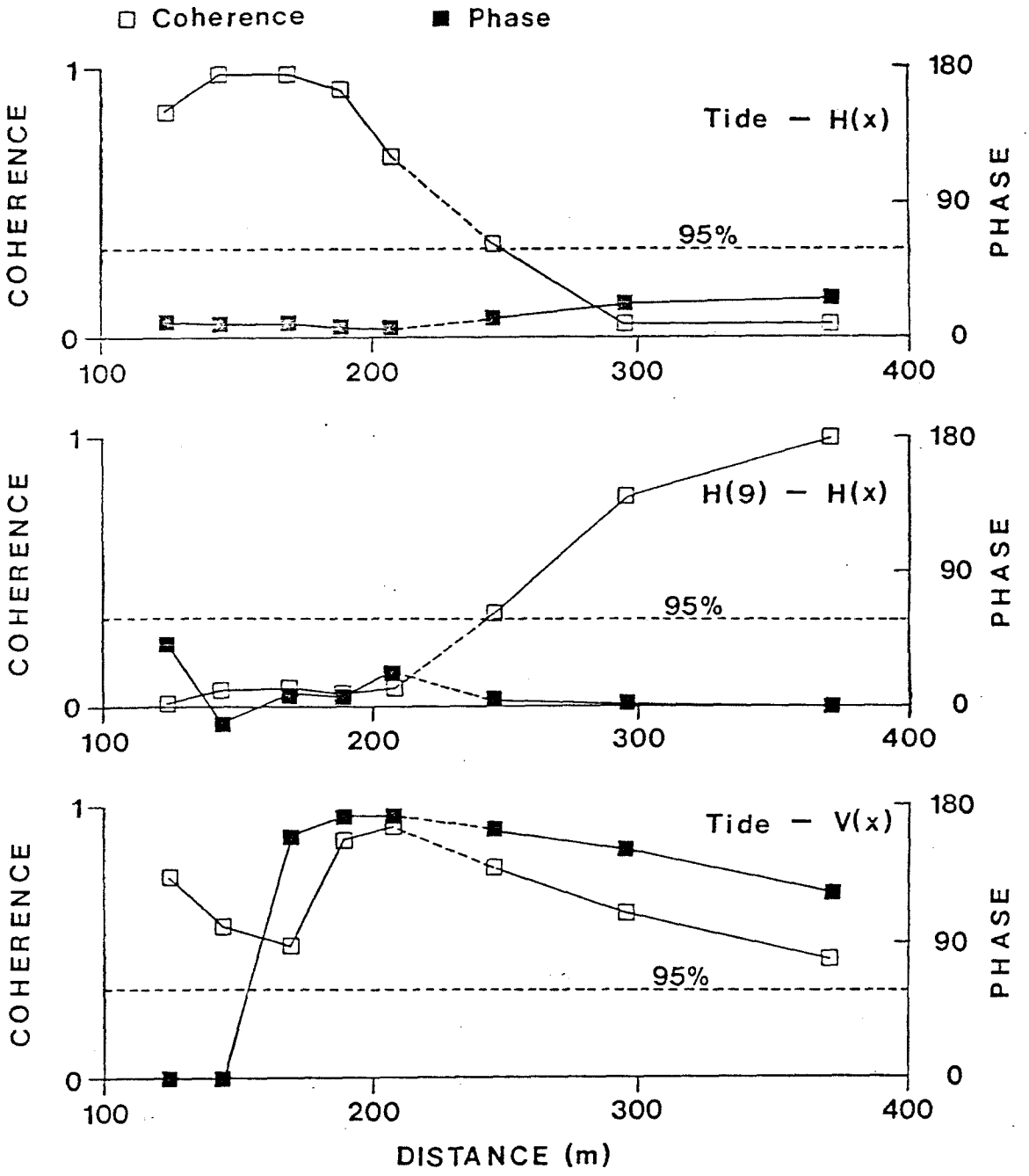
Coherence
Phase
COHERENCE
PHASE
Tide — H(x)
95%
H(9) — H(x)
Tide — V(x)
1
0
180
90
0
100
200
300
400
DISTANCE (m)

CONCLUSIONS

- o DELILAH Experiment provides the promising data for spatial and temporal variability study
- o Tidal signature in H_{rms} : surf zone
- o Tidal signature in V : strong near the shore and over the bar, weak in the trough
- o Dominant forcing for the variability due to tide
- o phase relationship between V and Tide tests the hypothesis ← verified
- o Modulation of H and V → O(1)
- o Needs further work on response to slowly–varying transient forcings such as wind and atmospheric pressure variations.

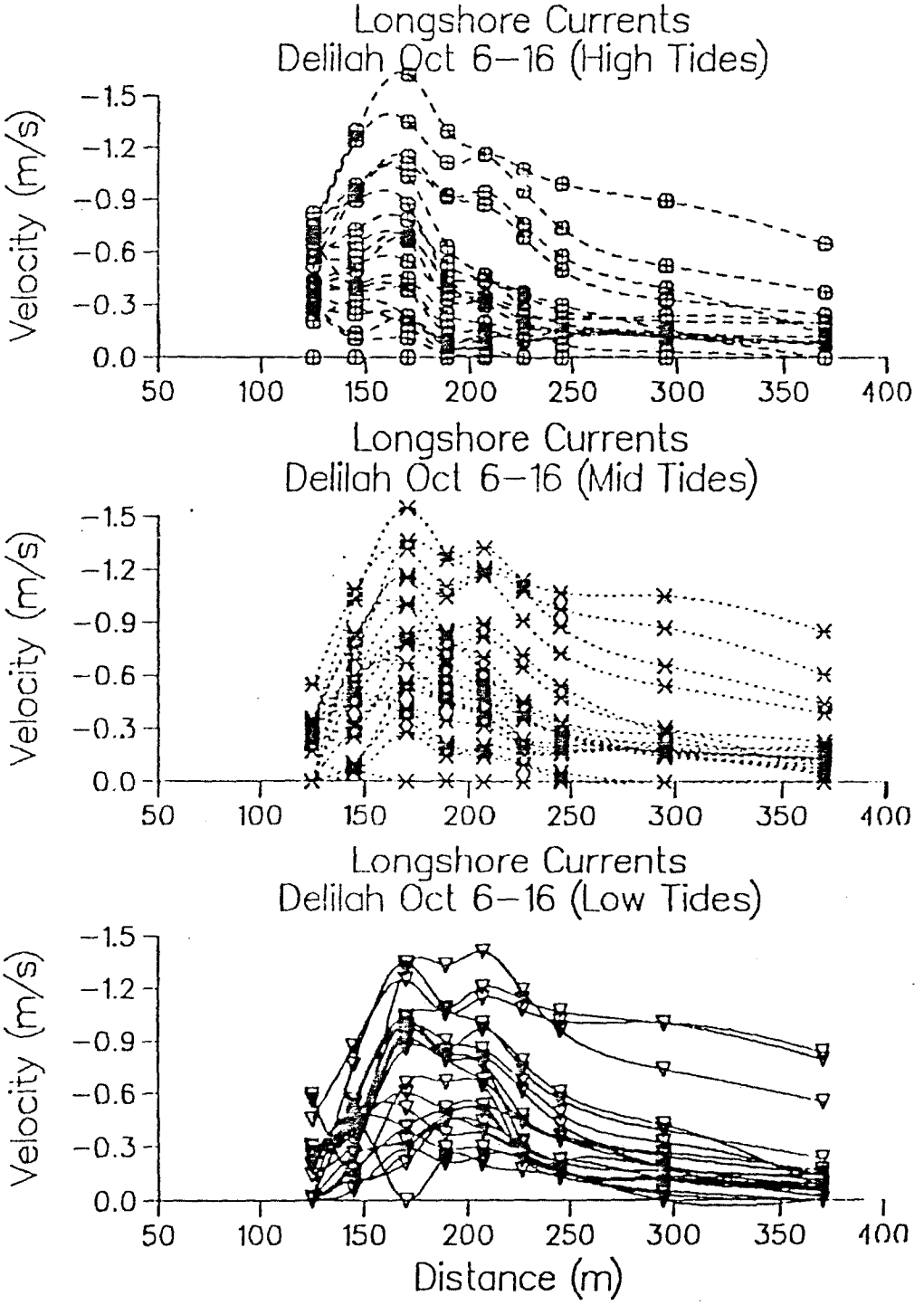
Longshore Currents
Delilah Oct 6–16 (High Tides)
Velocity (m/s)
-1.5
-1.2
-0.9
-0.6
-0.3
0.0
50
100
150
200
250
300
350
400
Longshore Currents
Delilah Oct 6–16 (Mid Tides)
Velocity (m/s)
Longshore Currents
Delilah Oct 6–16 (Low Tides)
Velocity (m/s)
Distance (m)

P9-V9

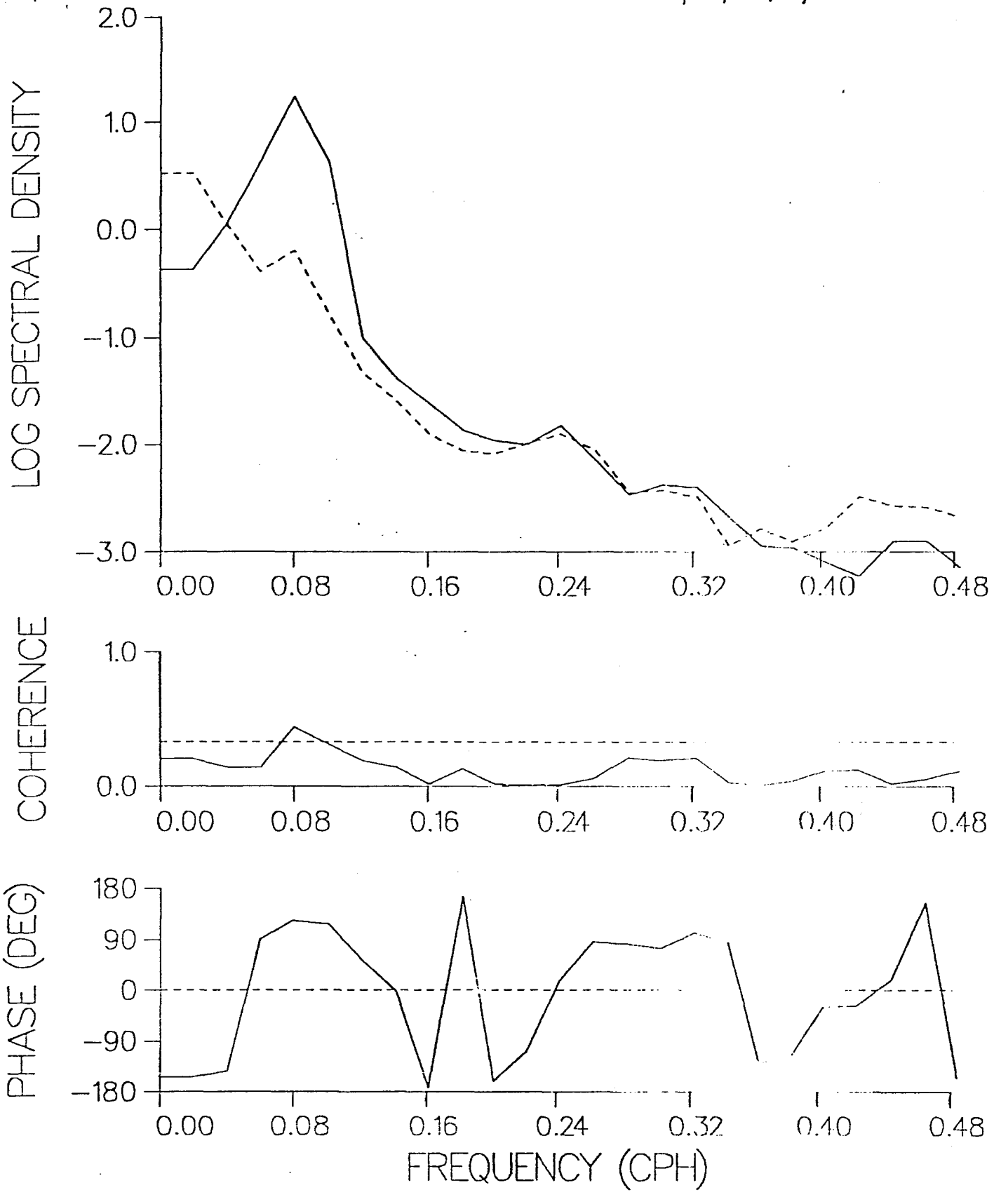
LOG SPECTRAL DENSITY
2.0
1.0
0.0
−1.0
−2.0
−3.0
COHERENCE
1.0
0.0
PHASE (DEG)
180
90
0
−90
−180
0.00
0.08
0.16
0.24
0.32
0.40
0.48
FREQUENCY (CPH)

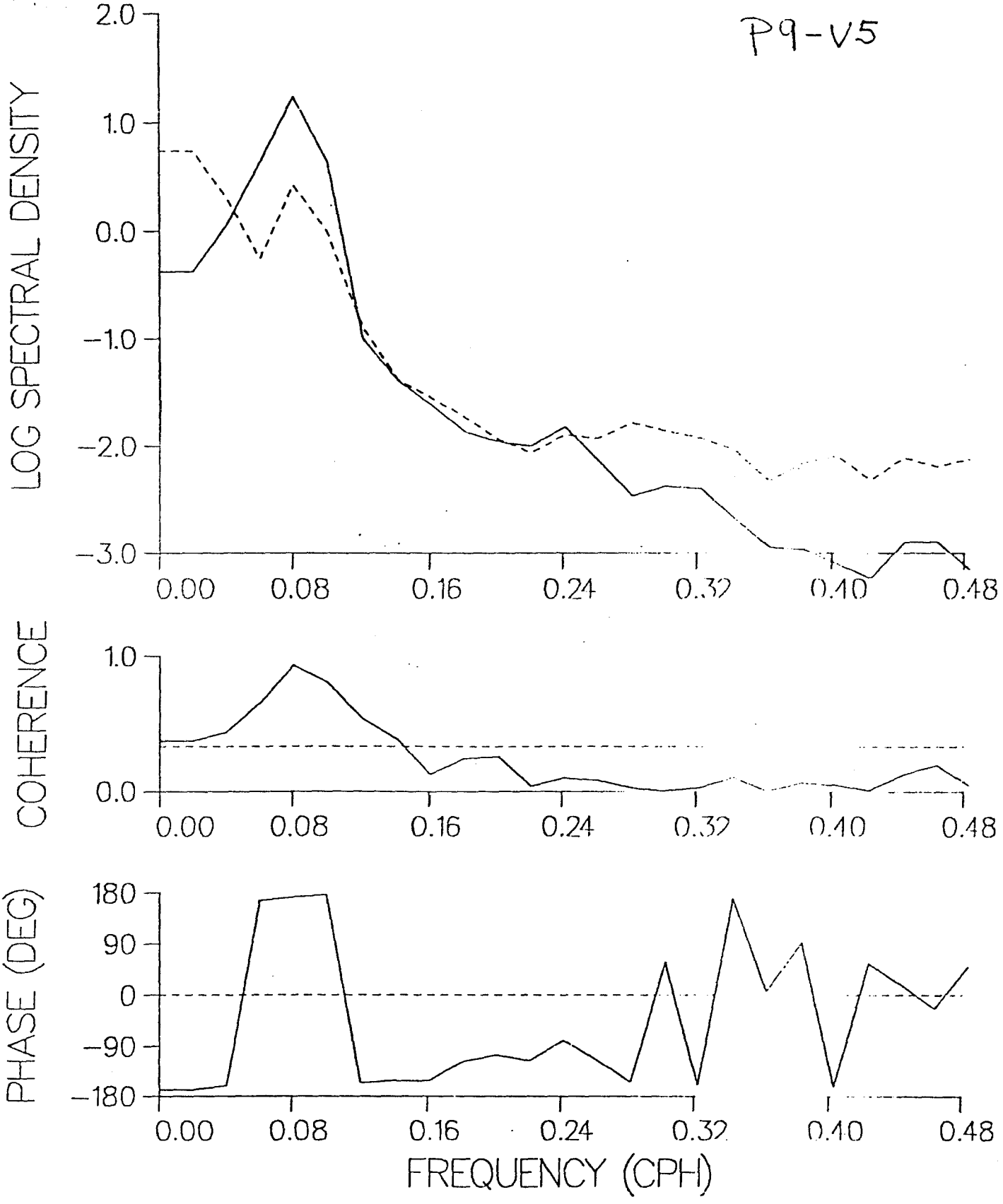
P9-V5
LOG SPECTRAL DENSITY
2.0
1.0
0.0
-1.0
-2.0
-3.0
0.00
0.08
0.16
0.24
0.32
0.40
0.48
COHERENCE
1.0
0.0
0.00
0.08
0.16
0.24
0.32
0.40
0.48
PHASE (DEG)
180
90
0
-90
-180
0.00
0.08
0.16
0.24
0.32
0.40
0.48
FREQUENCY (CPH)

Pg-V2

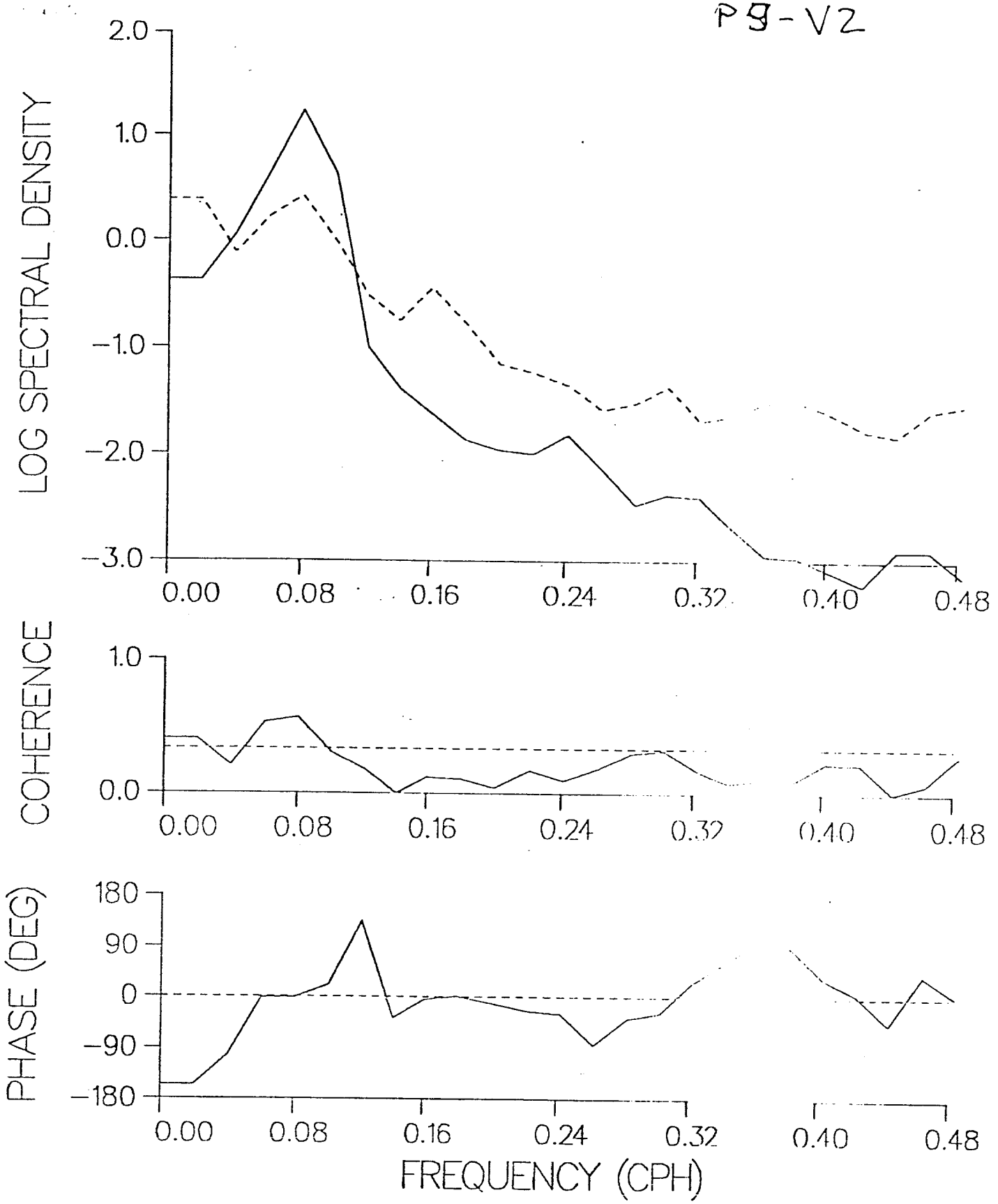
LOG SPECTRAL DENSITY
2.0
1.0
0.0
-1.0
-2.0
-3.0
0.00
0.08
0.16
0.24
0.32
0.40
0.48
COHERENCE
1.0
0.0
0.00
0.08
0.16
0.24
0.32
0.40
0.48
PHASE (DEG)
180
90
0
-90
-180
0.00
0.08
0.16
0.24
0.32
0.40
0.48
FREQUENCY (CPH)

제 3 장

JGR Ocean에 기고된 논문

92. 8. 기고
93. 3. 현재 1차수정본 Review 중.

Sept. 15/92
From EBT

TIDAL MODULATION OF WAVE HEIGHTS AND LONGSHORE CURRENTS INSIDE THE SURF ZONE

EDWARD B. THORNTON and CHANG S. KIM*

Oceanography Department

Naval Postgraduate School, Monterey, CA

ABSTRACT

Data were acquired continuously during the 19 day DELILAH nearshore experiment with the specific objective of examining variability of the longshore current at tidal frequencies. The hypothesis is that wave heights inside the surf zone are a strong function of the depth modulated by the tide due to wave breaking, and since radiation stress is a function of the wave height, it will force the longshore current at the tidal frequency inside the surf zone. The measured longshore current variations at tidal frequency are the same order of magnitude as the mean longshore current variations for moderate wave height conditions, indicating that the tide is a dominant forcing mechanism for longshore current variability. Simulations of the magnitude and phase of the longshore current variability with tide elevation using the model by Thornton and Guza (1986) are used to explain observations. The measured phase between tide elevation and longshore current are in-phase in the inner surf zone and out-of-phase in the outer surf zone as predicted by the model, verifying the hypothesis.

*Sabbatical from Korea Ocean R&D Institute, Seoul, Korea

INTRODUCTION

During the SUPERDUCK experiment conducted at the U.S. Army Field Research Facility (FRF) at Duck, North Carolina, Howd et al (1991) found high correlation of wave heights inside the barred beach with the tidal elevation. Only limited data were available during SUPERDUCK since measurements were only for four hours over the low and high tides. Data were acquired continuously during the DELILAH experiment at the same FRF, with the specific objective of examining variability of longshore currents at tidal frequencies. Waves and longshore currents inside the bar during the DELILAH experiment appear to have a strong tidal signature, suggesting a modulation of wave amplitude and consequently radiation stress. The order of fluctuation of longshore currents at tidal frequency is up to one m/sec, which is comparable to the mean value.

There are only a few forcing mechanisms for causing longshore current fluctuations at tidal frequencies. These are the changes in water depth due to the tide, tidal currents, atmospheric pressure variations, and wind forcing. The atmospheric pressure may be ruled out due to the time scale of variability generally varying greatly and on the order of a few days. The wind forcing often has a frequency component very similar to the semi-diurnal tide due to "diurnal sea breeze"; however, during the experiment, the wind varied in speed and direction during the experiment, but not in a clear semi-diurnal cycle. The most obvious possible cause for the observed fluctuations are the tidal currents themselves. However, the observed current fluctuations increased towards shore on the order of 1 m/sec, whereas tidal current would be expected to go to zero at the shore.

The wave heights inside the surf zone have been observed to a first approximation to be linearly related to the wave depth h, such that $H_{rms}=\gamma h$, where γ is a constant (Thornton an Guza, 1982). Thus, if the depth of water varies inside the surf zone, the H_{rms} will vary inside the surf zone. It is hypothesized that depth dependent breaking wave heights are modulated by time varying depth due to the tide, and that the waves inside the barred profile are dependent on the breaking wave height over the bar; the resulting

waves inside the surf zone will have a strong tidal signature.It is further hypothesized that the longshore current will have a tidal signature in response to the wave forcing.

In the following, time series of wave height and longshore current measured during the DELILAH experiment are shown to have a strong tidal signature. The hypothesis that depth dependent wave breaking modulated by the tidal elevation is responsible for this variability is examined by simulating the amplitude of wave heights and magnitude of longshore currents and their phase relationships with tide elevation using the model of Thornton and Guza (1986). A simple planar beach case is first examined to explain the expected amplitude and phase relations. Then the wave heights and currents are simulated over the actual barred profiles. If the currents are due to a progressive tidal wave propagating up the coast, the longshore currents and tide elevation would be expected to be around ninety-degrees out of phase. It is found the measured wave heights and currents are near either in-phase or out-of-phase with the tide elevation, verifying the hypothesis put forth. This study shows the tide is a dominant forcing mechanism for the variability of longshore currents.

EXPERIMENT AND DATA PREPARATION

The multi-institutional, comprehensive nearshore experiment DELILAH was conducted at the U.S. Army Field Research Facility (FRF) at Duck, North Carolina during the period of October 2-20, 1990. Nineteen days of continuous data were acquired with the object of examining wave, tide and wind forcing of longshore currents, vertical structure of mean currents, shear instabilities, infragravity waves, wave/current/morphology interactions and spectral wave transformations. DELILAH was conducted to coincident with the SAMSON experiment, which had the objective to measure microseism noise generated by wind-waves. The combined offshore directional wave instrumentation included a 26 element array in 13m and a 14 element array in 8m. In the nearshore, a 9 electromagnetic current meter/pressure sensor array was located in the cross-shore, and alongshore current meter arrays of six sensors in the trough and

five sensors offshore of the bar (see Fig. 1). Also shown in Figure 1 are one-hour averaged current vector plot for when 2m waves were incident at 40 degrees generating 1.5 m/s currents. In addition, a 5 electromagnetic current meter vertical array with pressure sensor and wave staff were mounted on a moveable sled. A detailed description of the experiment is given in Birkemeier (1991).

A wide variety of wave conditions occurred during the experiment. The wind speed and direction measured at the end of the pier, the significant wave height, period and mean direction measured in 8m depth, longshore current measured in the trough of the barred profile, and tide elevation are shown in Figure 2. A short "northeaster" occurred at the beginning of the experiment driving longshore current to the south. This was followed by 6 days of low swell from the south and concomitant longshore current to the north. On the 10th, a frontal system from the south arrived resulting in waves up to 2m incident at relatively large angles from the south quadrant driving strong longshore currents (up to 1.5 m/s). Two days later on the 13th, swell waves up to 2.5m arrived from hurricane Lili; although these waves were larger, the incident angle was less and the resulting longshore currents were not as large. After the 15th, local weather patterns and distance swell intermingled to give variable current direction and speeds, depending on the dominant component.

The bar at this location is highly mobile and responded to the variable wave conditions during the experiment. The changing of the bar location has a significant effect on the resulting longshore current profile. A well-formed bar was present at the beginning of the experiment. The bar then migrated shoreward during the swell waves between 2 and 7 October, eventually welding to the shoreface. The bar was re-established during the larger hurricane waves between 8 and 13 October with a steepening of the foreshore; the profile remained stationary for the remainder of the experiment. The active region of the profile was between the outer bar and the shoreface, with no noticeable change in the offshore profile and high-up the beach face (Figure 3.) The bar tends to be three-dimensional, or rhythmic, during times of moderate waves (2-9 October; Fig. 4a, typical) and becomes linear during times of strong longshore

currents (10-19 October; Fig. 4b typical). The vertical lines on the bathymetry plots are the locations of the instruments.

A primary objective of the DELILAH experiment was to measure the tidal forcing of the longshore currents. This required that the waves and currents be measured continuously throughout the experiment. Previous comprehensive experiments (eg. NSTS and SUPERDUCK) measured parameters only over the low and high tides with the objective of obtaining a long (approx. 4 hours) stationary time series in which the changes in water depth would be minimized. A secondary reason for not having continuous data was the problems of dealing with large data sets. A new data acquisition was designed specially for DELILAH taking advantage of microprocessor technology which simplified the data acquisition allowing near continuous acquisition. The data were sampled at 8 Hz. Only short (approximately 5 minute) gaps occurred approximately every eight hours in the data due to magnetic tape changes.

The data analyzed in this study were acquired by the cross-shore array of instruments consisting a two-component electromagnetic current meter and pressure sensor at each of 9 locations. The location and elevation of the current meters relative to selected beach profiles are shown in Figure 3. For convenience, sensors are numbered from 1 in the swash to 9 offshore. The current meters were kept at the same elevation relative to mean-sea-level, with the exception of current meter 1 whose elevation had to be adjusted during the experiment to accommodate changes in the beach profile. The top of the bar was at sensor 5 early in the experiment and moved offshore to 6 with the increase in wave height on 9 October. The cross-shore array was designed to measure more intensely over the bar where the largest changes in the wave height occur due to wave breaking.

To examine the fluctuations of wave height and longshore currents at tidal frequency, five minute average time series was prepared for the ten day period from October 6, 1990 to October 16, 1990. The data gaps due to tape changes were linearly interpolated. During this period of time, the wave height

generally increased from calm (Hrms < 0.5m) to severe condition (Hrms > 1.2m) (see Fig. 2). The tidal elevation fluctuations are measured using 5 minute mean values of pressure head. Tidal range in the study area is less than 1m, and the general rise in mean water level on October 12 is due to wind set-up during the passage of hurricane Lili.

The H_{rms} wave heights were calculated from the variance of the surface elevation spectra by summing the spectra across the wind-wave band of frequencies from 0.05 to 0.3 Hz, and assuming the waves are Raleigh distributed. The surface elevation spectra were obtained by applying a linear wave theory transfer function to the calculated pressure record spectra. The spectra were calculated every 8.4 minute (coinciding with an even number of data blocks and power of 2). The wave heights were then interpolated back to every 5 minutes (to coincide with velocity averages and so that time would plot as even hours). The wave height time series (Figure 5) show little tidal signature outside the surf zone and a strong tidal signature inside the surf zone. In the swash at sensor 1, the waves were low and the sensor was high in the profile; therefore, waves were only measured at high tide, and at lower tides the sensor was out of the water. As the waves increased in height, the surf zone width increased and the bar moved offshore (Figure 3); this resulted in the primary breaker region moving offshore. The tidal signature is even obvious at a depth of over 4m at sensor 8 during the height of the storm on October 12 and 13. Outside the surf zone, the waves show little tidal signature, but considerable variability in the wave height associated with wave generation by local winds and distant storms.

Continuous time series of longshore currents were calculated as simple five minute averages of the raw data. The longshore currents show similar significant tidal signature and slowly varying transient response at time scales of the wave height variations (Figure 6). At current meter V1 in the swash, the zero velocities are when the current meter was no longer in the water. The strongest tidal signatures appear near the shore and over the bar at sensors V4 and V5, with a decrease in tidal signature in the trough. The location of the maximum tidal signature in velocity is generally further offshore than that of

the wave heights. Tidal signature is observed even at the furthest offshore velocity sensor, suggesting that tidally driven longshore currents are present in addition to the wave driven longshore currents modulated at tidal frequency.

An expanded view of a segment of the longshore current time series for October 9th is shown in Figure 7. Large fluctuations in the longshore current velocities are superposed on the tidal variation even at the five minute averages; these fluctuations are assumed due to infragravity waves or shear instabilities of the longshore current as suggested by Bowen and Holman (1989) and Dodd et al. (1992). Again, the zero velocities at sensor V1 occurred when the current meter came out of the water at low tide. The strength of the tidal signature is seen to generally decrease offshore.

To test the hypothesis that the variations in the longshore currents at tidal frequencies are due to the modulation of the breaker heights over the bar by the tide, the phases between tide elevation and longshore currents across the surf zone are examined. If the currents are tidal currents, the currents across the surf zone should be in-phase with each other and 90 degrees-out -of phase with a tide progressing up the coast. If the longshore current variations are a consequence of variable wave heights due to changes in water depth at breaking, the longshore current could have other phase relations with the tide. The next section simulates longshore currents to explain the dominant cause for the variations at tidal frequency.

SIMULATION OF LONGSHORE CURRENT VARIABILITY DUE TO TIDE

To gain a qualitative understanding of the variability in the longshore current due to the tide, longshore current variations are first simulated on a simple planar beach. The present study adapts the model of Thornton and Guza (1986) to simulate the mean longshore currents along with tidal variation using discrete-step transient. Variation in both wave height and longshore current and their phase relations with the tide are examined in this simulation. Then, a similar qualitative simulation of wave height and longshore current is calculated over the actual barred bathymetry measured during DELILAH to further

explain the observed variations due to the tide.

It is assumed the bottom contours are straight and parallel, the wave heights offshore are stationary with time (over a tidal cycle) and wind stress can be ignored. Time averaging is done over times short compared with tidal changes, such that the wave height and longshore current can be considered quasi-stationary. The wave height cross-shore distribution is solved first using the energy balance

$$\frac{\partial EC_{gx}}{\partial x} = \langle \epsilon_b \rangle \qquad (1)$$

where the right-handed coordinate system is x positive offshore and y alongshore, E is the energy per unit area of the waves, C_{gx} is the cross-shore component of the group velocity and $\langle \varepsilon_b \rangle$ is the dissipation due to wave breaking. The waves are assumed narrow banded in frequency and direction with the random wave height variability described by the Rayleigh distribution everywhere, both outside and inside the surf zone. Describing the waves using linear wave theory, the ensemble averaged wave energy based on the Rayleigh distribution is

$$E = \frac{1}{8}\rho g H_{rms}^2 \qquad (2)$$

Dissipation is modeled after a linear bore and only applies to those waves that are breaking, which are described by a weighing function of the Rayleigh distribution. Thus, at a particular location, some of the waves are described as breaking and the rest are not with the percent of breaking increasing towards shore, until well inside the surf zone all waves are breaking. In this manner, wave dissipation is spread over a region and the cross-shore variations in wave height are well described compared with measurements (see eg. Thornton and Guza, 1986; Thornton and Whitford, 1992).

Longshore currents are solved for using the alongshore momentum equation, which based on the

above assumptions simplifies to a balance between the changes in the alongshore directed momentum flux, S_{yx}, and the bottom shear stress in the alongshore direction,

$$\frac{\partial S_{yx}}{\partial x} = -\tau_y^b = -\rho c_f |\overline{u}| V \qquad (3)$$

where the bottom shear stress on the rhs has been linearized assuming the longshore current is weak compared with the magnitude of the wave velocity (Longuet-Higgins, 1970), and ρ is the water density and c_f is the bottom shear stress coefficient; the ensemble averaged wave velocity magnitude is specified using linear theory, $|u| = Hrms(g/4\pi h)^{1/2}$. The S_{yx} can be partitioned into wave and turbulent momentum fluxes

$$S_{yx} = \tilde{S}_{yx} + S'_{yx} \qquad (4)$$

Using linear wave theory, the wave-induced momentum flux (radiation stress) is given by

$$\tilde{S}_{yx} = E \frac{C_{gx}}{C} \sin\alpha\cos\alpha \qquad (5)$$

The turbulent momentum flux formulation by Battjes (1975) is used, which assumes the primary source of turbulent energy within the surf zone is due to wave breaking and that the mean rate of wave energy dissipation equals the rate of turbulent energy production locally. The effect of the presence of the longshore current shear is to stretch the isotropic generated turbulent eddies, inducing horizontal anisotropy resulting in a negative correlation of turbulent velocity components u' and v'. The characteristic size of the turbulent eddies is limited by the local depth. The turbulent momentum flux, or Reynolds stress integrated over depth, is given by

where

$$S'_{yx} = \int_{-h}^{0} \overline{\rho u' v' dz} = \rho A h \frac{\partial}{\partial x} V \qquad (6)$$

$$A = Nh \left[\frac{\langle \epsilon_b \rangle}{\rho} \right]^{1/3} \qquad (7)$$

and N should be O(1). The longshore current is numerically solved using Equation 3 (Thornton and Guza, 1986), where the H_{rms} (and E) are obtained by first solving Equation 1. Model coefficients used for wave height transformation are B=0.8 and γ=0.4, and for longshore currents c_f=0.006 and N=1.

The longshore current simulation over the planar beach for a tidal cycle is shown in Figure 8, where the velocity, wave height and depth profiles are shown at various tidal stages in the upper panels, and the time variation of V with tidal amplitude at various cross-shore locations is shown in the lower panel. The H_{rms} values for all tidal stages start at the same value offshore (stationary wave conditions). As the waves progress shoreward the waves start to break, with breaking starting further offshore at lower tides. Although the mean water level is changing with the tide, the longshore current profile is invariant in its profile shape on a planar beach with the profile simply sliding back and forth with the tide. The maximum longshore current migrates from offshore during low tide towards the shore during high tide. The behavior of the maximum current migrating in the on-offshore direction illustrates the relative phase difference between two regions separated by a position (node) where current does not change with tide. The lower panel clearly indicates the opposite phase in time variations between these two regions. The sign of the phase between longshore current and tide elevation depends upon whether the currents are negatively or positively flowing. For positive flowing current, the longshore current is in-phase with the tide nearer the shoreline and out-of-phase in the outer surf zone. To examine this phase relationship, let x_s be the distance of the time-varying shoreline measured relative to the shoreline at mid-tide, x_o, and the tidal fluctuations given by

$$\zeta = \zeta_T \sin\sigma t \tag{8}$$

where ζ_T is tidal amplitude and σ is the tidal frequency (eg. 12.4 hr for M_2 semi-diurnal tide). The shoreline position x_s is given as

$$x_s = -\frac{\zeta}{\tan\beta} = -\frac{\zeta_T}{\tan\beta}\sin\sigma t \tag{9}$$

where $\tan\beta$ is the beach slope. Therefore, the offshore position at time t is expressed by $x = x_o - x_s$. Solving for the longshore current as a function of the tide elevation using a change of variables by applying the chain rule

$$V(x, t) = \int \frac{dV(x, t)}{dt} dt = \int \frac{dV(x_o)}{dx} \frac{dx}{dt} dt \tag{10}$$

Substituting Equation 9 and integrating,

$$V(x, t) = \frac{dV(x_o)}{dx} \frac{\zeta_T}{\tan\beta}\sin\sigma t \tag{11}$$

where the constant of integration is zero satisfying the boundary condition that $\partial V/\partial x = 0$ as $x \rightarrow \infty$. Equation 11 implies that the time variations of the longshore currents partitions into two regions separated by the inflection point at $\partial V/\partial x = 0$ with opposite phase. The longshore current is in-phase with the tide in the inshore portion of the surf zone where dV/dx is positive, and is out-of-phase with the tide offshore the velocity peak where $\partial V/\partial x$ is negative.

The ideas presented for a planar beach are applicable to the barred system, where the longshore

current profiles are more sensitive to changes in the bathymetry in response to wave breaking over the barred profile. Longshore current profiles are simulated over the observed bathymetry for October 7 (low wave, poorly-developed bar case; Figure 9) and October 12 (high wave, well-developed bar case; Figure 10). Again, the H_{rms} values all start at the same value offshore, and as the waves progress shoreward the waves start to break, with breaking starting further offshore at lower tides. The low wave, poorly-developed bar case is similar to the plane beach case with the longshore current profile sliding on and offshore with the tide, but with distortions in the profile shape due to variations in the dissipation intensity due to the non-planar beach profile.

The wave height and longshore current distributions are more complex for the well-developed bar case (Figure 10). The simulated waves break most strongly on the outer bar, with a large decrease in wave height over the bar, reform in the trough as noted by the increase in wave height due to shoaling and break strongly again on the foreshore; the shapes of the cross-shore H_{rms} profiles are similar once the waves start to break. The simulated V profile is more complicated. At higher tidal stages, the velocity profile has a single maximum located just inside the bar with the strongest longshore current occurs at high tide. At low tidal stages the longshore current maximum moves onto the outerside on the bar in response to waves breaking more intensely offshore the bar at low tide; the waves then reform over the trough and break on the foreshore causing a another maximum in longshore current near the beach. Again, the fluctuations of longshore current indicates a possible reversal of the phase between two regions separated by a node. The results of the simulation on the variation of longshore currents clearly suggest a possible reversal of the phase between two regions, which is examined with observed data.

OBSERVED VARIABILITY OF LONGSHORE CURRENTS

The time series of longshore currents shown in Figure 6 are grouped into 3 different tidal stages; high, mid, and low tides, and the resulting cross-shore distribution of longshore currents for the ten days

are shown in Figure 11. The markers represent the locations of the sensors, and the connecting lines are cubic spline interpolations. The range of variation at each stage gives an idea about the response of longshore current to the wave variability. The relatively large values observed at the inner most sensor during high tide suggests that the shoreline position with zero longshore current is further inshore of the expected tidal shoreline, or significant longshore current is present even at the shoreline.

Mean wave height and longshore current profiles for consecutive tidal stages from low to high tides on three different days are shown in Figures 12-14: 7 October (low waves, weak bar), 9 October (moderate waves, moderate bar with tidal plateau) and 11 October (higher waves and well-developed bar). Examining wave height transformation first, the waves were nearly stationary for each day, i.e. offshore wave height is nearly the same for all tide stages. The waves initially increase in height due to shoaling and then decrease due to breaking. The wave heights decrease more rapidly where the depth decreases more rapidly due to enhanced dissipation due to wave breaking. For the larger waves on the 11th, the waves broke first on the bar, reformed in the trough, increasing slightly due to shoaling, and then broke again on the foreshore. For the lower wave case on the 7th, the waves broke further offshore at lower tide with breaking initiated by the rapidly decreasing depth of the residual bar formation, and then broke closer to shore on the steeper foreshore at high tide. The behavior of observed changes in H_{rms} at various tidal stages is similar to the simulations shown in Figures 8-10.

The longshore current responds to the displacement of the location of the changes in the Hrms with the V peak moving shoreward as the tide increases, similar to the simulations. A possible discrepancy of the measurements with the simulations occurs on the 11th at high tide. In the simulations the strongest velocities occur at high tide, whereas on the 11th the velocity is less; this is due to the initial wave height being less at high tide, and not a conflict with the simulations. Interestingly, the longshore current velocities at high tide on 7 and 9 October are near maximum at the apparent shoreline where the wave heights are near zero.

The contribution of the variance of wave height and velocity associated with the semi-diurnal tide to their total variance is examined by calculating energy density spectra. The spectra are ensemble-averaged over 9 records of 49.6 hours (four tidal periods) with fifty percent overlap, giving approximately 18 degrees of freedom. Using record lengths of exact multiples of the primary diurnal tidal period negates bias due to leakage. Examples of energy density spectra for tidal elevation and velocity are shown in Figures 15 a,b,c (upper panels).

The fraction of the variance at the semi diurnal tide is obtained by summing the adjacent spectral bands centered on the semi-diurnal tidal frequency (0.08cph), and comparing it with the variance obtained from the time series of the entire record; these are presented as ratios of standard deviations in Table 1. Little of the wave height variability outside the surf zone is associated with the tide, while significant variability is associated with the tide inside the surf zone. The longshore current associated with the tide is greater than that associated with the wave height outside the surf zone; this fraction shows a general increase in across the surf zone, with the exception of a decrease in the trough. The maximum longshore current variability at tidal frequency is at the foreshore.

The H_{rms} varied at tidal frequency across the entire surf zone (Figure 5). On the other hand, there is an observed decrease in longshore current response to tide variations in the trough of the profile, compared with enhanced variations at tidal frequency both nearshore and over and offshore the bar as reflected in the timeseries (Figure 6) and quantized in the portion of the standard deviation associated with the tide (Table 1). The decrease in the response at the tidal frequency can be explained by examining the longshore current formulation. Manipulating Equation 3,

$$V(x,t) = \frac{1}{\rho c_f |u|} \frac{\partial \tilde{S}_{yx}}{\partial x} \qquad (12)$$

where mixing has been ignored for simplicity. Substituting the linear wave theory formulations for S_{yx} (Eq. 5), E (Eq. 2) and $|u|$, into the alongshore momentum balance gives

$$V(x,t) \sim -[h(x) + \zeta(t)] \frac{\partial H_{rms}(x,t)}{\partial x} \qquad (13)$$

where angle information is constant as described by Snell's law for straight and parallel contours and a higher order term has been neglected. The magnitude of the longshore current is temporally modulated by the tidal elevation and spatially dependent on the total water depth and the gradient of H_{rms}. Referring to the depth profiles in Figure 3 and the H_{rms} transformations shown in Figure 11, the largest gradients of H_{rms} occur on the seaward face of the bar and on the foreshore coinciding with enhanced longshore current variations at the tidal frequency. The trough is a region of wave reformation and low wave height gradients, and hence a lack of tidal signature in the longshore current. The tidal variation dependence in the total depth term, $h(x)+\zeta(t)$, increases with decreasing depth over the bar and close to the shore; this acts to amplify the relative tidal variations.

The cross-spectra between the tide and longshore current and wave heights are calculated to examine the coherence and phase difference information; examples between the tide elevation (P9) and V sensors are shown in Figures 15a,b,c. The longshore current is coherent with the tide at the semi-diurnal frequency (significantly different from zero at 95% confidence) at all locations across the surf zone (see Table 2). The phases at this frequency band change from 124 degrees offshore (P9-V9) to out-of-phase at mid-surf zone (P9-V5) to in-phase at the inner surf zone (P9-V2). The observed current at tidal frequency at the offshore sensor V9 is weak (Fig. 6), but the coherence and phase suggests the presence of tidal currents offshore. The change in the phase towards the shoreline corresponds to the behavior observed in the simulations (Fig. 8-10).

The coherences and phases at the semi-diurnal tidal frequency between tide elevation (P9) and wave heights across the surf zone (H(x)) between the wave height furthest offshore (H9) with other wave heights (H(x)), and between the tide elevation (P9) and the longshore currents across the surf zone (V(x)) are shown Figure 16 and listed in Table 2. The values for location 6 have not been included in the Figure

do we need both?

as the time series was considerable shorter and the results inconsistent. The coherence gives a measure of the linear cross-correlation between two sinusoids at a particular frequency. The wave heights offshore of the bar (locations 8 and 9) are not coherent with the tide elevation indicating their variability is due to processes other than the tide. The wave heights are coherent with the tide elevation inshore of location 7 with the coherence increasing shoreward; the slight decrease of coherence in the swash at location 1 is because of distortions of the sinusoidal wave form due to no waves at low tide. The wave heights inside the surf zone are in-phase with the tide indicating they are responding to the tide. These results tend to substantiate the hypothesis that variations at tidal frequency are due to changes in the depth modulating the breaking wave height over the bar and controlling the wave heights inside the bar.

On the other hand, the coherences between the wave height offshore (H9) with shoreward wave heights generally decreases shoreward and are not significant inside the surf zone, indicating another mechanism is controlling the wave height other than the initial conditions, namely the modulation of the depth of water by the tide resulting in changes in the wave height due to breaking over the bar. The offshore wave height is in-phase with the shoreward wave heights outside the surf zone where the coherence is significant; the phase inside the surf zone has no meaning as the wave heights are not coherent. The anonymously high coherence at location 6 is due a shortened record in which most of the measurements were for low wave heights during the earlier part of the experiment when this location was well outside the surf zone (see Figure 5).

The coherence between the tide elevation and longshore current velocities is significant at all locations with maximum values over the bar and near the shoreline and decreased over the trough. The phase difference between the tide elevation and longshore current is out-of-phase in the outer surf zone and in-phase in the inner surf zone, which is in accord with the simulations.

SUMMARY AND CONCLUSIONS

Nineteen days of continuous data of wave height and longshore current were acquired during the DELILAH experiment to examine tidal variability. Wave height time series outside the surf zone show considerable variability in the wave height associated with wave generation by local winds and distant storms, but little tidal signature; on the other hand, the wave heights inside the surf zone show a strong tidal signature. The longshore currents inside the surf zone show similar significant tidal signature and slowly varying transient response at time scales of the offshore wave height variations. The strongest tidal signatures in the longshore currents appear near the shore and over the bar, with a decrease in tidal signature in the trough. Some tidal signature is observed even at the furthest offshore sensor, suggesting that tidally driven longshore currents are present in addition to the wave driven longshore currents modulated at tidal frequency. This study shows the tide is a dominant forcing mechanism for the variability of wave height and longshore currents inside the surf zone.

It was hypothesized that time varying water depth due to the tide modulates the depth dependent breaking wave heights over the bar resulting in the waves inside the barred profile having a strong tidal signature, and that the longshore currents have a tidal signature in response to the wave forcing. To test this hypothesis, the phases between the tide elevation and the longshore currents across the surf zone were examined using model simulations and data analysis. The random wave driven longshore current model of Thornton and Guza (1986) was used to simulate the mean longshore currents along with tidal variation using discrete-step transient. Variation in both wave height and longshore current and their phase relations with the tide for both a planar beach and the actual bathymetry were examined in these simulations. It was found that the longshore currents are in-phase with the tide elevation in the inner surf zone and out-of-phase in the outer surf zone with no variation outside the surf zone. The tidal variations were strongest nearshore and over the bar, and weaker in the trough. If the currents were simply tidal currents, the currents across the surf zone should all be in-phase with each other and 90 degrees-out-of phase with the tide progressing up the coast.

These expected phase relations were examined in the data by calculating cross-spectra between tide elevation and wave heights and longshore currents. The energy density and coherence were maximum at the semi-diurnal tidal frequency. The phases betweem the tide elevation and longshore current at this frequency vary from in-phase near the shore, to out-of phase in the outer surf zone, to around 90 degrees offshore. At the semi-diurnal tidal frequency, the coherence between tide elevation and wave height is significant within the surf zone and not outside. The coherence between the tide elevation and longshore current are greatest near the shoreline, less over the trough, increased over the bar and then approaching zero offshore. These results are in accord with the simulations and substantiate the hypothesis that the tidal variations at tidal frequency are due to the depth modulating the breaking wave height over the bar and controlling the wave heights and longshore currents inside the surf zone.

The modulation of the wave height and longshore current velocity by the tides must have an O(1) influence on the sediment transport processes inside the surf zone integrated over time. Obviously this is true at the shoreline where the beach is dry approximately half the time and covered by water over the high tide, but also applies across the surf zone due to the nonlinearity of the process described by high order velocity moments (Bailard, 1981). It is conjectured that for at least moderate waves, such as swell building a summer beach, much of the accretion of sediments occurs over high tide. This is the topic of a forthcoming paper analyzing the DELILAH data.

ACKNOWLEDGEMENTS

The authors wish to express their appreciation to all those who participated in the DELILAH experiment and in particular the staff of the U.S. Army Field Research Facility under the direction of B. Birkemeier. In addition, special appreciation is expressed to R. Wyland, Naval Postgraduate School, and K. Scott, University of California, Santa Cruz, for their roles in acquisition of wave and current data, and to Mary Bristow, Naval Postgraduate School, for help in processing the data. EBT was funded by ONR Coastal Sciences Grant N00014-92-AF-0002 and CSK was funded by ONR and Korean R&D Institute.

REFERENCES

Bailard, J., 1981, An energetics total load sediment transport model for a plane sloping beach. J. Geophysical Research, (11), 10938-10954.

Battjes, J.A., 1975. Modeling of turbulence in the surf zone. Proc. of the Symposium on Modeling Techniques, ASCE, 1050-1061.

Birkemeier, W.A. 1991. Samson and Delilah at the FRF. The CERCular. U.S. Army Coastal Engineering Research Center, CERC-91-1, 1-6.

Bowen, A.J. and R.A. Holman. 1989. Shear instability of the mean longshore current. J. Geophys. Res. 94, 18023-18030.

Dodd, N.J., Oltman-Shay and E.B. Thornton. 1992. Shear instabilities in the longshore current: A comparison of observation and theory. J. Phys. Oceanogr. 22(1), 62-82.

Howd, P.A., J. Oltman-Shay and R.A. Holman, 1991, "Wave variance partitioning in the trough of a barred beach", J. Geophysical Research, 96(C7), 12781-12,796.

Longuet-Higgins, M.S., 1970: Longshore currents generated by obliquely incident sea waves, 2. J. Geophys. Res. 75, 6790-6801.

Thornton, E.B. and R.T, Guza. 1982. Energy saturation and phase speeds measured on a natural beach. J. Geophysical Research, 87, 9499-9508.

Thornton, E.B. and R.T. Guza. 1986. Surf zone longshore currents and random waves: Field data and models. J. Phys. Oceanogr., 16, 1165-1178.

Thornton, E. B. and D. J. Whitford. Longshore currents over a barred beach, II: Model, (resubmitted to the J. of Physical Oceanography).

Table 1. Fraction of wave height and velocity standard deviations associated with the semi-diurnal tide.

Location	H(x)	V(x)
1	.27	.67
2	.57	.40
3	.69	.17
4	.68	.30
5	.46	.31
6	.12	.24
7	.18	.23
8	.11	.23
9	.10	.27

Table 2. Coherences and phase differences at the semi-diurnal tidal frequency (0.08 cph) between tide elevation (P9) and wave heights across surf zone, between wave height at the offshore location (H9) with wave heights, and between tide elevation (P9) and longshore current. Values of coherence greater than 0.33 are significantly different from zero at 95% confidence level.

Location	Tide, H(X)		H(9), H(X)		Tide, V(X)	
	Coherence	Phase	Coherence	Phase	Coherence	Phase
1	.84	11	.01	43	.74	-1
2	.98	10	.06	-11	.56	-1
3	.98	10	.07	9	.49	160
4	.92	8	.05	7	.88	173
5	.66	6	.07	24	.93	173
6	.61	67	.85	13	.91	169
7	.35	13	.35	4	.78	164
8	.05	22	.78	2	.61	152
9	.05	26	1.00	0	.44	124

FIGURE CAPTIONS

Figure 1. Layout of instruments deployed during the DELILAH experiment overlying bathymetry with one hour mean longshore current vectors superposed for 11 October 1990.

Figure 2. Wind speed and direction measure at end of pier, significant wave height, period and direction in 8m depth, longshore current measured in trough, and tide elevation during DELILAH experiment.

Figure 3. Bottom profiles during experiment with current meter elevation and locations indicated.

Figure 4. Examples of bathymetry showing a) three-dimensional morphology during mild conditions early in the experiment, and b) linear bar as a result of strong longshore currents after 10 October.

Figure 5. Time series of five minute mean H_{rms} values, 6-16 October 1990.

Figure 6. Time series of five minute mean longshore current values, V, 6-16 October 1990.

Figure 7. Expanded view of five minute mean V values on 9 October 1990.

Figure 8. Simulated longshore currents and wave heights and depths on a planar beach during a tidal cycle (upper panels). Variation of longshore currents at various cross-shore locations with tidal cycle (lower panel).

Figure 9. Predicted longshore currents and wave heights and depths over the measured barred bathymetry 7 October for case of low waves and poorly-developed bar during a tidal cycle (upper panels). Variation of longshore currents at various cross-shore locations with tidal cycle (lower panel).

Figure 10. Predicted longshore currents, wave height and depth over the measured barred bathymetry 12 October for case of low waves and well-developed bar during a tidal cycle (upper panels). Variation of longshore currents at various cross-shore locations with tidal cycle (lower panel).

Figure 11. Observed longshore currents grouped into three tidal stages.

Figure 12. Observed H_{rms} and longshore currents for consecutive tidal stages, 7 October.

Figure 13. Observed H_{rms} and longshore currents for consecutive tidal stages, 9 October.

Figure 14. Observed H_{rms} and longshore currents for consecutive tidal stages, 11 October.

Figure 15a. Cross-spectra between tide elevation (P9) and longshore currents at V9.
15b. Cross-spectra between tide elevation (P9) and longshore currents at V5.
15c. Cross-spectra between tide elevation (P9) and longshore currents at V2.

Figure 16. Coherences (open squares) and phase differences (closed squares) at the semi-diurnal tidal frequency (0.08 cph) between tide elevation (P9) and wave heights across surf zone (upper panel), between wave height at the offshore location (H9) with wave heights (middle panel), and between tide elevation (P9) and longshore current (lower panel). Values of coherence greater than 0.33 are significantly different from zero at 95% confidence level.

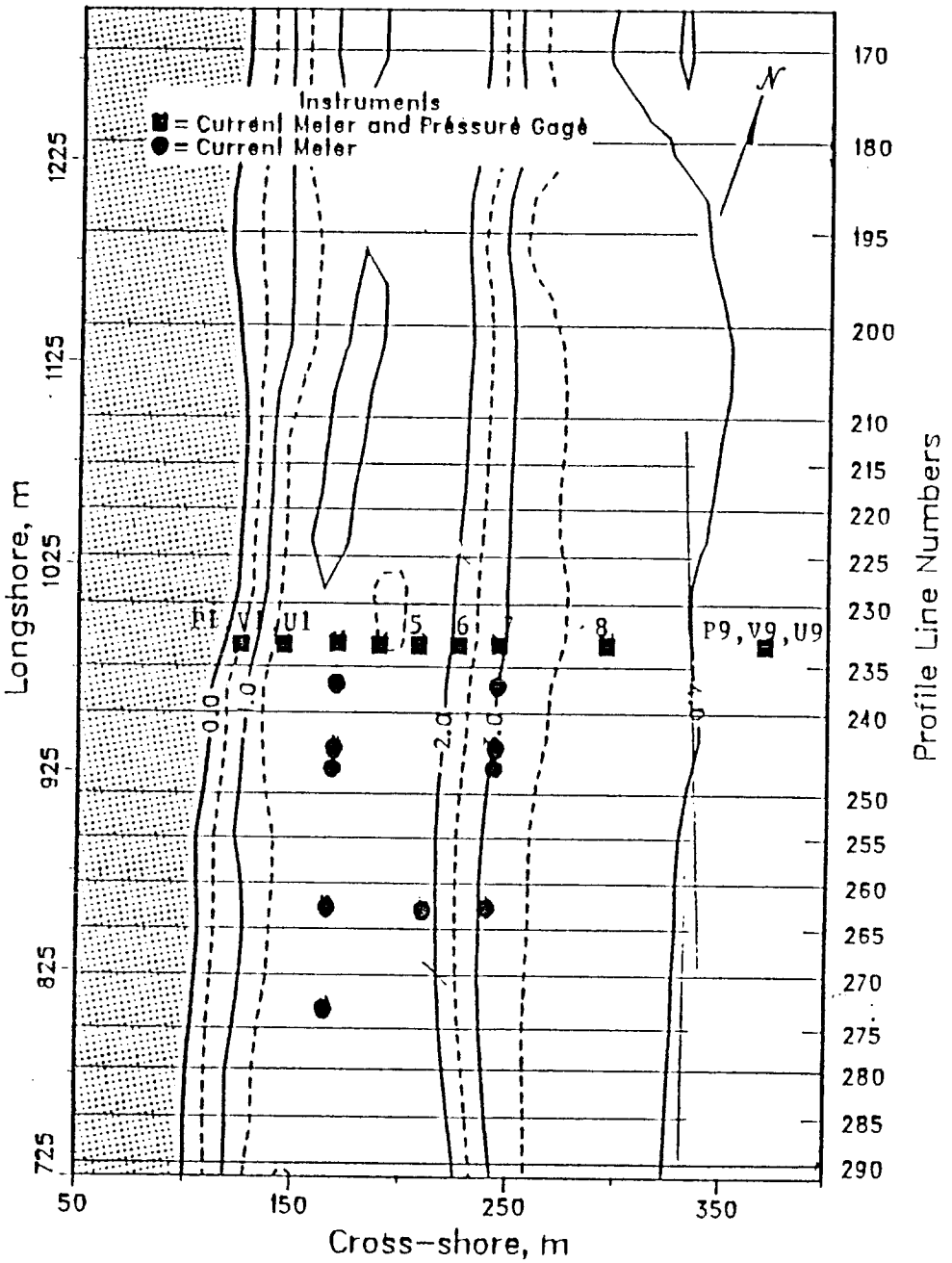

DELILAH Mini-Grid 11 OCT 90

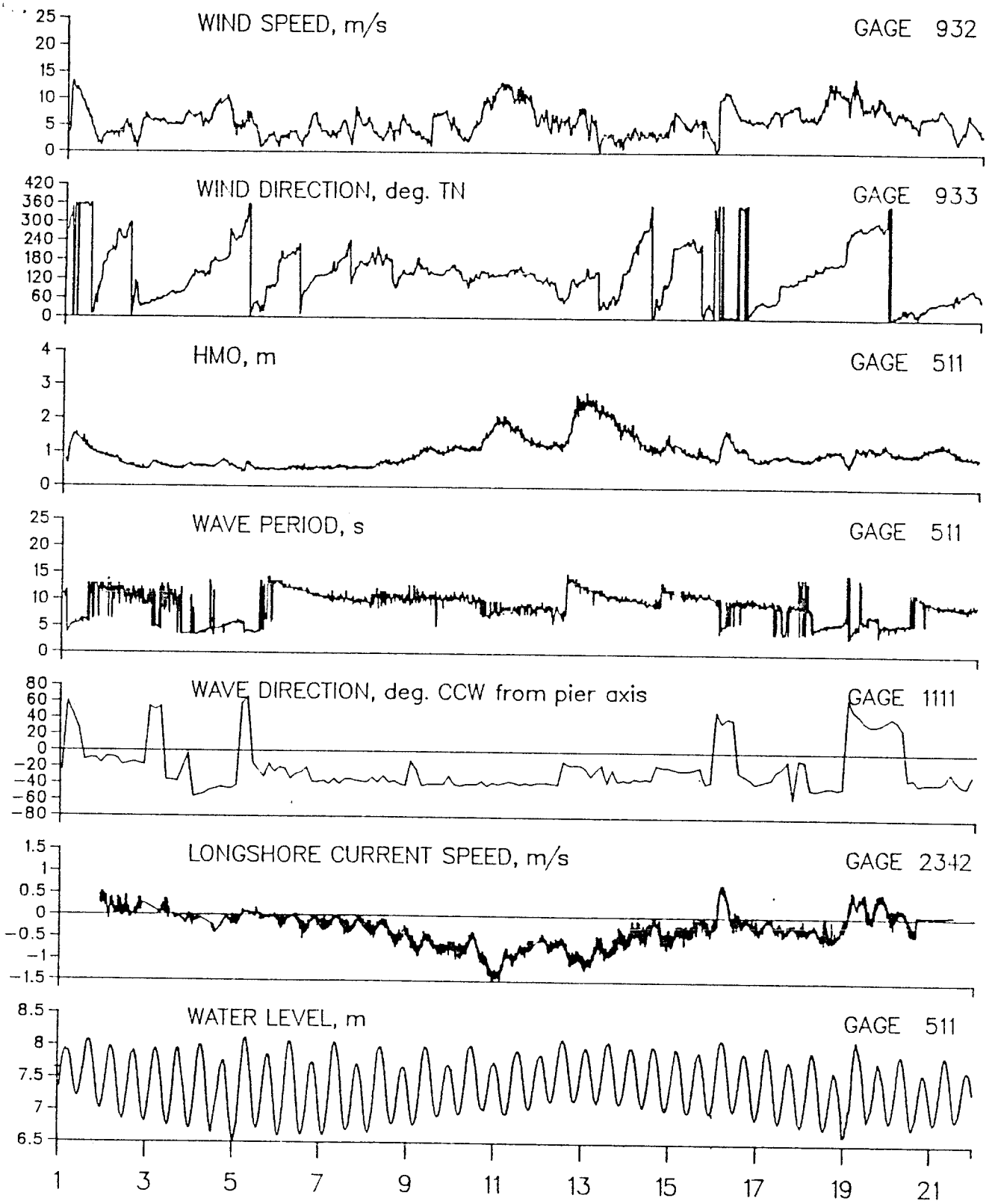
WIND SPEED, m/s
GAGE 932
25
20
15
10
5
0
WIND DIRECTION, deg. TN
GAGE 933
420
360
300
240
180
120
60
0
HMO, m
GAGE 511
4
3
2
1
0
WAVE PERIOD, s
GAGE 511
25
20
15
10
5
0
WAVE DIRECTION, deg. CCW from pier axis
GAGE 1111
80
60
40
20
0
−20
−40
−60
−80
LONGSHORE CURRENT SPEED, m/s
GAGE 2342
1.5
1
0.5
0
−0.5
−1
−1.5
WATER LEVEL, m
GAGE 511
8.5
8
7.5
7
6.5
1
3
5
7
9
11
13
15
17
19
21
OCTOBER
1990

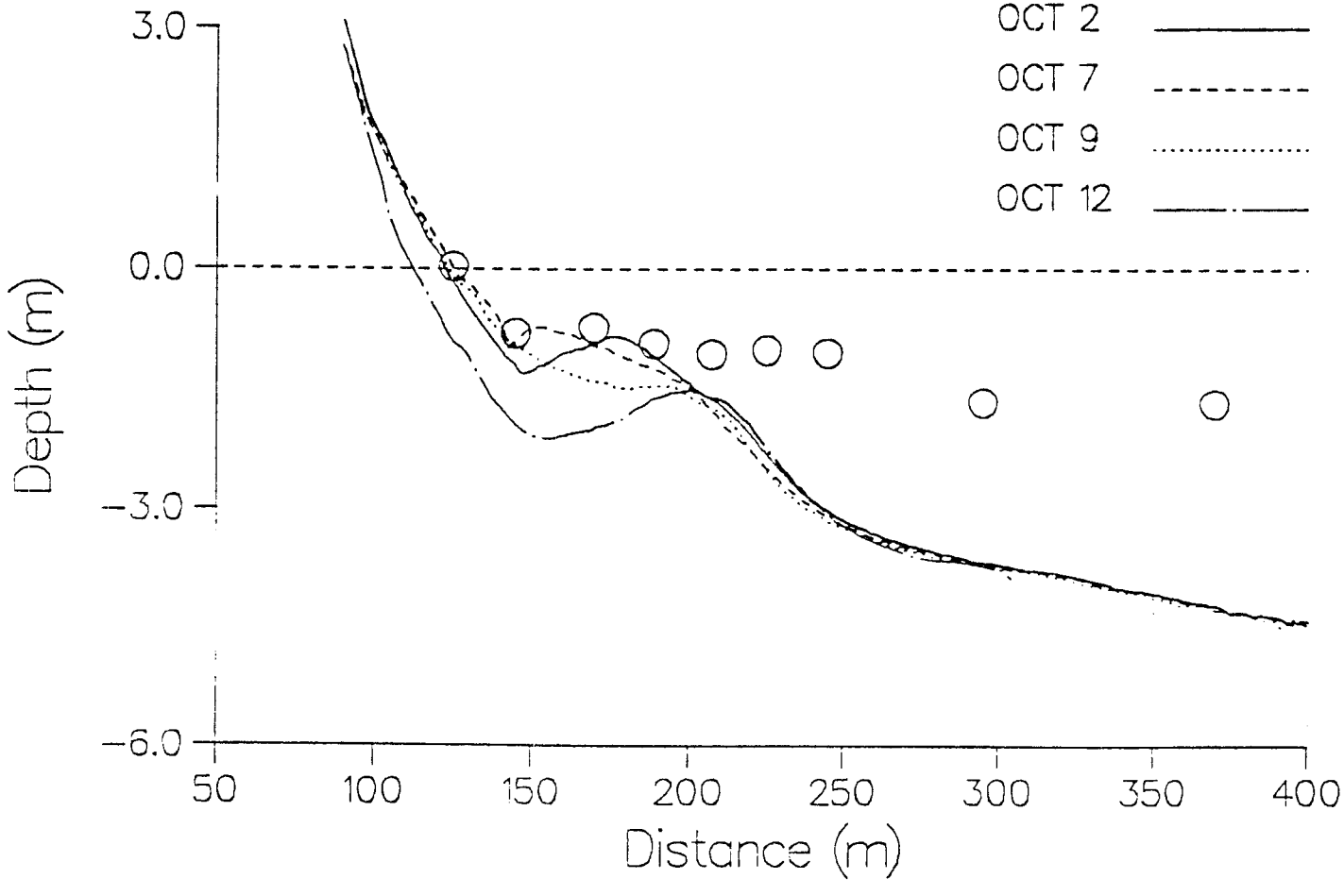
OCT 2
OCT 7
OCT 9
OCT 12
3.0
0.0
-3.0
-6.0
Depth (m)
50
100
150
200
250
300
350
400
Distance (m)

1 OCT 90

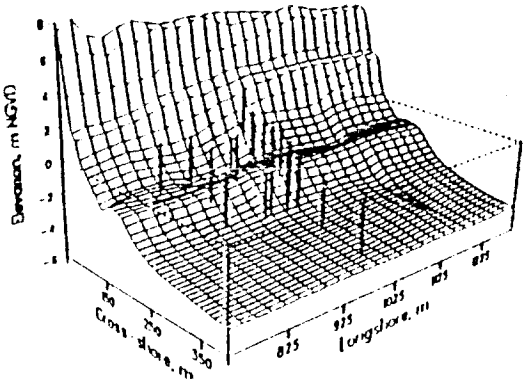

9 OCT 90

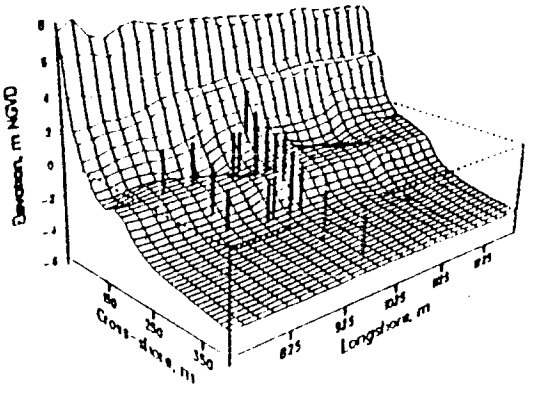

11 OCT 90

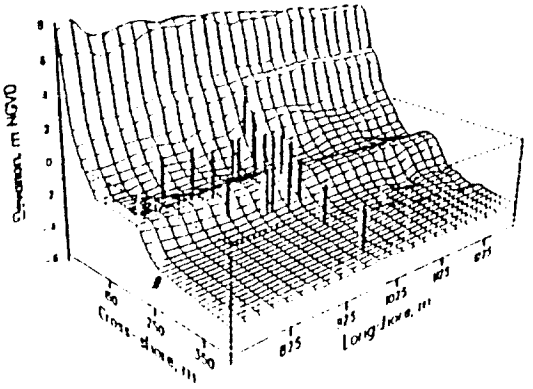

19 OCT 90

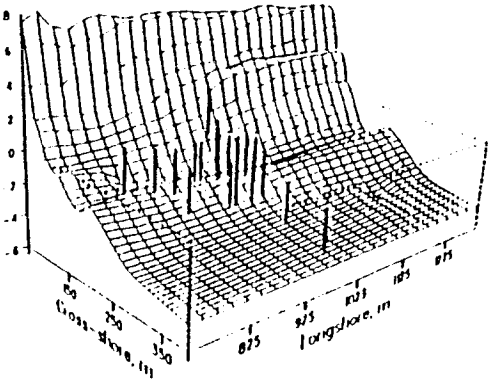

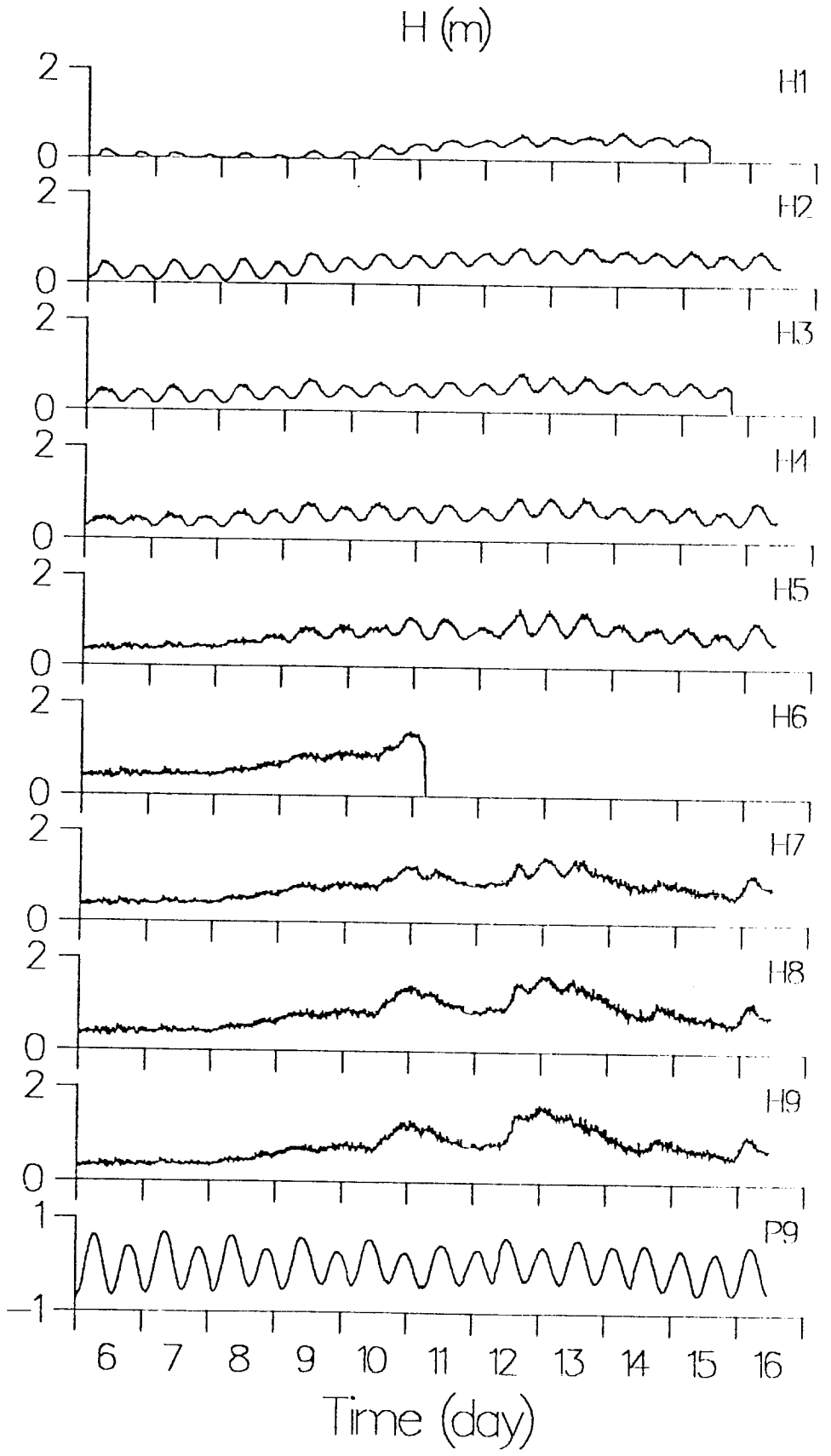
H (m)
H1
H2
H3
H4
H5
H6
H7
H8
H9
P9
2
0
1
−1
6
7
8
9
10
11
12
13
14
15
16
Time (day)

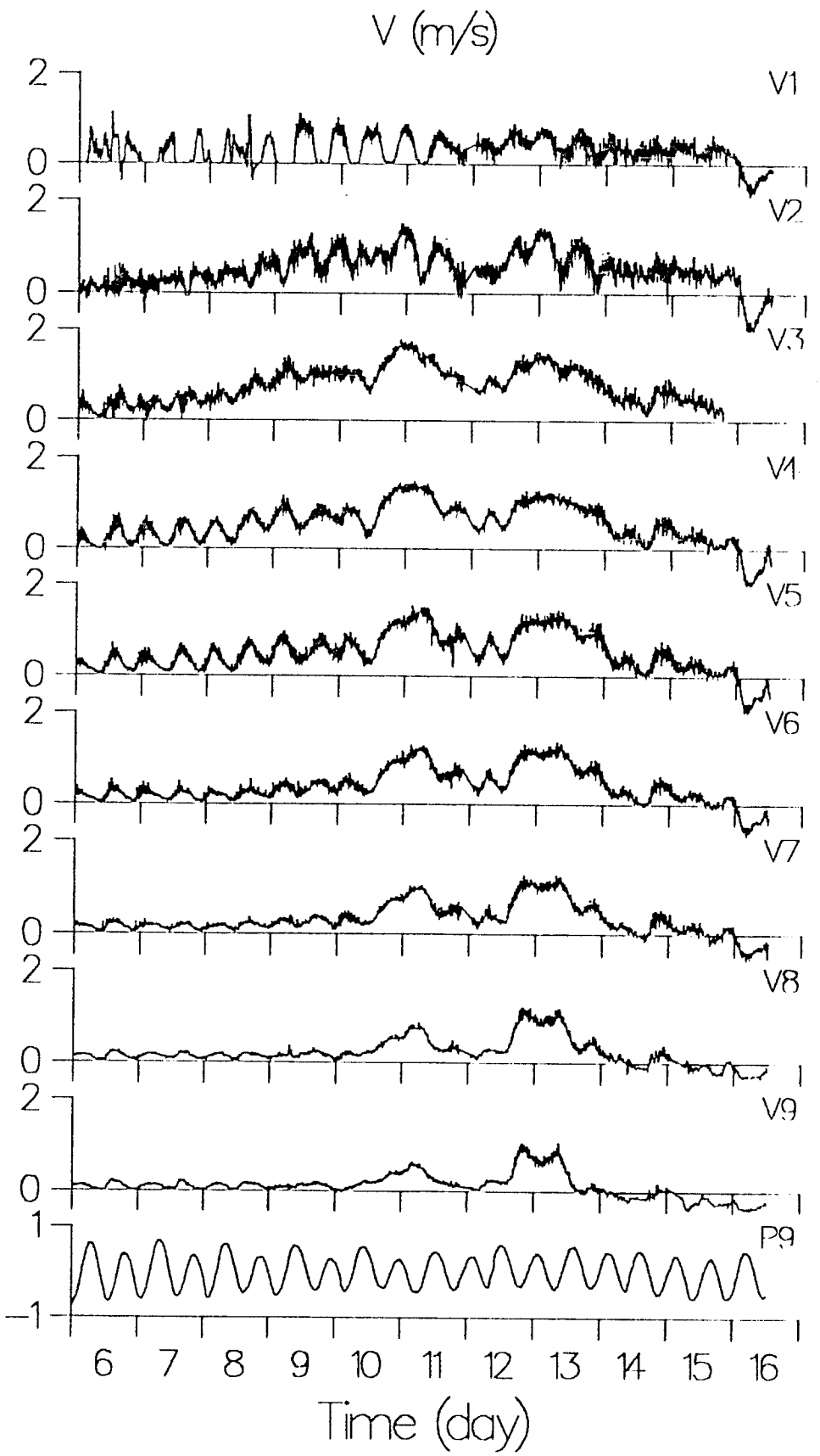
V (m/s)
V1
V2
V3
V4
V5
V6
V7
V8
V9
P9
2
0
1
-1
6
7
8
9
10
11
12
13
14
15
16
Time (day)

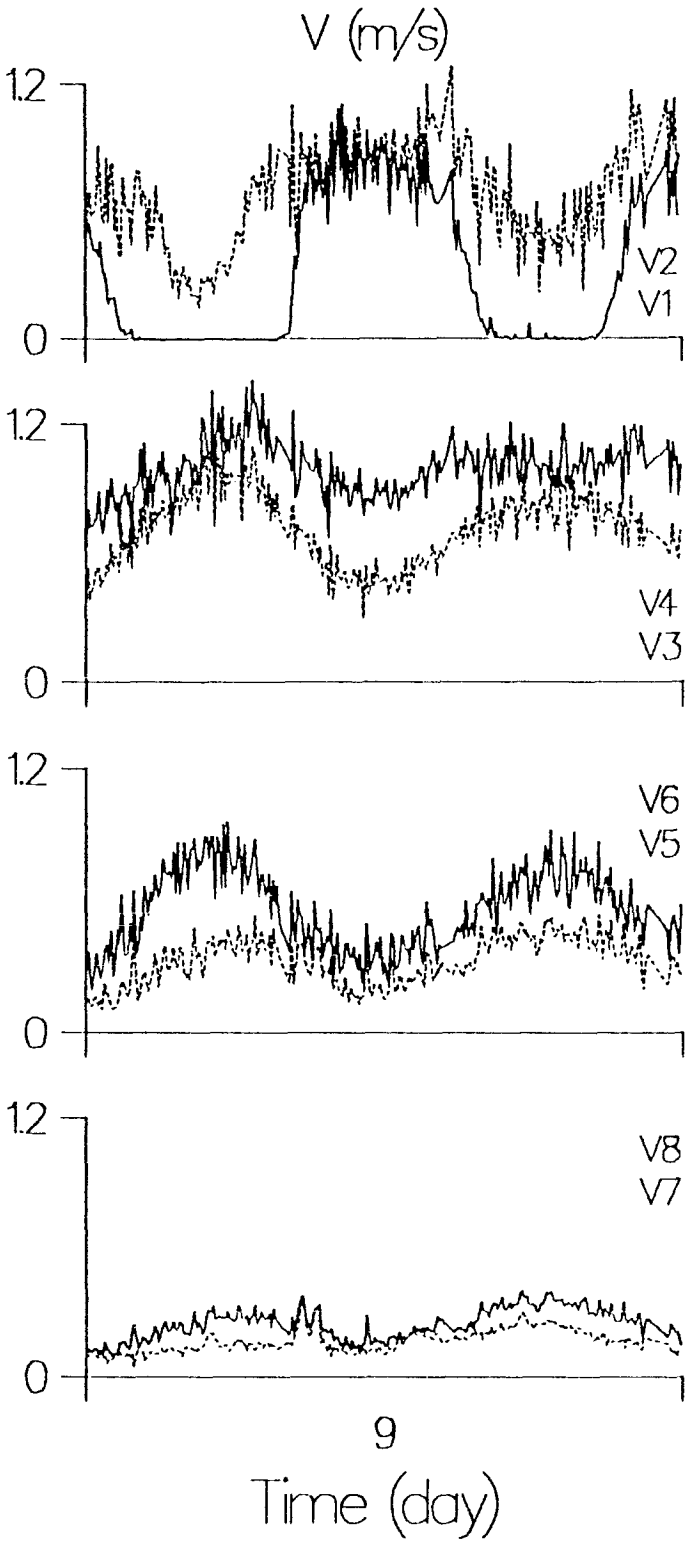
V (m/s)
1.2
0
V2
V1
1.2
0
V4
V3
1.2
0
V6
V5
1.2
0
V8
V7
9
Time (day)

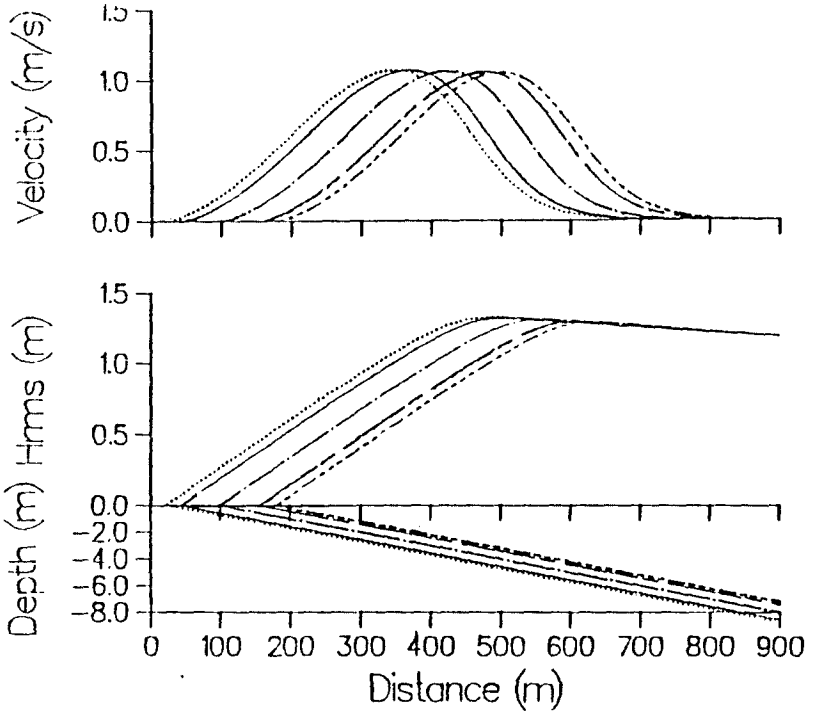
Velocity (m/s)
1.5
1.0
0.5
0.0
Depth (m) Hrms (m)
1.5
1.0
0.5
0.0
-2.0
-4.0
-6.0
-8.0
0
100
200
300
400
500
600
700
800
900
Distance (m)

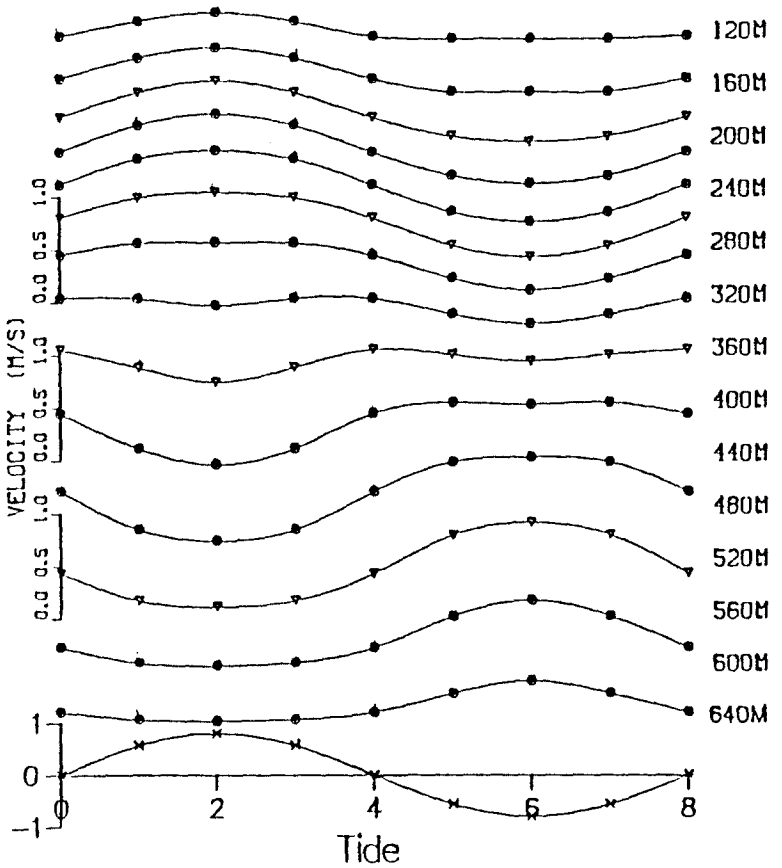
120M
160M
200M
240M
280M
320M
360M
400M
440M
480M
520M
560M
600M
640M
VELOCITY (M/S)
1.0
0.5
0.0
1
0
-1
0
2
4
6
8
Tide

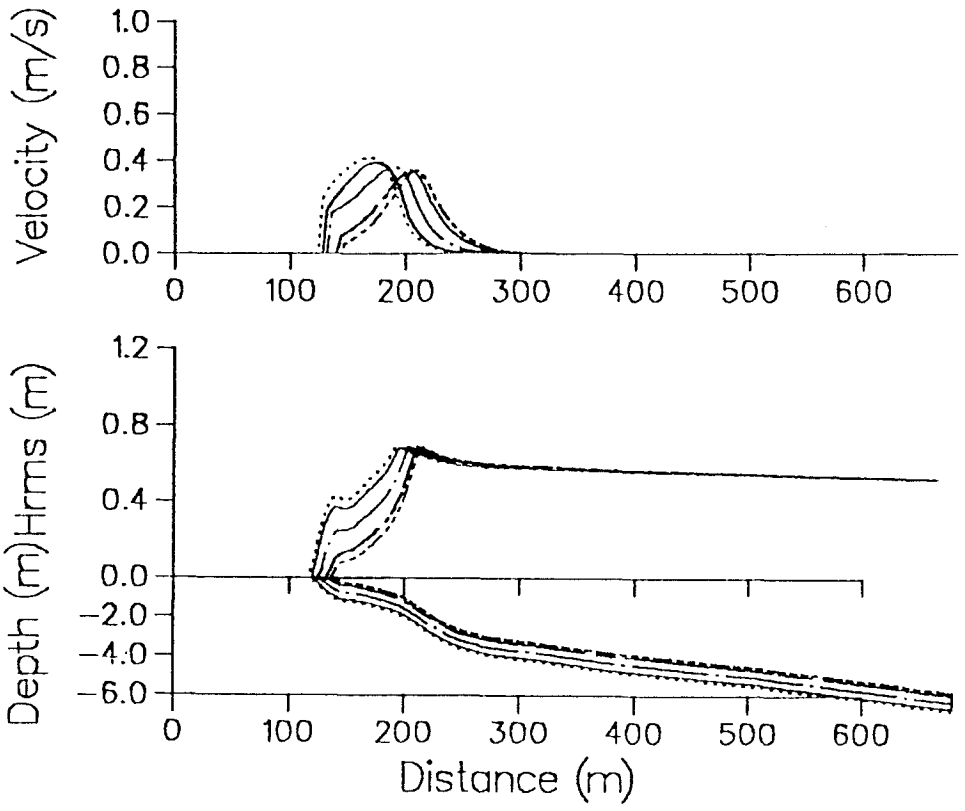
Velocity (m/s)
1.0
0.8
0.6
0.4
0.2
0.0
0
100
200
300
400
500
600
Depth (m)Hrms (m)
1.2
0.8
0.4
0.0
-2.0
-4.0
-6.0
0
100
200
300
400
500
600
Distance (m)

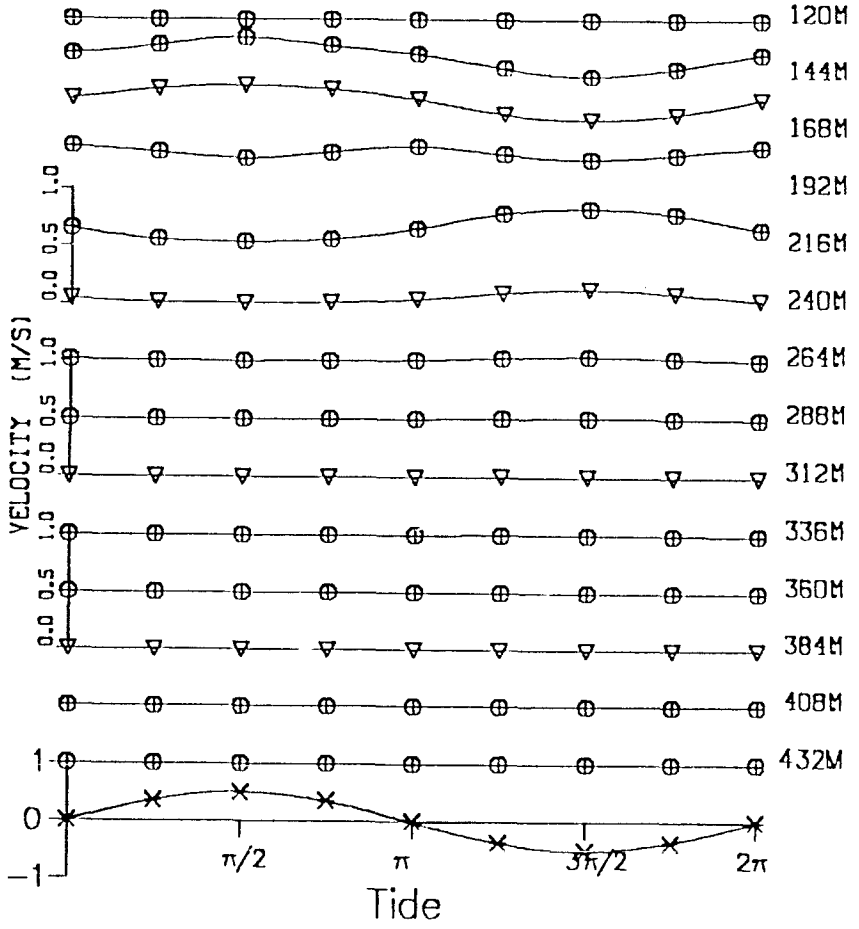
120M
144M
168M
192M
216M
240M
264M
288M
312M
336M
360M
384M
408M
432M
VELOCITY (M/S)
1.0
0.5
0.0
1
0
-1
π/2
π
3π/2
2π
Tide

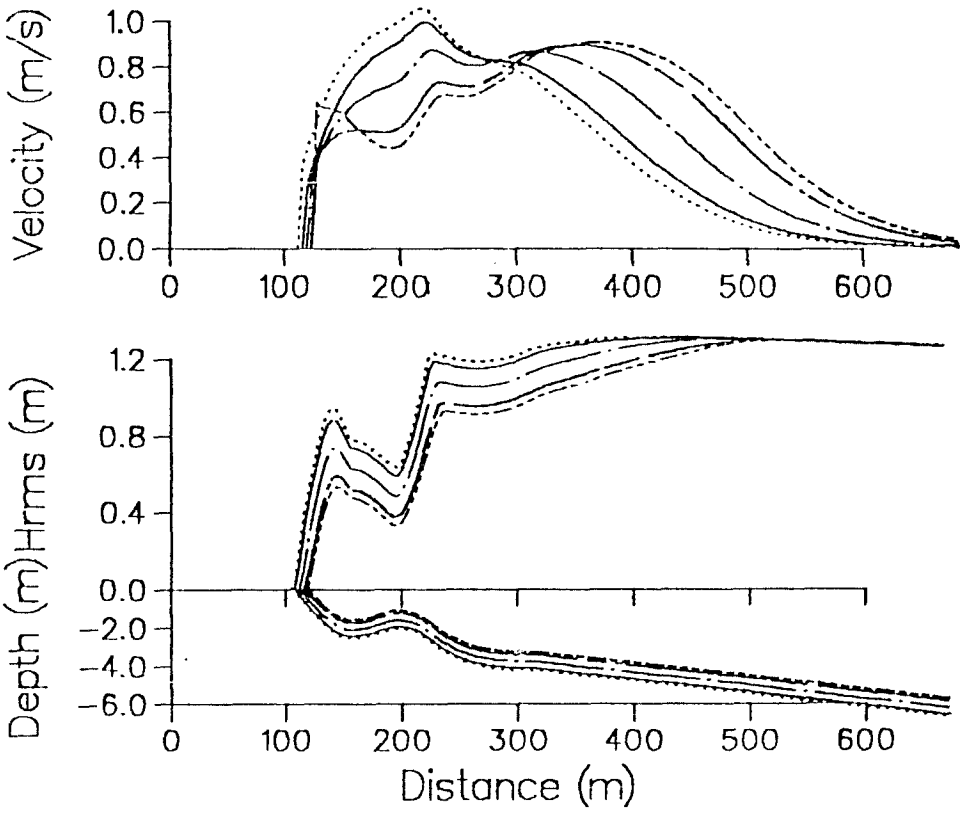
Velocity (m/s)
1.0
0.8
0.6
0.4
0.2
0.0
0
100
200
300
400
500
600
Depth (m)Hrms (m)
1.2
0.8
0.4
0.0
-2.0
-4.0
-6.0
0
100
200
300
400
500
600
Distance (m)

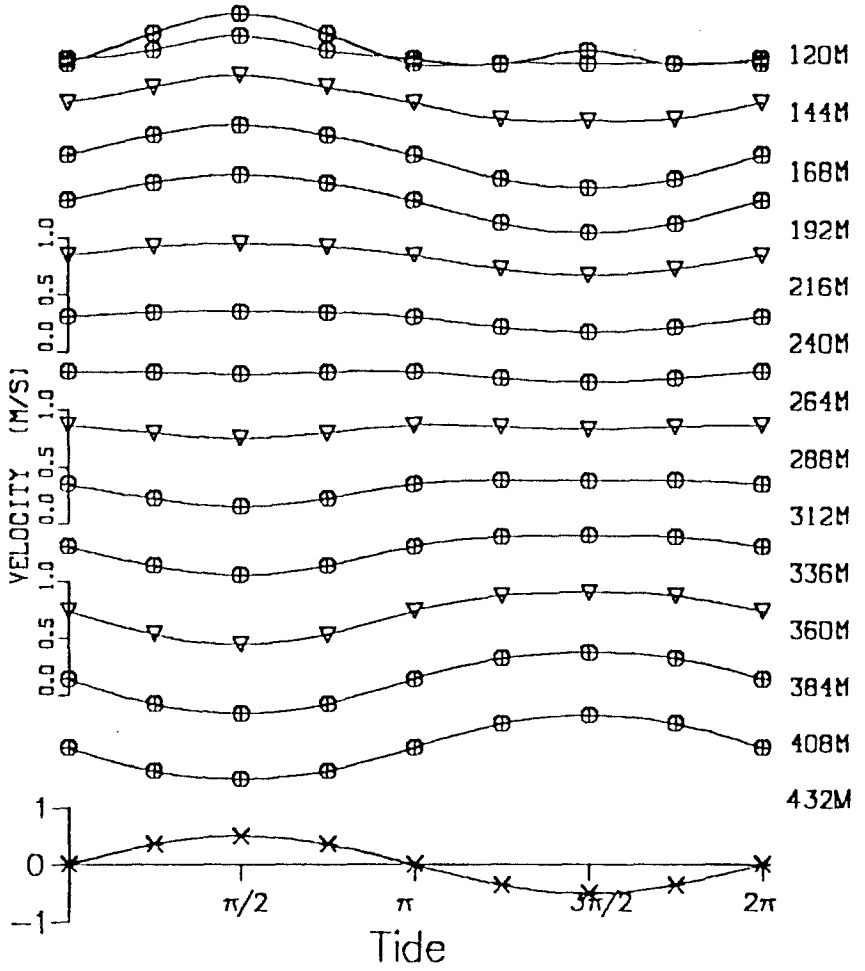
VELOCITY (M/S)
1.0
0.5
0.0
120M
144M
168M
192M
216M
240M
264M
288M
312M
336M
360M
384M
408M
432M
1
0
-1
π/2
π
3π/2
2π
Tide

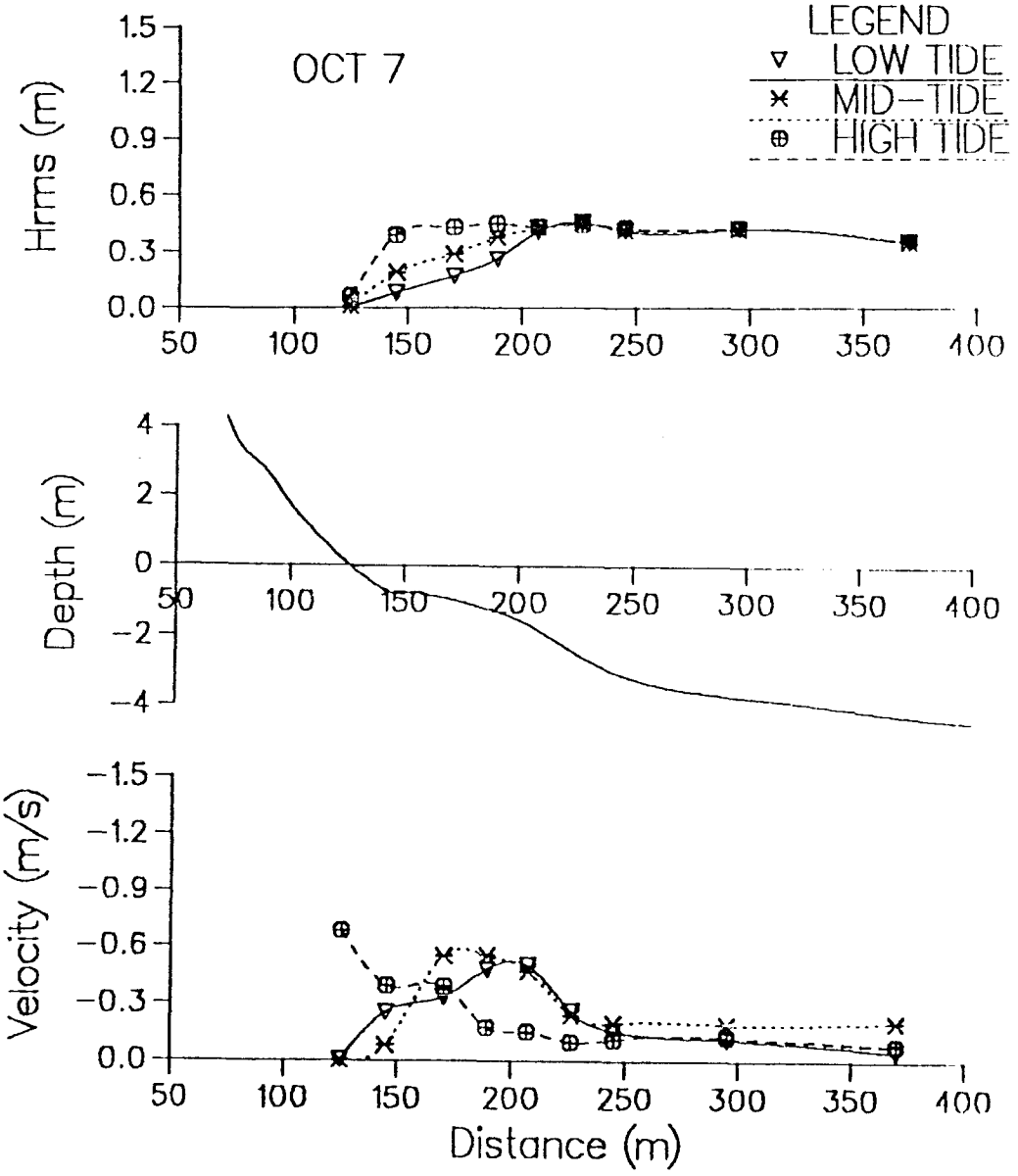
OCT 7
LEGEND
LOW TIDE
MID-TIDE
HIGH TIDE
Hrms (m)
1.5
1.2
0.9
0.6
0.3
0.0
50
100
150
200
250
300
350
400
Depth (m)
4
2
0
-2
-4
Velocity (m/s)
-1.5
-1.2
-0.9
-0.6
-0.3
0.0
Distance (m)

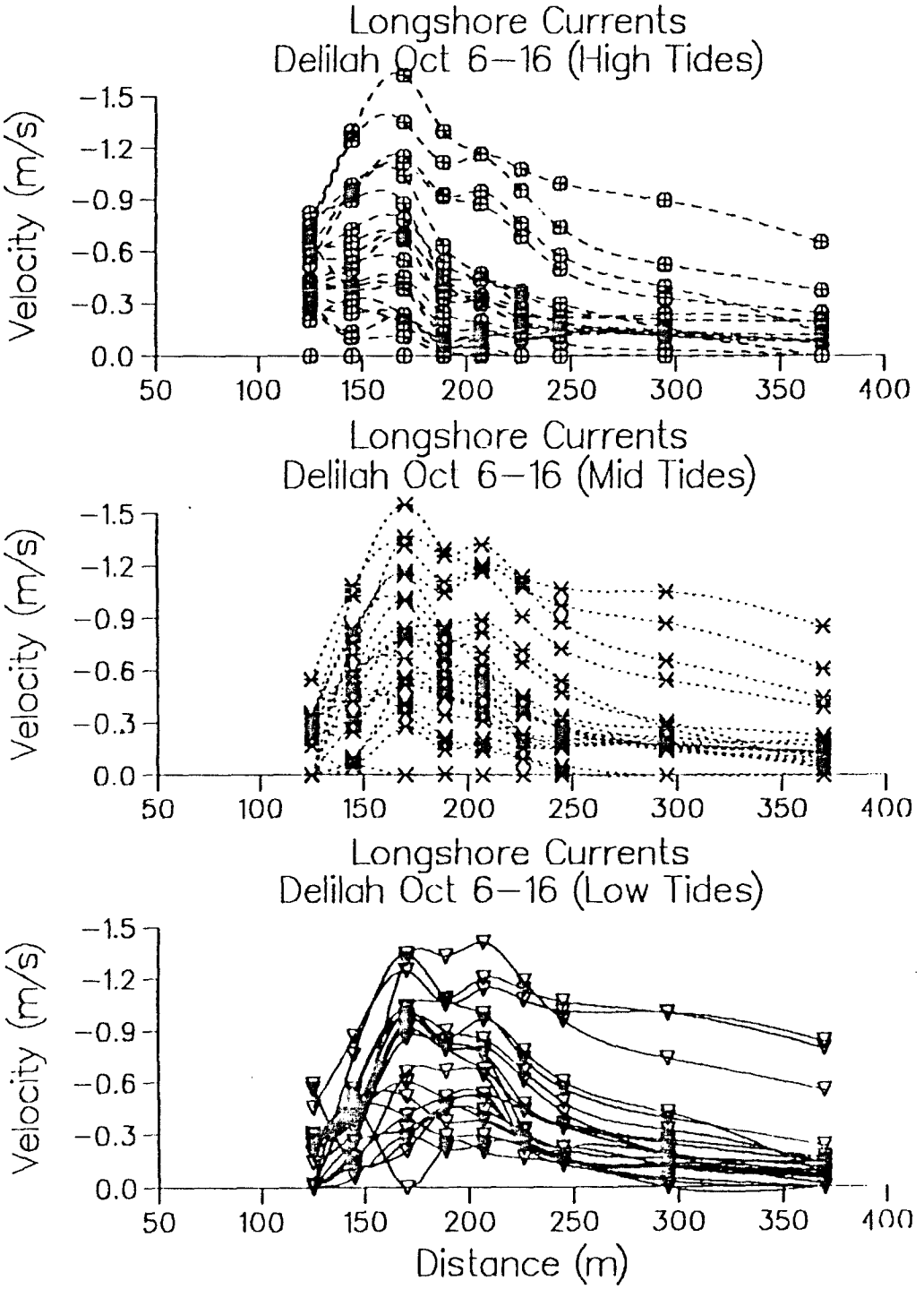
Longshore Currents
Delilah Oct 6–16 (High Tides)
Velocity (m/s)
−1.5
−1.2
−0.9
−0.6
−0.3
0.0
50
100
150
200
250
300
350
400
Longshore Currents
Delilah Oct 6–16 (Mid Tides)
Velocity (m/s)
Longshore Currents
Delilah Oct 6–16 (Low Tides)
Velocity (m/s)
Distance (m)

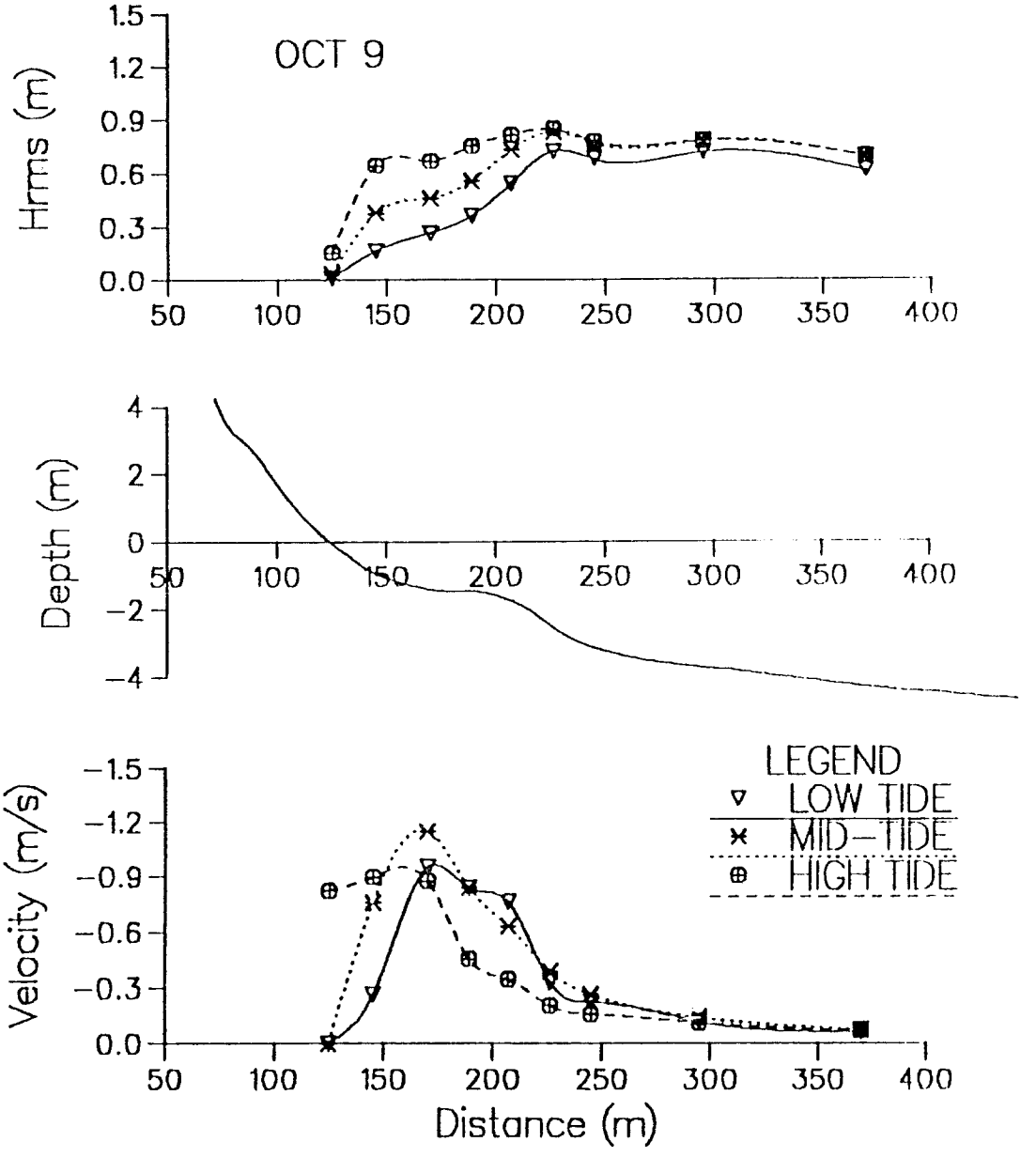
OCT 9
Hrms (m)
1.5
1.2
0.9
0.6
0.3
0.0
50
100
150
200
250
300
350
400
Depth (m)
4
2
0
−2
−4
Velocity (m/s)
−1.5
−1.2
−0.9
−0.6
−0.3
0.0
LEGEND
LOW TIDE
MID−TIDE
HIGH TIDE
Distance (m)

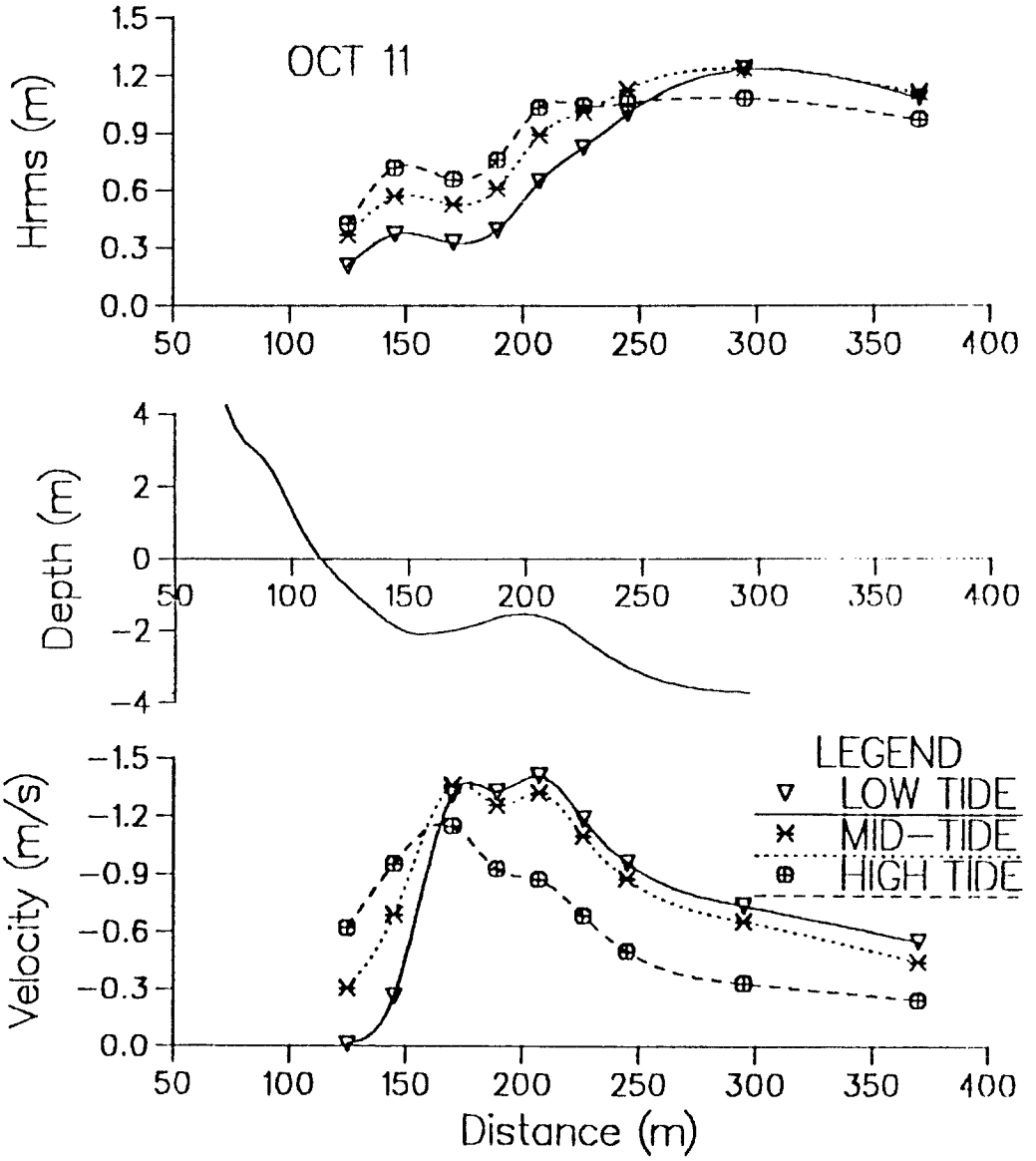
OCT 11
Hrms (m)
1.5
1.2
0.9
0.6
0.3
0.0
50
100
150
200
250
300
350
400
Depth (m)
4
2
0
−2
−4
Velocity (m/s)
−1.5
−1.2
−0.9
−0.6
−0.3
0.0
LEGEND
LOW TIDE
MID−TIDE
HIGH TIDE
Distance (m)

P9-V9

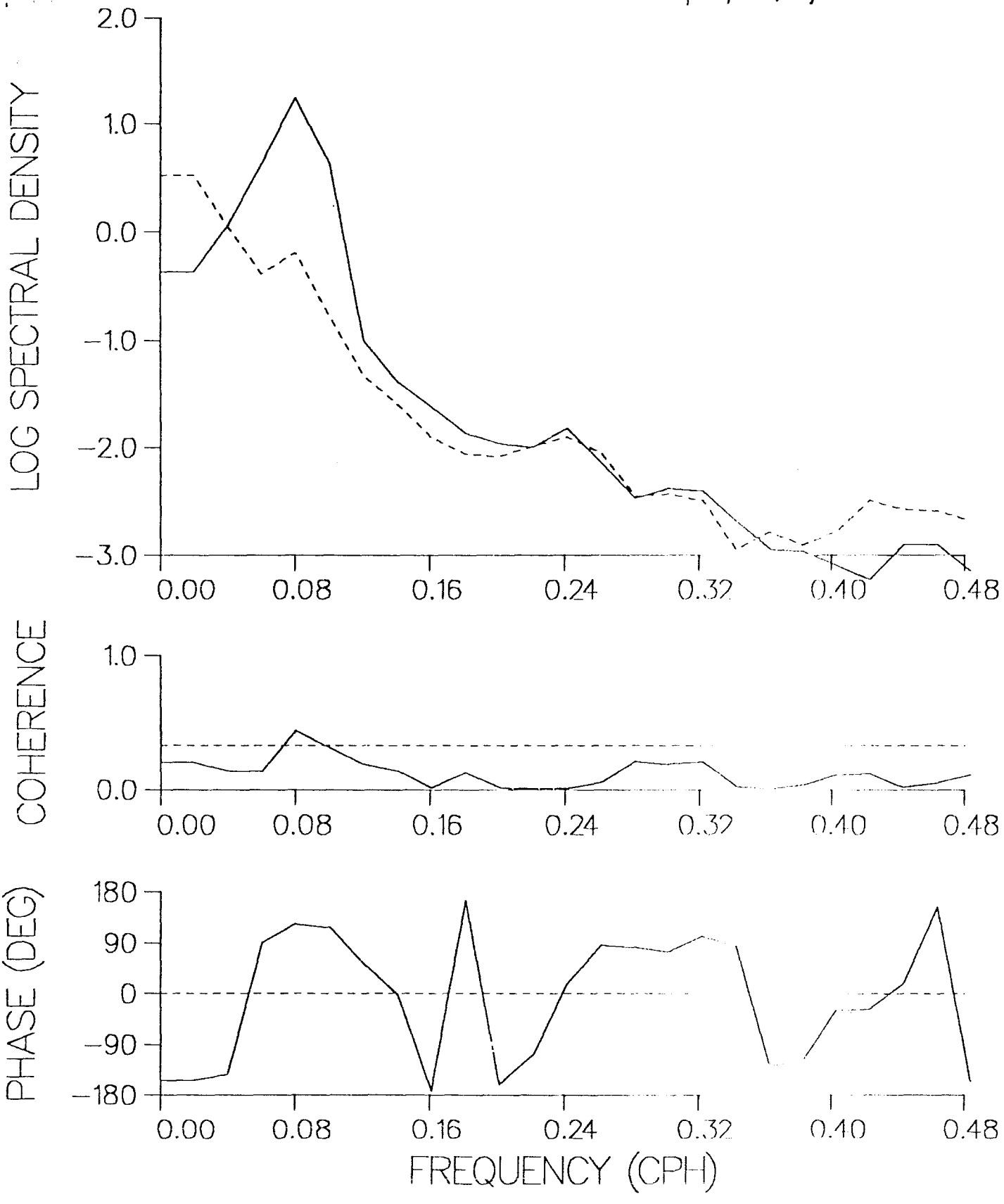
LOG SPECTRAL DENSITY
2.0
1.0
0.0
-1.0
-2.0
-3.0
0.00
0.08
0.16
0.24
0.32
0.40
0.48
COHERENCE
1.0
0.0
0.00
0.08
0.16
0.24
0.32
0.40
0.48
PHASE (DEG)
180
90
0
-90
-180
0.00
0.08
0.16
0.24
0.32
0.40
0.48
FREQUENCY (CPH)

P9-V5

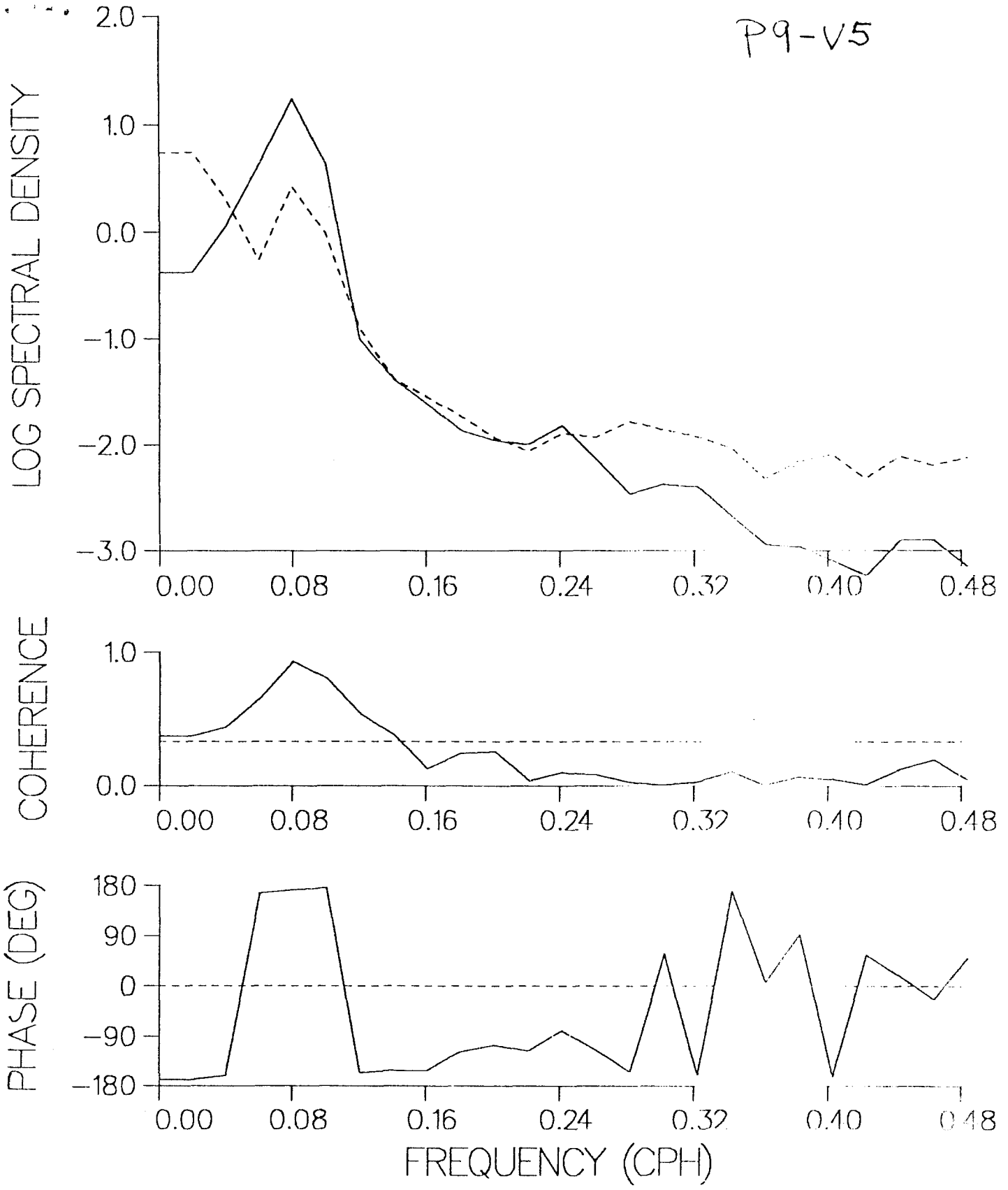
LOG SPECTRAL DENSITY
2.0
1.0
0.0
-1.0
-2.0
-3.0
0.00
0.08
0.16
0.24
0.32
0.40
0.48
COHERENCE
1.0
0.0
0.00
0.08
0.16
0.24
0.32
0.40
0.48
PHASE (DEG)
180
90
0
-90
-180
0.00
0.08
0.16
0.24
0.32
0.40
0.48
FREQUENCY (CPH)

P9-V2

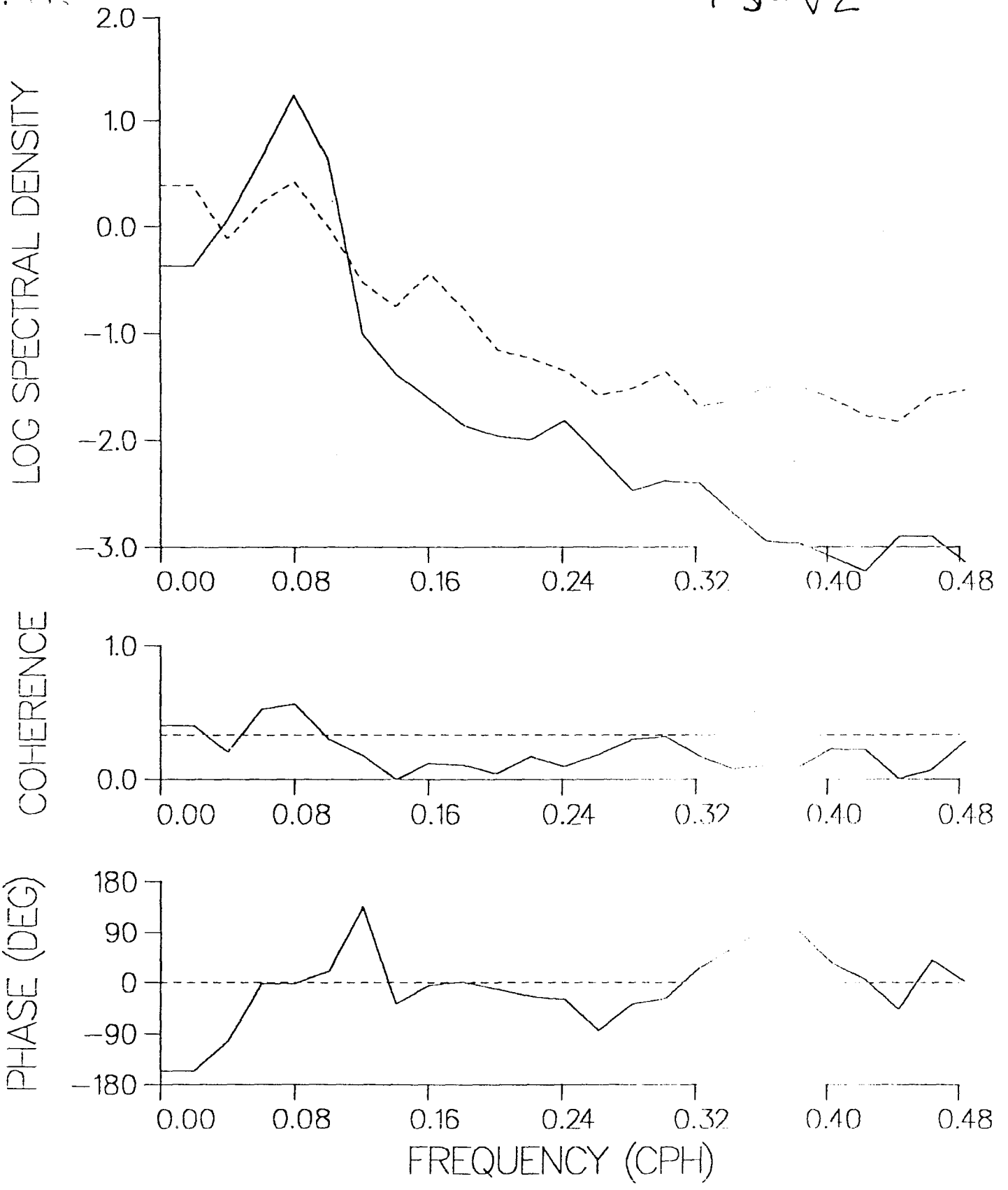
LOG SPECTRAL DENSITY
2.0
1.0
0.0
-1.0
-2.0
-3.0
0.00
0.08
0.16
0.24
0.32
0.40
0.48
COHERENCE
1.0
0.0
0.00
0.08
0.16
0.24
0.32
0.40
0.48
PHASE (DEG)
180
90
0
-90
-180
0.00
0.08
0.16
0.24
0.32
0.40
0.48
FREQUENCY (CPH)

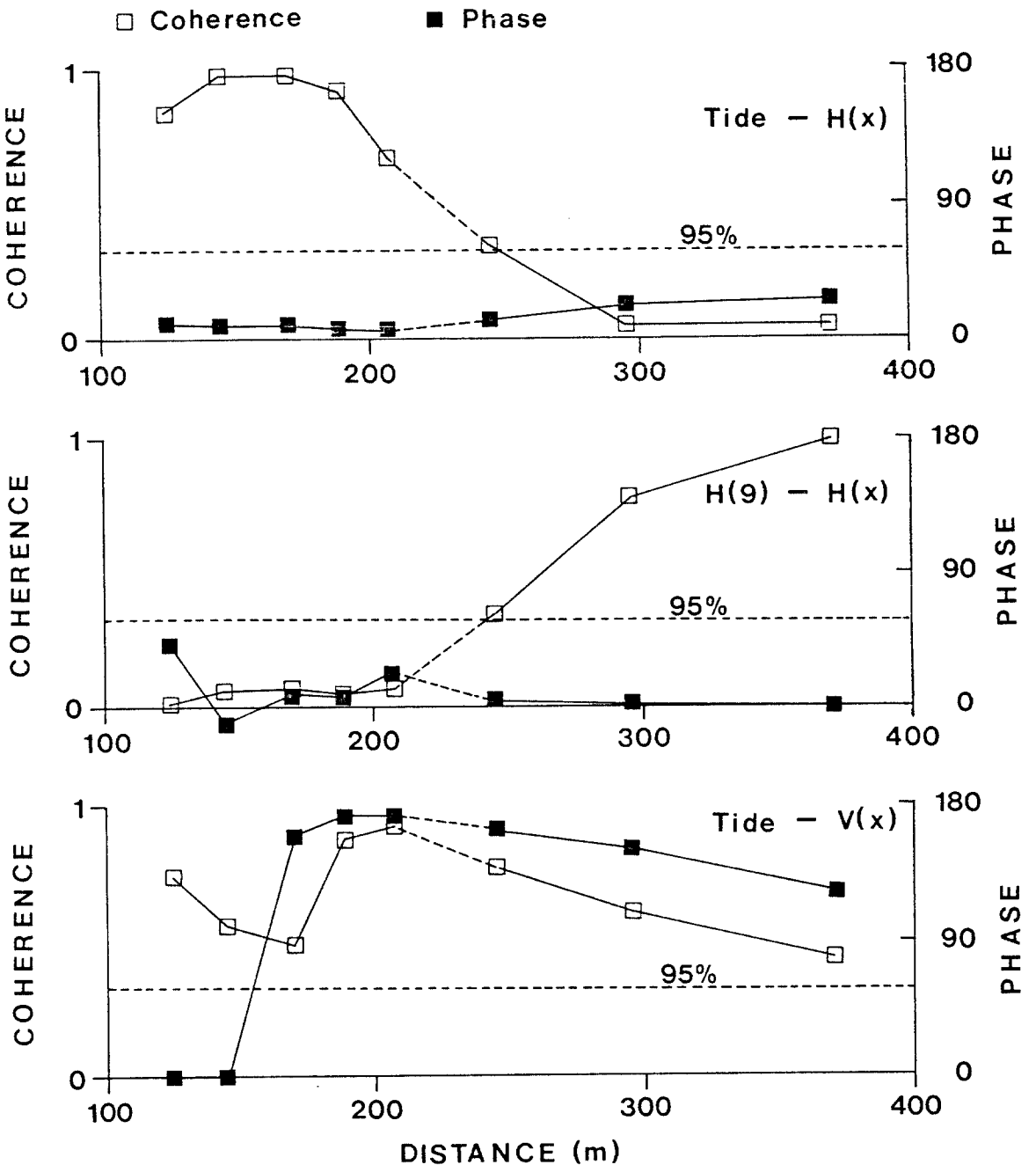
Coherence
Phase
COHERENCE
PHASE
Tide – H(x)
H(9) – H(x)
Tide – V(x)
95%
1
0
180
90
0
100
200
300
400
DISTANCE (m)